

Final Report to



Phase I Final Technical Report

10121.4302.01.Final1

***Ultra-High Conductivity Umbilicals:
Polymer Nanotube Umbilicals (PNUs)***

10121-4302-01

June 24, 2013

Christopher A. Dyke
Principal Investigator
NanoRidge Materials, Inc.
15850 Vickery Drive
Houston, Texas 77032

LEGAL NOTICE

THIS REPORT WAS PREPARED BY NANORIDGE MATERIALS, INC. AS AN ACCOUNT OF WORK SPONSORED BY THE RESEARCH PARTNERSHIP TO SECURE ENERGY FOR AMERICA, RPSEA. NEITHER RPSEA MEMBERS OF RPSEA, THE NATIONAL ENERGY TECHNOLOGY LABORATORY, THE U.S. DEPARTMENT OF ENERGY, NOR ANY PERSON ACTING ON BEHALF OF ANY OF THE ENTITIES:

- a. MAKES ANY WARRANTY OR REPRESENTATION, EXPRESS OR IMPLIED WITH RESPECT TO ACCURACY, COMPLETENESS, OR USEFULNESS OF THE INFORMATION CONTAINED IN THIS DOCUMENT, OR THAT THE USE OF ANY INFORMATION, APPARATUS, METHOD, OR PROCESS DISCLOSED IN THIS DOCUMENT MAY NOT INFRINGE PRIVATELY OWNED RIGHTS, OR**

- b. ASSUMES ANY LIABILITY WITH RESPECT TO THE USE OF, OR FOR ANY AND ALL DAMAGES RESULTING FROM THE USE OF, ANY INFORMATION, APPARATUS, METHOD, OR PROCESS DISCLOSED IN THIS DOCUMENT.**

THIS IS A FINAL REPORT. THE DATA, CALCULATIONS, INFORMATION, CONCLUSIONS AND/OR RECOMMENDATIONS REPORTED HEREIN ARE THE PROPERTY OF THE U.S. DEPARTMENT OF ENERGY.

REFERENCE TO TRADE NAMES OR SPECIFIC COMMERCIAL PRODUCTS, COMMODITIES, OR SERVICES IN THIS REPORT DOES NOT REPRESENT OR CONSTITUTE AN ENDORSEMENT, RECOMMENDATION, OR FAVORING BY RPSEA OR ITS CONTRACTORS OF THE SPECIFIC COMMERCIAL PRODUCT, COMMODITY, OR SERVICE.

THIS PAGE INTENTIONALLY LEFT BLANK

In witness whereof, the duly authorized representatives of RPSEA and NanoRidge Materials, Inc. have executed this document on the dates shown below.

SUBCONTRACTOR:

NANORIDGE MATERIALS, INC

By: *Chris Dyke*

(Signature)

Name: Christopher A. Dyke

Title: Principal Investigator

Date: July 24, 2013

**Phase I Final Technical Report Draft
NanoRidge Materials, Inc.
Contract Number 10121-4302-01**

Abstract

This final technical report draft details the Phase I technical effort. NanoRidge Materials, the Prime Subcontractor, was responsible for management, reporting, and technical development. Rice University, a Subcontractor to NanoRidge, was responsible for research. The deliverable for Year 1 was a CNT conductor with resistivity of $10^{-5} \Omega \cdot \text{cm}$. This was achieved. The report includes results of the NanoRidge, Rice technical effort and details the achievement of the deliverable. The highlights from Year 1 are a) installation of a lab scale furnace outfitted for continuous wire formation, b) optimization of purification, doping, and testing protocols, c) characterization of several wires and relating CNT composition to conductivity, and d) technology transfer opportunities. Since the technical deliverable was achieved, our recommendation is to transition to Phase II.

TABLE OF CONTENTS

1.	EXECUTIVE SUMMARY	7
2.	REPORT DETAILS	8
2.1	EXPERIMENTAL METHODS.....	9
2.1.1	SUBTASK 5.1.1.1 – SPECIFY EQUIPMENT.....	10
2.1.2	SUBTASK 5.1.1.2 – PROCUREMENT	11
2.1.3	SUBTASK 5.1.1.3 – INSTALLATION	11
2.1.4	SUBTASK 5.1.1.4 – CONTINUOUS FIBER.....	11
2.1.5	SUBTASK 5.1.1.5 – START-UP REVIEW	12
2.1.6	SUBTASK 5.1.1.6 – OPTIMIZATION	12
2.1.7	RICE 1.1 – NANOTUBE MANIPULATION.....	13
2.1.8	RICE 1.2 – NANOTUBE PURIFICATION	15
2.1.9	RICE 1.3 – MANIPULATION AND CONNECTIONS.....	15
2.1.10	RICE 1.4 – NANOTUBE GROWTH STUDIES	15
2.1.11	RICE 1.5 – EXTENDED LENGTHS OF NANOTUBES	16
2.1.12	RICE 1.6 – REDUCE DEFECTS OF THE CONDUCTOR.....	16
2.1.13	RICE 1.7 – OPTIMIZE NANOTUBE GROWTH BY TYPE	16
2.1.14	RICE 1.8 – OPTIMIZE ALIGNMENT FOR CONDUCTIVITY AND STRENGTH.....	16
2.1.15	RICE 1.9 – DOPING AND CONDITIONING	17
2.2	RESULTS AND DISCUSSIONS	17
2.2.1	ELECTRICAL PROPERTY MEASUREMENTS	18
2.2.2	MATERIAL CHARACTERIZATION METHODS	22
2.2.3	CARBON NANOTUBE WIRES	28
2.2.4	CNT PURIFICATION	65
2.2.5	CNT GROWTH	65
2.2.6	MANIPULATION AND CONTACT	67
2.2.7	IMPACT TO PRODUCERS.....	71
2.2.8	TECHNOLOGY TRANSFER EFFORTS	73
2.2.9	CONCLUSIONS	74
2.2.10	RECOMMENDATIONS	74
3.	FIGURES AND TABLES	74
4.	REFERENCES.....	77
5.	LIST OF ACRONYMS AND ABBREVIATIONS.....	80
6.	APPENDICES.....	81

1. EXECUTIVE SUMMARY

This document constitutes the Phase I Final Technical Report (Draft) and details the technical work performed to achieve the first year deliverable, a carbon nanotube wire with $10^{-5} \Omega \cdot \text{cm}$ resistivity. Phase I corresponds to the first year's effort. This is a three-year, \$3.2 M phased project with NanoRidge Materials, Inc. as the lead organization.

In a previous Department of Energy (DOE) Research Partnership to Secure Energy for America (RPSEA) project, NanoRidge Materials, Inc. (NanoRidge) and Rice University (Rice) teamed up to advance a new conductive wire based on carbon nanotubes [1]. In this project, Technip, USA (Technip) and DUCO were industrial partners. In this one year project, an electrical conductor was produced with an electrical resistivity of $60 \Omega\text{-kcmil/ft}$ ($1 \times 10^{-2} \Omega \cdot \text{cm}$). While this resistivity was similar to the best conducting polymers, resistivity of $6 \Omega\text{-kcmil/ft}$ ($1 \times 10^{-3} \Omega \cdot \text{cm}$) was achieved by Rice immediately after the RPSEA project ended. A novel approach was employed and a patent was filed [2]. Rice continued its work following the RPSEA project and improved the resistivity of a carbon nanotube wire from $0.6 \Omega\text{-kcmil/ft}$ ($1 \times 10^{-4} \Omega \cdot \text{cm}$) and finally as low as $0.9 \Omega\text{-kcmil/ft}$ ($1.5 \times 10^{-5} \Omega \cdot \text{cm}$) for a small laboratory scale wire conductor. This work led to two patents and one high impact journal publication [3-5]. The present three-year project can be considered a follow-on effort from this initial RPSEA project.

In year 1 of the current effort, Dr. Christopher Dyke (NanoRidge) and Professor Enrique Barrera of Rice University served as principal investigators. The work was performed at both NanoRidge and Rice University. The cost share partners include DUCO, Shell, Total, and Baker Hughes. Each organization specified an individual to serve on the Working Project Group and provide industrial guidance throughout the course of this project. Herve de Naurois, Total, was unanimously appointed Project Champion. Communication of progress with the project sponsor, RPSEA, was maintained via monthly reports and routine updates.

The purpose of this program is to develop a unique conductor for use in subsea umbilicals and power transmission. As offshore developments move into deeper water and have longer step-out distances, subsea umbilicals must be improved. Offshore umbilicals must withstand substantial installation and service loads and deliver significant amounts of power along with an extended operational life. As drilling depths increase, conventional copper wire cannot support its own weight. Design engineers have considered this issue and determined one solution is a lighter, higher current carrying capacity conductor. *This is what the three-year project shall produce, a carbon-nanotube based conductor with less resistivity and higher current carrying capacity than copper at 1/6th the weight.* The technical team maintains a wire with $10^{-5} \Omega \cdot \text{cm}$ resistivity in year 1 is a prerequisite to the overarching goal.

The three-year development effort culminates with a prototype umbilical for use in a demonstration project. The conductor is comprised of double-walled carbon nanotubes (DWNT) in wire form and jacketed with a polymer; this is termed the polymer nanotube umbilical (PNU[®]) cable. The polymer provides electrical insulation, adds mechanical integrity, abrasion resistance, and ease of handling to the conductor. In the first phase of the project, Year 1, the technical team focused on the production of the conductor. The Year 1 tasks involved a) synthesis of DWNT, b) drawing the as-produced material into wire form, c) doping

the product, and d) optimization of the product. *The Phase I deliverable is a conductor with $10^{-5} \Omega \cdot \text{cm}$ resistivity.* In addition to the continuous production of the DWNT conductor, second year activities include jacketing the wire with polymer, optimizing and developing production processes, and extensive characterization of the wire (with and without jacket). Characterization is to include formation of wire connections and terminations. The Year 2 deliverable is a polymer jacketed DWNT conductor with $10^{-5} \Omega \cdot \text{cm}$ resistivity operational at a pressure of 5500 psig. In the third and final year of the project, the team shall optimize the conductor performance, produce the jacketed conductor, and insulate the wire. The insulated wire shall be used to form a prototype umbilical for the demonstration project. The prototype umbilical is to have resistivity as low as copper ($10^{-6} \Omega \cdot \text{cm}$) yet the conductor is $1/6^{\text{th}}$ the weight of copper. The working umbilical must be operational at 5500 psig pressure.

This document contains: **Section 2 – Report Details** that specifies our **2.1 Experimental Methods, 2.2 Results and Discussions, and 2.6 Recommendations**. This is a comprehensive technical report and describes achievement of the technical deliverable, carbon nanotube wire with $10^{-5} \Omega \cdot \text{cm}$ resistivity. In order to protect intellectual property being created at this time, the discussion shall be limited to published or patented topics [2-6].

2. REPORT DETAILS

This section documents and summarizes all worked performed during Phase I. The ultra-high conductivity umbilical project is a three-year, \$3.2 million stage-gated effort with three deliverables and one key milestone. At successful program completion, the following shall be realized:

- The carbon nanotube-based conductor has $10^{-6} \Omega \cdot \text{cm}$ resistivity.
- The polymer nanotube umbilical (PNU[®]) cable is capable of operating at 5500 psig pressure.
- Formation of a prototype umbilical that uses the PNU[®] cable for power transmission shall be completed. This is the milestone and shall be used for a demonstration program.

To satisfy the program objectives and initiate the demonstration program, the plan is divided broadly into 1) Research and 2) Technical Development. The research effort, **Task 5.0**, is focused on the formation and optimization of the carbon nanotube-based, polymer jacketed conductor; i.e., the PNU[®] cable. The remaining tasks, **Tasks 1.0 to 4.0**, although not technical in nature, are critical to the success of the project. The remainder of this document shall focus on Year 1. **Figure 1** is a tree structure view of the Year 1 tasks and contains the work described in this document. The following list shows the tasks, technical lead and principal investigator responsible for directing the work:

- Task 3.0 – Technology Transfer, NanoRidge Materials, Christopher Dyke. This work is described in **Section 2.2.2**.
- Subtask 5.1.1 – Carbon Nanotube (CNT) Growth, NanoRidge Materials, Christopher Dyke. This effort was supported by Rice University but headed by NanoRidge.
- Subtask 5.1.2 – CNT Junctions, Rice University, Enrique Barrera.
- Subtask 5.1.3 – CNT Doping, Rice University, Enrique Barrera.

- Subtask 5.1.4 – Reports, NanoRidge Materials, Christopher Dyke. This document, once finalized, constitutes the product of work package 5.1.4.1.

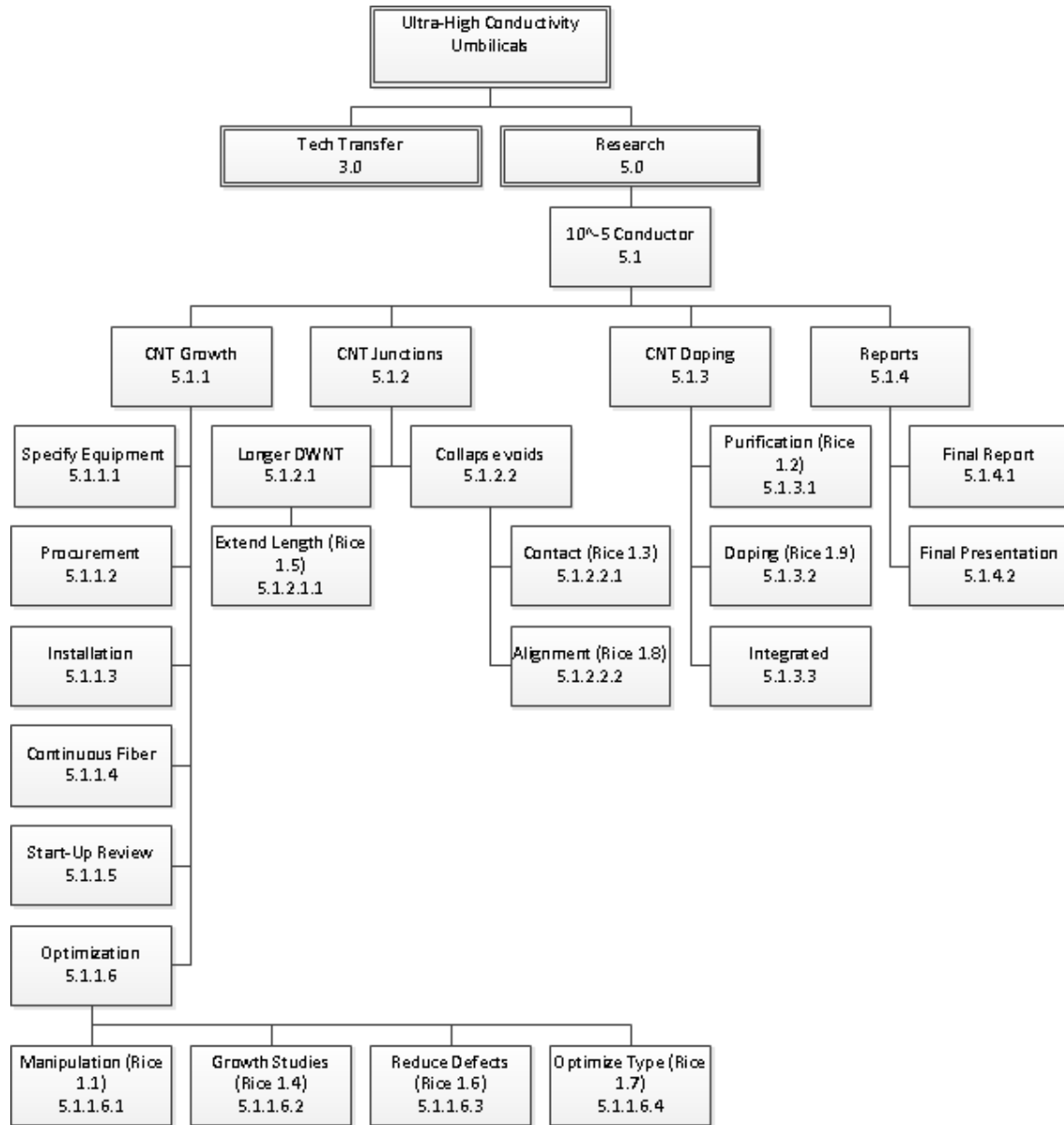


Figure 1. Tree structure view of the Phase I tasks and subtasks.

2.1 EXPERIMENTAL METHODS

This section is divided into the following tasks, subtasks:

- 2.1.1. Subtask 5.1.1.1 – Specify Equipment
- 2.1.2. Subtask 5.1.1.2 – Procurement
- 2.1.3. Subtask 5.1.1.3 – Installation
- 2.1.4. Subtask 5.1.1.4 – Continuous Fiber

- 2.1.5. Subtask 5.1.1.5 – Start-Up Review
- 2.1.6. Subtask 5.1.1.6 – Optimization
- 2.1.7. Rice 1.1 – Nanotube Manipulation
- 2.1.8. Rice 1.2 – Nanotube Purification
- 2.1.9. Rice 1.3 – Manipulation and Connections
- 2.1.10. Rice 1.4 – Nanotube Growth Studies
- 2.1.11. Rice 1.5 – Extended Lengths of Nanotubes
- 2.1.12. Rice 1.6 – Reduce Defects of the Conductor
- 2.1.13. Rice 1.7 – Optimize Nanotube Growth by Type
- 2.1.14. Rice 1.8 – Optimize Alignment for Conductivity and Strength
- 2.1.15. Rice 1.9 – Doping and Conditioning

Each task is discussed separately below. Described are the methods, materials, and equipment used to complete the tasks.

2.1.1 SUBTASK 5.1.1.1 – SPECIFY EQUIPMENT

The primary equipment used in Year 1 was a furnace and take-up spool. During the course of technical due diligence and completion of Task 2.0 – Technology Status Assessment, several features were specified for the furnace. The furnace must a) be operated in the vertical and horizontal positions, b) be specified for hydrogen use, c) have a maximum operating temperature of 1200 °C, d) be sized to accommodate an 80 mm diameter quartz tube, and e) have a 36-inch heated zone. This is considered a lab scale furnace. Larger furnaces are specialty items with long lead times. We opted for a split combustion tube furnace from CM Furnaces, Inc. in Bloomfield, New Jersey. The model number is 1000K-0412-36-3Z-HTFS-240V-1PH. **Figure 2** is the engineering schematic of the furnace in the vertical configuration. Specification of the furnace was completed within the 15-day allotment. The take-up spool we selected, a modular take-up system MTS-120912, was from Showmark, LLC.

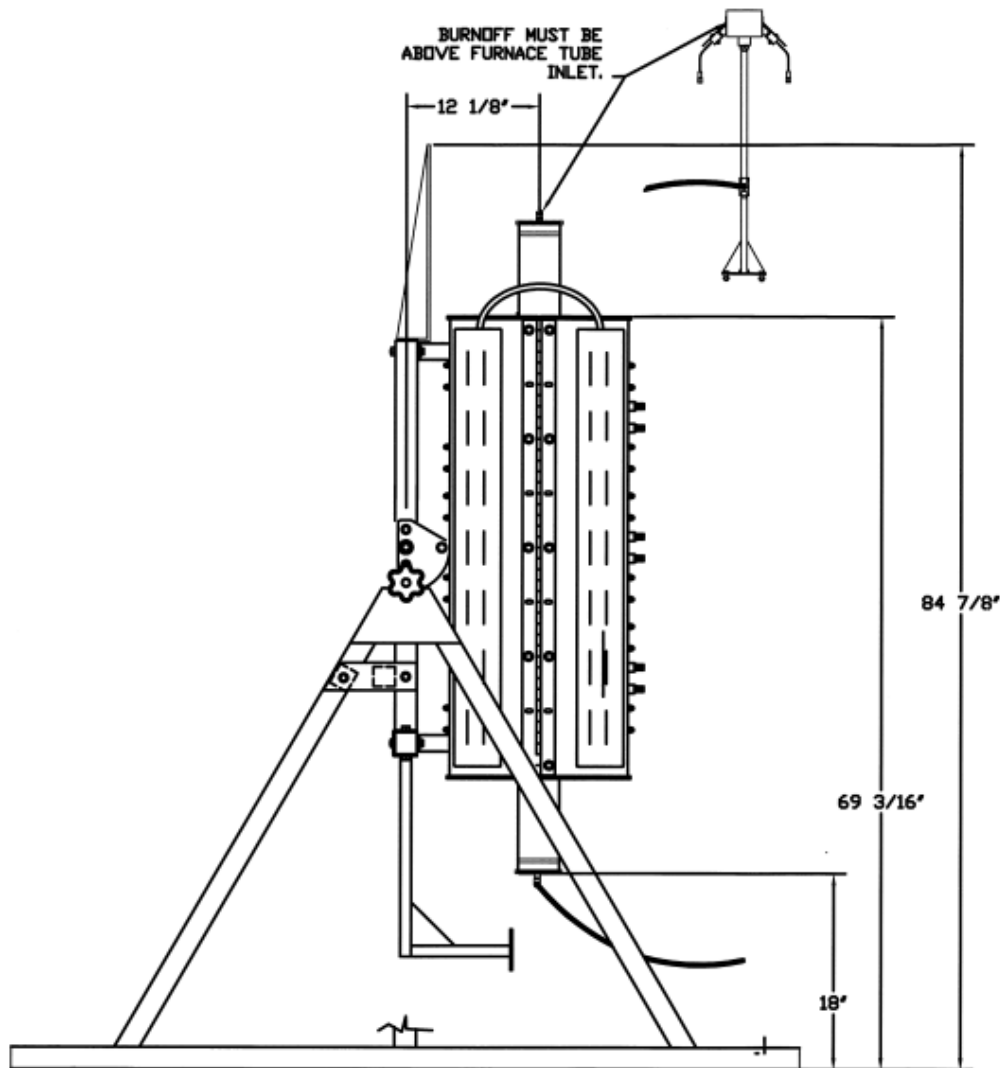


Figure 2. Engineering schematic of CM Furnace 1000K-0412-36-3Z-HTFS-240V-1PH.

2.1.2 SUBTASK 5.1.1.2 – PROCUREMENT

Once specified, procurement of the furnace was initiated. A 60-day lead time was anticipated. Changes were made to the furnace and Hurricane Sandy delayed procurement considerably. The furnace was actually received on December 03, 2012. This corresponds to a 125-day lead time, based on a 5-day work week. The take-up spool equipment was received on January, 23 2013.

2.1.3 SUBTASK 5.1.1.3 – INSTALLATION

Once the furnace was received installation was completed after five days, although initially scheduled for 15 days.

2.1.4 SUBTASK 5.1.1.4 – CONTINUOUS FIBER

This subtask was designed to attach the take-up spool to the end of the furnace for a brief time to observe the process and specify modifications. Initially the furnace was operated in the horizontal, and the take-up spool was positioned on the end (**Figure 3**). Attempts to string the take-up spool by hand were not successful. In addition, as the nanotubes continued to grow, the exit ports were blocked. This led to variability of the flow profile in the growth zone and inconsistencies in the product.

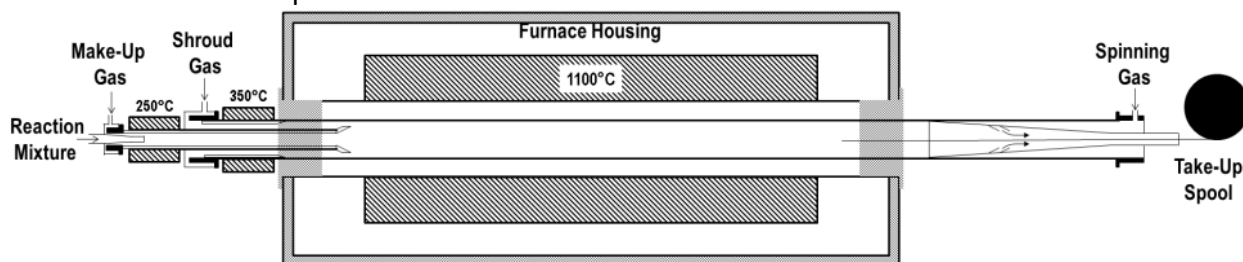


Figure 3. Schematic of furnace in the horizontal.

To make the process continuous in the least amount of time, a spindle approach was adopted. This approach is detailed in another publication [7]. In brief, a shaft was extended into the growth zone at an angle of 15° and rotated at approximately 90 RPM. As the carbon nanotubes grew and migrated through the growth zone with the carrier gas, they came in contact with the spindle. The CNT adhered to the spindle and thus were removed from the growth zone in a continuous manner. This protocol gave a consistent product throughout the entirety of a run. Modifications were made to the feedstock, flow rates, and preheater, furnace temperatures. The material collected from the spindle was twisted into a wire and provided to Rice for further characterization (vide infra).

2.1.5 SUBTASK 5.1.1.5 – START-UP REVIEW

The Start-Up Review was conducted after the Steering Committee Meeting held on April 16, 2013. Christopher Dyke, Enrique Barrera, and Professor Alan Windle attended this review. Prof. Windle discussed his current approach to continuous wire formation. This was adopted by the NanoRidge team and is currently the technical focus.

2.1.6 SUBTASK 5.1.1.6 – OPTIMIZATION

Several optimization studies were performed during Year 1. They include:

- Feedstock composition
- Feedstock weight ratio
- Carrier gas flow rate
- Shroud gas flow rate
- Carrier to shroud gas ratio
- Spinning strategy
- Reduction in pressure at exit port
- Flow profile in the growth region
- Temperature
- Temperature profile

The product formed is consistent, clean, and has small diameter nanotubes. The decided feedstock mixture gives a spinnable system. Currently the focus is continuous wire forming processes in the vertical configuration.

2.1.7 RICE 1.1 – NANOTUBE MANIPULATION

One of the primary research objects is the manipulation of the smallest units of the electrical conductor (PNU[®]), the carbon nanotubes. Carbon nanotubes are considered nanometer scale carbon fibers. In order to use them in an electrical conductor, they have to be prepared and assembled into a multi-fiber wire. This gives the conductor. These small diameter wires can be twisted or braided into a larger wire or cable. Nanotube manipulation has a considerable impact on the conductivity of the wire. In fact, most of the tasks in this project can be considered nanotube manipulation activities. Carbon nanotubes exist in a variety of forms (**Figure 4**) including single-walled carbon nanotubes (SWNT), double-walled carbon nanotubes, and multiwalled carbon nanotubes (MWNT). **Figure 5** shows SWNT can be conducting or semiconducting depending on the arrangement of the carbon hexagons on the nanotube. The most conducting carbon nanotubes are metallic SWNT but they are not easily separated from semiconducting SWNT or other CNT. Also, SWNT have only been grown in very short lengths. Therefore, this project has focused more on DWNT since they can be grown in high concentrations and at longer lengths [8].

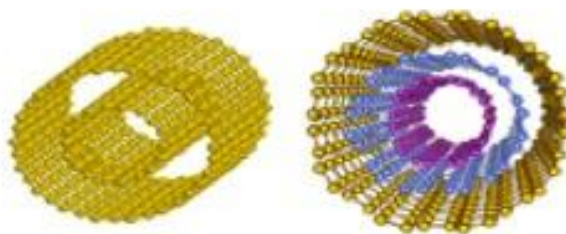


Figure 4. A DWNT and an MWNT [9].

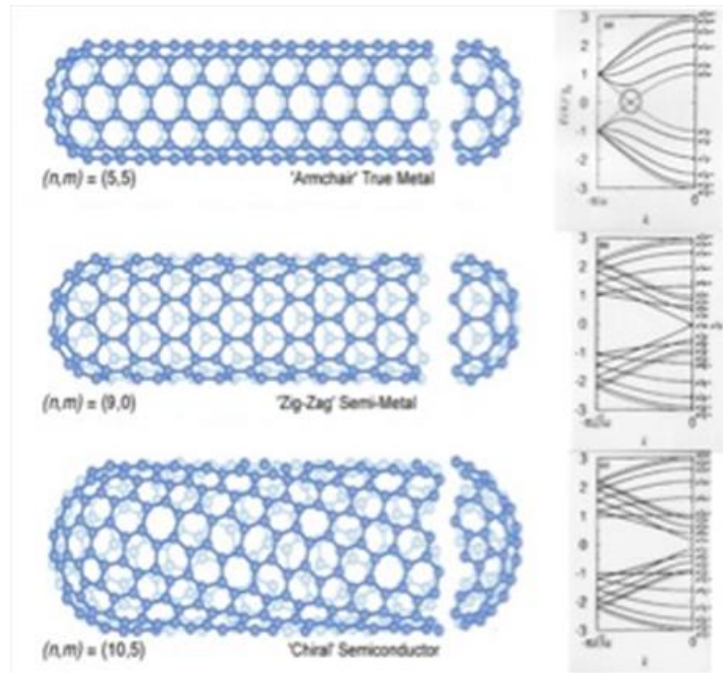


Figure 5. SWNT of distinct chiralities with band structure for each. Metallic SWNT have no band gap.

For **Rice 1.1**, manipulation is centered on altering the nanotubes to enable other manipulation. For example, two approaches to adjusting the nanotube conditions were used that included a) heat treating the nanotubes and b) wetting the nanotubes. Heat treatment is a type of purification but is not the traditional chemical purification described later. The second treatment, an ethanol wash, makes the nanotubes more hydrophilic. While this is not a purification step, it does improve purification by shortening the purification time. An acid doping can also be used but is an alteration of purification. While acid treatment does not change the conductivity very much, it does lead to improved iodine doping; i.e., a bigger change in the resistivity occurs when the nanotubes are acid treated first [6].

A larger component of nanotube manipulation is the CNT/polymer interaction. For this aspect, a study is being conducted on the interaction of nanotubes, particularly in wire form, with polymers. This shall allow us to better understand their stability and observe changes as they interact. In this case, several approaches are being used to study the interface between nanotubes and polymers. They include:

- Forming a nanotube rich membrane then placing droplets of polymer on the surface.
- Applying polymer to preformed CNT wires under several conditions
- Dispersing nanotubes in polymer to look at local interactions on an almost individual basis.

Each of these approaches provides important insight to better understand the nanotube/polymer interactions. Results of this study shall lead to a patent disclosure on the

topic of nanotube wire packaging and insulation (to be discussed in **Section 2. Results and Discussion**).

2.1.8 RICE 1.2 – NANOTUBE PURIFICATION

In this task several approaches have been used to “clean” the carbon nanotubes. These methods are usually chemical treatments and are intended to remove amorphous carbon and metal catalysts (typical impurities caused by the nanotube growth process) [5]. Current production methods do not produce nanotubes of high purity. For an electrical conductor, impurities reduce the effective conductivity as impurities disrupt the alignment and connections between discontinuous nanotubes or atoms in the case of copper wire. The impurities can also lead to defect formation and nanotube entanglement. Both reduce the conductivity of nanotube wires. Therefore, removal of impurities leads to a higher level of conductivity [5, 6]. Currently, most methods of purification still clean nanotubes to 99.6 percent pure at best. Higher levels of purity require more extensive purification and increase process cost. In this work, a goal of 96 percent purity has been set for Phase I. Purification improves conductivity provided the process does not damage the nanotubes.

In Phase I three basic paths were used to purify wires. They are:

- Purification, Wire forming, Wire treatment, Conditioning
- Wire forming, Purification, Wire treatment, Conditioning
- Wire growth, Purification, Wire treatment, Wire conditioning

These routes have led to repeated outcomes of resistivity in the 10^{-5} $\Omega\cdot\text{cm}$ range, the deliverable for Phase I.

2.1.9 RICE 1.3 – MANIPULATION AND CONNECTIONS

This form of nanotube manipulation involves the optimization of nanotube connects and junctions. When connectors, such as nanotubes, get joined, the connections can lead to electrical losses if the connection is not done in such a way as to reduce contact resistance. Therefore, nanotube length, type, and alignment all influence contact resistance and are therefore, their own tasks for this project. There are a number of ways to reduce contact resistance; the published routes include:

- Using metal contacts between the nanotubes [11],
- Producing end functionalized nanotubes to join together [11],
- Adjusting the overlap of nanotubes with each other [1], and
- Doping the nanotubes in various ways [1].

Therefore, this task is a long term manipulation of the nanotubes to achieve higher conductivity and several new methods are being studied that are priority.

2.1.10 RICE 1.4 – NANOTUBE GROWTH STUDIES

While NanoRidge takes the lead on nanotube growth for this project, Rice studies growth as well because there are a number of aspects about growth that lead to improved conductivity.

The role of Rice is to study growth a) to reduce the cost of nanotube production, b) to increase the rate of nanotube formation, and c) to optimize a range of properties that enhance conductivity (nanotube length, single type growth, and alignment). Rice's role for this task is particularly on studying the defects that result from growth and how to reduce and eliminate them. Rice also looks for ways to lower temperature, reduce powder requirements, and broaden the process window for ease of production.

2.1.11 RICE 1.5 – EXTENDED LENGTHS OF NANOTUBES

As the carbon nanotube length is extended, wire conductivity improves [3, 6]. Therefore, growth with an emphasis on extending the lengths of the nanotubes is an important focus area. While this is known about growth, extending the lengths is not an easy task. The Armchair Quantum Wire project is a project to produce continuous SWNT, but they are typically some of the shortest nanotubes produced [12]. Research has shown that MWNT can be grown to longer lengths, but greater length increases are still sought. What is important to understand is that as they get longer, their ability to assemble gets more difficult for some assembly methods. So for a given conductor this becomes an optimization process; i.e., how long should they be versus ease of assembly.

2.1.12 RICE 1.6 – REDUCE DEFECTS OF THE CONDUCTOR

While there are defects produced by nanotube production and growth, there are a host of other defects that can influence conductivity. Therefore, manipulation via defect reduction and elimination is a separate task. The PIs in this project have been studying nanotubes for many years and have seen all types of nanotube, nanotube wire, and assembled nanotube defects. As growth and processing is altered, new types of defects emerge. The goal is to track the defect to its source so it can be eliminated. Rice has a patent for the elimination of nanotube defects [14], and, therefore, not only has a unique understanding of defects but has determined ways to manage defects to advance properties.

2.1.13 RICE 1.7 – OPTIMIZE NANOTUBE GROWTH BY TYPE

Growth by type can lead to improved wire conductivity [1, 5, 6, 8, 11]. Expectations are that SWNT to SWNT junctions would give the lowest contact resistance [1]. Indications are that DWNT to DWNT junctions can give an equally low contact resistance condition. Growth of primarily DWNT (the specific nanotube type) is sought in this project, and this property has already been demonstrated by researchers in this project [3, 5]. Typical nanotube growth leads production of different nanotube types, including a range of chiralities. Nanotubes of same type and chirality lead to better nanotube/nanotube junctions and lower contact resistance.

2.1.14 RICE 1.8 – OPTIMIZE ALIGNMENT FOR CONDUCTIVITY AND STRENGTH

Nanotube alignment tends to lower contact resistance, increase wire density, and reduce defect population. This leads to enhanced conductivity and strength. Several approaches are being used to study alignment. These approaches start with growth and continue through wire formation and conditioning.

2.1.15 RICE 1.9 – DOPING AND CONDITIONING

Nanotubes are a unique carbon-based conductor. The mechanism for electron transport is different as compared to copper (Cu) and aluminum (Al). For nanotubes two mechanisms are emphasized and include a) ballistic transport and b) resonant quantum tunneling [14, 15]. Ballistic transport is the migration of an electron along the nanotube surface. They are practically uninhibited in their motion as nanotubes have minimal defects. Resonant quantum tunneling, also referred to as “hopping”, is the migration of electrons from one tube to another. The nanotube to nanotube distance or d-spacing determines ease of electron transport. For instance, nanotubes spaced 1.8 nm apart do not form a conduction pathway.

The conduction of carbon nanotubes can be an order of magnitude higher than Cu. Additionally and as the transport mechanism is different, conduction can be further improved by employing other approaches.

In our previous work, doping was used to enhance the number of charge carriers, and in turn, enhance the conductivity of carbon nanotubes [3-5]. Doping is performed to increase the number of charge carriers in a wire by the intercalation of atoms, iodine (I) or antimony (Sb). These elements collect on the surfaces of the nanotubes and provide additional charge carriers to the wire system. Doping similar to that for semiconductors can also be used in which direct carbon replacement with atoms like boron adds holes or electrons within the nanotube structure [16]. Other methods to introduce better charge-carrying capabilities to the nanotubes also exist [17].

Wires can still undergo additional steps to advance the electrical properties. These steps are generally termed conditioning. In this task, a range of methods can be used or introduced in the production process in order to eliminate batch type processing steps. Conditioning can include a) heating in electric fields, b) drawing, c) twisting, and d) braiding. Many of these strategies shall be explored during continuous wire formation.

Each of these tasks has been the subject of the Phase I study. Their better understanding has been made apparent by materials characterization in conjunction with the various methods. They have been used to improve properties. The results in later sections shall demonstrate these tasks yield advanced electrical properties.

2.2 RESULTS AND DISCUSSIONS

A variety of characterization methods were used to assess the wire product and the efficacy of processing conditions. Much time during Phase I was devoted to training members of the Rice team on these characterization techniques and analysis instrumentation. **Table 1** shows a list of project participants and the methods they were trained on to assist in this study. A number of these students were Rice undergraduates and they were only with the project for a short time.

Table 1. List of project participants and their characterization method training.

Participant	Time on Project	SEM	TEM	Raman	TGA	EDX	CVD
Eric Lange	One year	√		√	√		√

Adrian Yao	4.5 months	✓		✓	✓		✓
Chenpeng Huang	2 months	✓					✓
Nick Semon	4.5 months	✓		✓		✓	
Chris Hurd	1 month						✓
David Chan	1 month	✓			✓	✓	
Luke Boyer	1 year	✓			✓		✓
Travis Boyer	2 months	✓		✓	✓	✓	
Santoshkumar Biradar	1 month	✓		✓	✓	✓	
Liehui Ge	1 year	✓	✓	✓		✓	✓

Having several individuals trained to perform the different characterization methods enabled the team to reach the project goals. All of the members in the table went through safety training. In June, an Environmental Health & Safety (EH&S) meeting was held where the following members attended: Nick Semon, David Chan, Luke Boyer, Travis Boyer, Santoshkumar Biradar, and Liehui Ge. This was a very thorough safety presentation on how to work in the laboratory and handle chemicals and nanotubes. These members make up the current Rice Team. Spot inspections were also held for the laboratories used in this project.

Characterization methods used in this study are listed in **Table 1**. Descriptions of these methods are in the following sections.

2.2.1 ELECTRICAL PROPERTY MEASUREMENTS

Resistivity of the sample wires was computed using the formula below, where the length L , diameter D , and resistance R of the wires is measured.

$$\rho = R\pi D^2/4L,$$

The calculation is based on the assumption that wires are in a cylindrical shape. In fact, the cross-section of some wires is not an ideal circle but irregular. In the calculation, we used long axis length as the diameter. By this approximation, the real resistivity of the cable is lower than the calculated value. Diameter, D , was an average value based on the measurements at three different locations along the cable's long axis direction. The resistance was measured by a new Keithley 2400 in a four-probe configuration and measured a second time by an additional new Keithley 2400 four-probe configuration to verify results.

When the resistance is measured with a simple ohmmeter as shown in **Figure 6**, the resistance of its wires leading to the sample and the resistance of the contacts is measured as well as the resistance of the sample wire itself. Understanding this, simple two-point resistance measurements were unreliable.

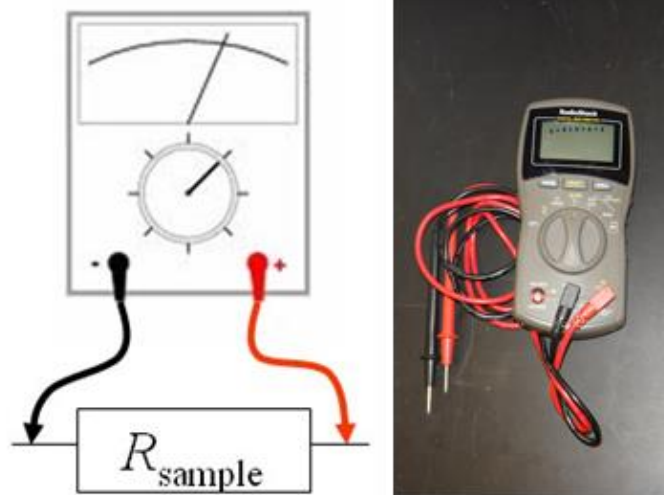


Figure 6. Two-point measurement setup.

The contact resistances can be a serious problem when electrical contact is made using the micromanipulators as the contact area with the wire is very small.

In order to overcome the problem of the contact resistances, we transitioned to a four-probe configuration. A current is passed through the two outer contacts while the voltage is measured between the two inner contacts. The equivalent circuit for a four-point measurement is shown in **Figure 7**.

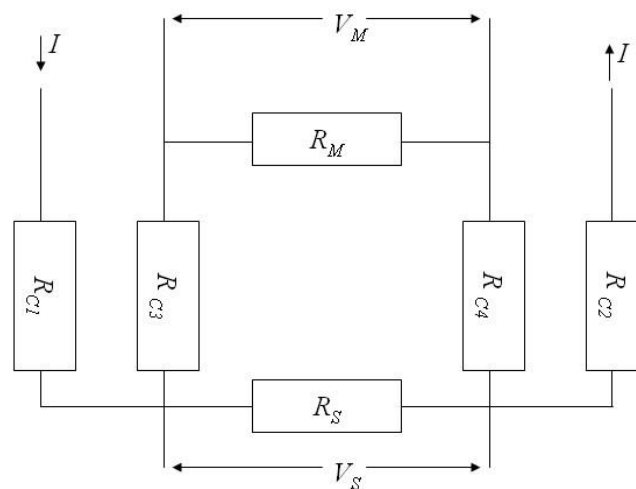


Figure 7. Four probe configuration.

Current flows into the sample at contact 1 and comes out of the sample at contact 2. Here R_{C_i} is the cable resistance and contact resistance of contact i . The contact resistance usually dominates over the cable resistance. R_S is the sample resistance, and R_M is the equivalent resistance of the voltmeter. The term V_S is the voltage across the sample, and V_M is the voltage measured by the voltmeter.

In the initial stages, concentration was focused on characterization and analysis of given raw material batches. In order to determine initial properties and resistivity, a four-point set up was created using gold-plated film as shown in **Figure 8**. This allowed for a conservation of material with a standardized, accurate resistance measurement.



Figure 8. Gold-plated four-point setup.

With the increase of production and wire length, other techniques of resistance measurement needed to be explored. A setup utilizing Cu tape on glass slides in a four-point set up was devised in order to more accurately allow measurements with a diversity of changing of wire length and diameter. To secure the wire to the Cu tape, a fast drying silver paint was used (**Figure 9**).



Figure 9. Wire secured by silver paint.

While this setup provided true measurement results, the setup proved to be somewhat destructive to the sample. A silver paint diluent (isobutyl methyl ketone) could remove the sample after measurements; however, to avoid creating any trace amounts of silver contaminating the authenticity of our readings, the idea was discarded to keep accuracy. The alternative method of clipping the wire from the nearest points of contact shortened the wire and proved to be destructive, especially when further purification techniques needed to be applied and re-measurement of resistance was necessary.

To overcome this complication, a non-destructive method was constructed using only the Cu tape, points of contact, and an additional layer acting as a non-conductive lid over the sample as shown in **Figure 10**. This method allowed for accuracy without unnecessary alteration of the

sample. Additionally, it shall allow for the testing of resistance under variation of pressure in stage 2.

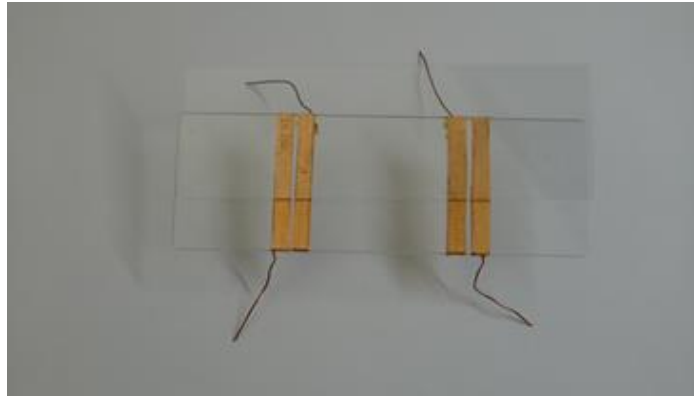


Figure 10. Basic Cu resistance measurement setup.

In-situ resistance measurements

In Phase II, electronic conditioning of the wires shall be explored, and its effects shall be captured with only a slight alteration from the current basic setup. Using the Keithley 2400, a program shall be written in LabVIEW that shall both control the variation of the conditioning and the means by which it is recorded.

Experiments have shown a positive correlation with iodine doping and resistance measurements for the wire samples. To better understand the effects of the doping and optimize the time/molarity needed to optimize resistance results, a system was formulated to measure the doping effects in-situ.

The setup (**Figure 11**) was erected using a system of Cu wires contained within two long, thin glass tubes. The individual wires had to maintain separation and insulation as to not short circuit the system and corrupt the measurements. As a steady vacuum as applied to the apparatus, a constant temperature of 70 °C was maintained to transform the iodine into a gas stage and dope the samples.

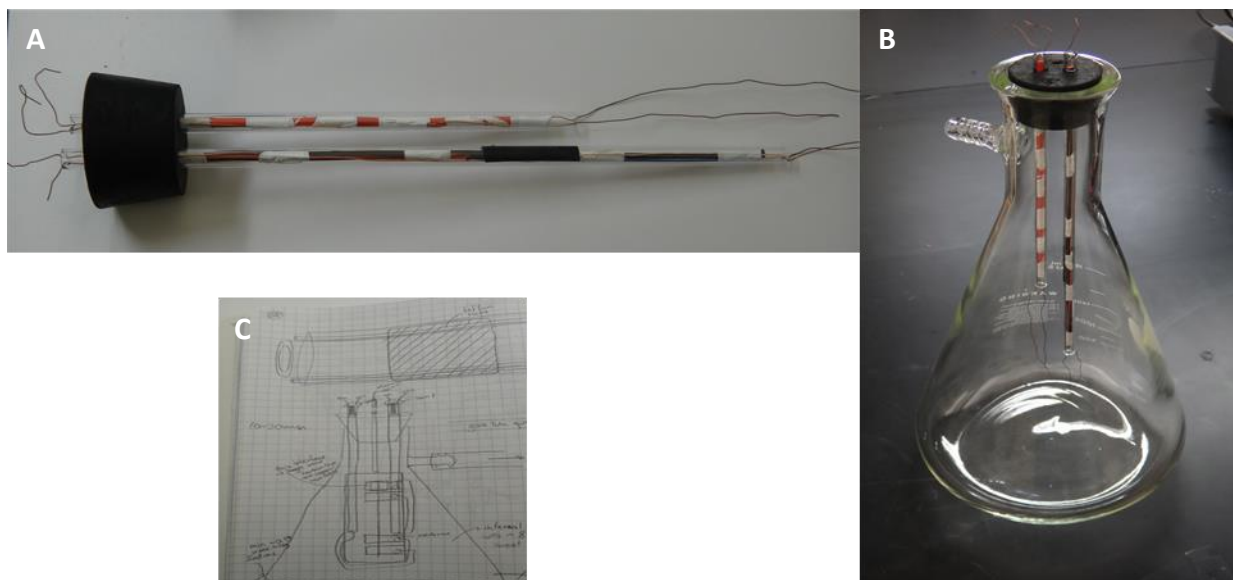


Figure 11. In-situ resistance measurement setup. A. Wire setup constructed to obtain resistance reading from attached sample. B. Empty chamber ready for wire sample, vacuum, and iodine crystals. C. Sketch of iodine doping measurement system.

At higher doping temperatures of 200 °C and longer periods of time; however, copper wire reacts with iodine and forms a coating as shown in **Figure 12**. The device was instead outfitted with platinum wire to maintain correct readings without contamination to the sample. Gold wire was considered and tested; however, while the gold wire worked better than copper, initial trial showed gold particles attaching to the sample. It was shown that platinum, rather than gold, wire would prevent any misgivings from showing in post-doping characterization.

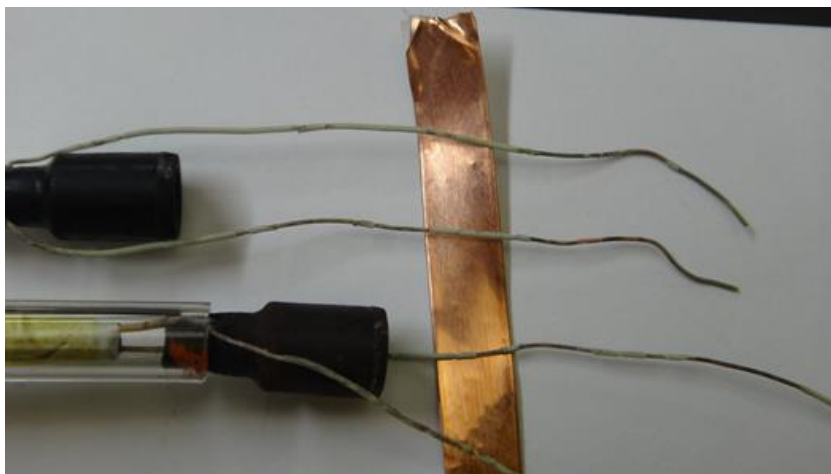


Figure 12. Cu wires with surface contamination (green) from iodine doping.

2.2.2 MATERIAL CHARACTERIZATION METHODS

Raman spectroscopy

Raman Spectroscopy is a non-destructive characterization testing method that observes vibrational, rotational, and other low-frequency modes in a system. For our analysis, we used laser wavelengths of 514 nm and 633 nm. As the laser is pointed at the sample, it has a backscattering effect causing energy of the laser photons being shifted up or down. **Figure 13** is an example of Raman spectrum for carbon nanotube.

The resulting shifts appear in the form of bands that give the wire characteristics. The G-band is a characteristic feature of the carbon nanotubes and corresponds to the lateral vibration of the carbon atoms. The D-band intensity is characteristic of defective, broken, or short nanotubes and loose carbon atoms. Looking at the ratio of these two peaks allows us to determine the quality of the wires in terms of tubes.

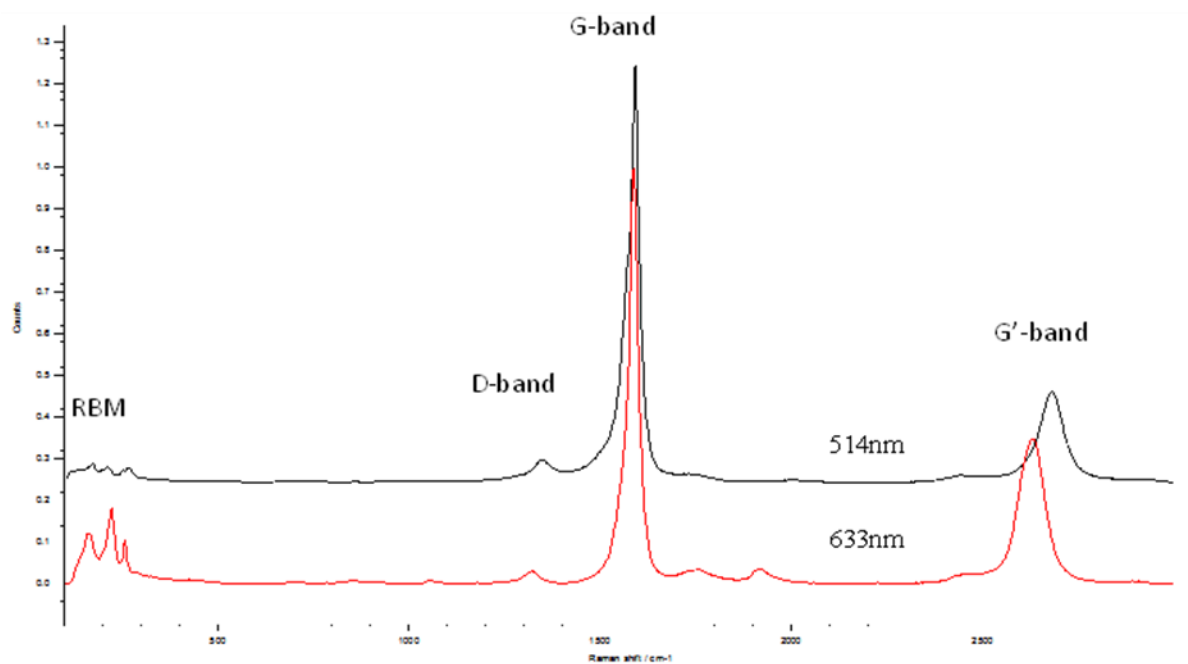


Figure 13. A typical Raman spectrum of carbon nanotube.

A third area, called the radial breathing mode (RBM), lies in the Raman shift of 0 to 500 cm^{-1} (shown above). This area is very sensitive to the diameter of SWNT and DWNT. The interlayer interaction between the inner and outer (or multiple layers) of nanotubes and enables us to distinguish between SWNT, DWNT, and MWNT. The band of higher Raman shift corresponds to the inner diameters and the ones with less Raman shift to outer diameters. Two distinct peaks would indicate the presence of primarily pure DWNT that have consistent diameters.

Impurities can also be identified through the Raman process. Additional peaks and fluorescence appearing on scans can indicate the presence of foreign substances. As seen in **Figure 14** on left is pure ferric oxide (Fe_2O_3) with a fluorescence hump. On the right is a NanoRidge Sample displaying potential fluorescence due to Fe_2O_3 impurity. Iron oxide presence can create a fluorescence hump, signifying a presence of the material on the wire sample and helping us to determine the needed steps for batch purification.

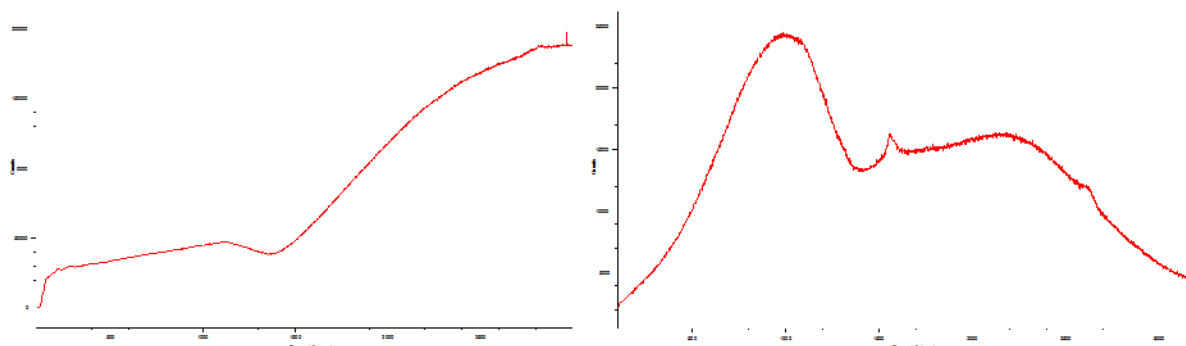


Figure 14. Fluorescence from impurity.

SEM

A second nondestructive analysis technique applied is Scanning Electron Microscope (SEM). SEM is a microscope that uses electrons instead of light to form an image. A beam of electrons is produced at the top of the microscope by an electron gun. The beam travels through electromagnetic lenses, which focus the beam down toward the sample. Once the beam hits the sample, electrons and X-rays are ejected from the sample. Detectors collect these X-rays, backscattered electrons, and secondary electrons and convert them into a signal that is sent to a computer. This produces the final image and spectrum.

Due to the nano-scale of material properties that we are investigating, a traditional light microscope was insufficient. Because the SEM uses electromagnets rather than lenses, we had much greater control in the degree of magnification as well as a much higher resolution, so impurities, tube spacing, and densification can be examined at much higher levels.

The SEM allowed us to do visual investigations of the wire samples, from a macroscopic view of 40 to 100,000 times magnification. **Figure 15** is an example of SEM image of carbon nanotubes. Performing this examination intermediately between each step of purification and doping procedure we were able to identify the reactions/interactions that took place. We were then able to focus on both the positive and the negative aspects of each step and adjust accordingly.

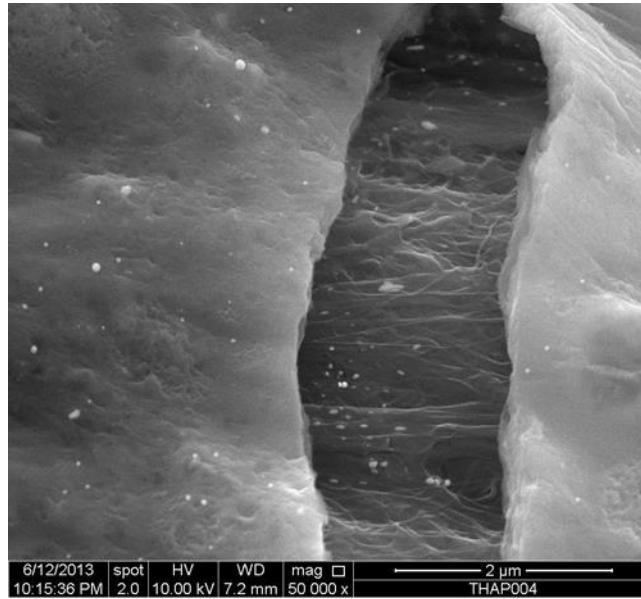


Figure 15. SEM sample of THAP002 at 50,000x magnification. Interior reveals dense tubes in alignment with an outer oxidation shell covering the bare wire.

EDX

A third nondestructive analysis technique utilized is the EDX (Energy Dispersive X-Ray), analytical device attached to the SEM used for elemental or chemical characterization of a wire sample. To identify the elemental composition of materials, the EDX creates data consisting of spectra showing peaks corresponding to the elements that make up the composition of the sample surface. These spectra are created from the interaction of X-ray excitation on the sample with each element having a unique set of peaks on its X-ray spectrum. **Figure 16** is an example of EDX data.

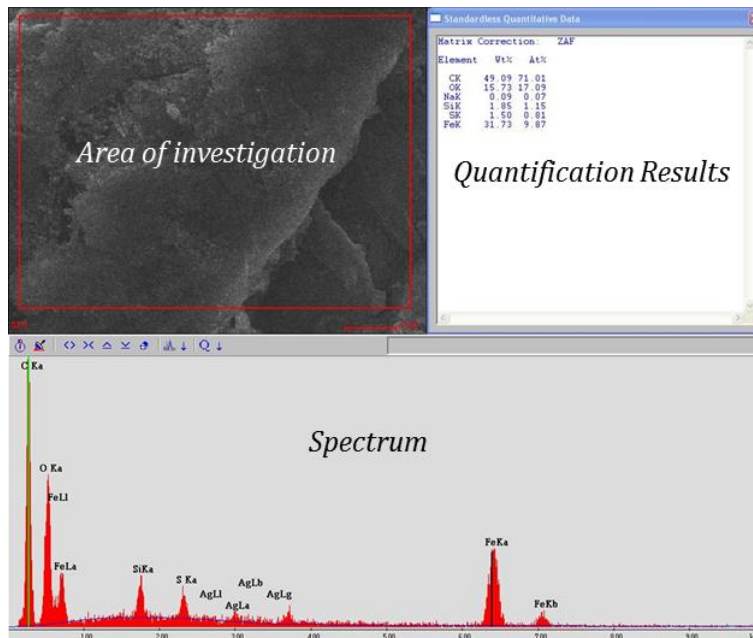


Figure 16. Example of EDX spectrum.

The EDX allows us to not only examine the surface makeup, but to map out selected areas of the sample as well. In order to better determine and identify defect catalysts, points of interests are identified and their origin is diagnosed. Through studying the collection of impurities and imperfections we are better able to understand and alter the manufacturing and purification methods needed to achieve more enhanced result.

TGA

The Rice Thermogravimetric Analysis with Infrared Spectroscopy (TGA/DSC) measures the amount and rate of change in the weight of a material as a function of temperature or time in a controlled atmosphere. We use the measurements to determine the composition of the batch samples for the wires and predict their thermal stability. It allows us to characterize the raw material that exhibits weight loss or gain due to decomposition, oxidation, or dehydration.

To date, TGA analysis has been limited to larger batch samples, but it is currently underway for the second stage of the project as larger amounts of material are manufactured and available for characterization. This is due to the nature of the TGA (**Figure 17**) to be a destructive analysis method and stage 1 required a conservation of samples. During the upcoming stage, deeper characterization using TGA shall be conducted with findings helping us to better understand a variety of material traits:

- Thermal stability of the wire
- Oxidative stability of the wire material
- Decomposition period of the wire material
- Kinetics of the wire material
- Reactions of the wire in various atmospheric (corrosive or non-corrosive) environments

- Moisture content of the wire material

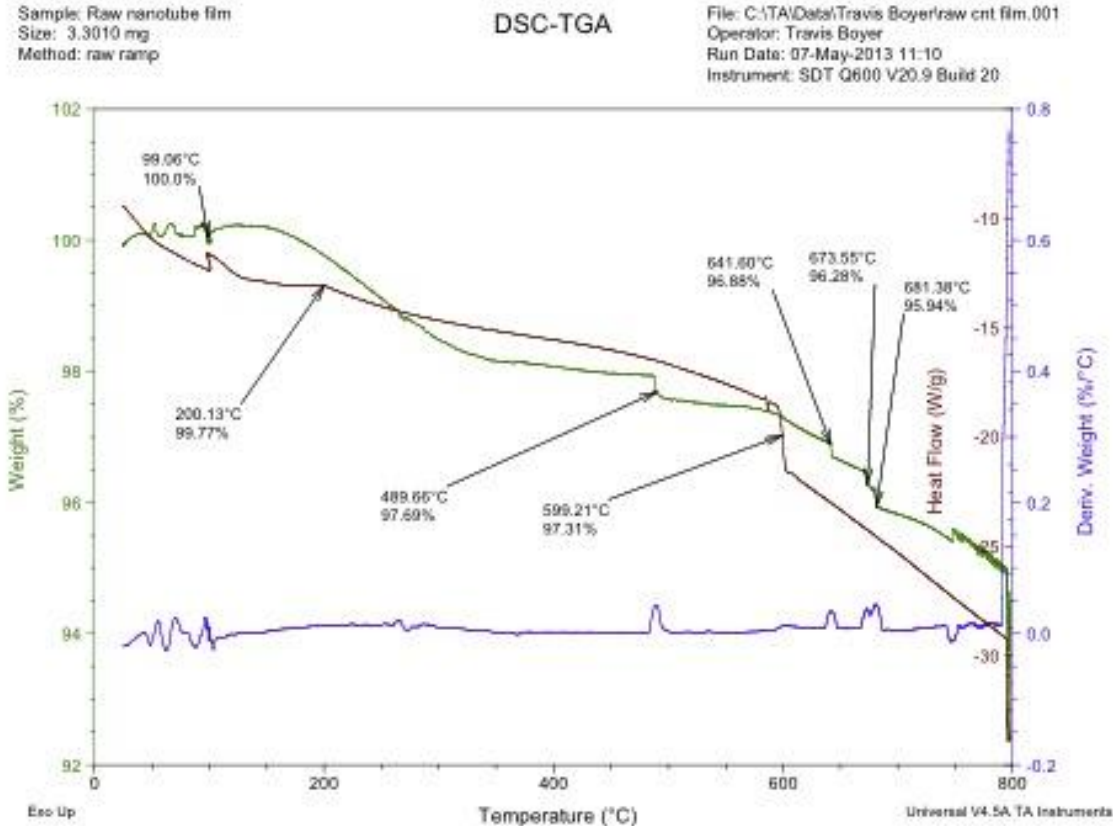


Figure 17. TGA of THB sample shown above. Different drops correspond to the release of water, amorphous carbon, and other impurities.

Processing Protocol

To accomplish the goals of Phase I the Rice Team followed a protocol identified by the co-Principal Investigator (co-PI): Barrera to achieve a uniform sample preparation procedure to use not only in Phase I but in subsequent Phases of this project. The items listed below identify the starting procedure for year one work:

- (1) Where the nanotubes have been purified to an acceptable level (meeting some defined approval condition).
- (2) Where the TGA shows the nanotubes to be clean (less than 4 percent impurities).
- (3) Where SEM does not show the presence of sizable impurities or dispersed particles.
- (4) Where the nanotubes have been characterized by Raman to show the presence of DWNT (although not 100 percent unless that is possible).
- (5) Where the nanotubes are processed into a wire with a reasonable large diameter and at least 3 inches (7.62 cm) long after all the characterizations; that means we may need to start with a length of 4 inches (10.16 cm).

- (6) Where the wire diameter is consistent along its length to be uniform within an acceptable standard deviation.
- (7) Where the diameter is accurately measured by both SEM and optically if possible.
- (8) Where we have a very good set of SEM micrographs of the wire at high and low magnifications.
- (9) Where the resistivity is measured several times using both four-point and two-point probe contact approaches.
- (10) Where the sample is doped using previous used approaches so that the resistivity is measured in real time (iodine doping).
- (11) Where again the diameters are measured by SEM and optically if possible.
- (12) Where SEMs of the wire are taken at both high and low magnifications.
- (13) Where resistivity measurements are taken by both four-point and two-point probe contact measurements.

2.2.3 CARBON NANOTUBE WIRES

With consideration to the various steps above, the Rice Team set out to manipulate nanotubes into wires and to better understand the steps to advance the conductivity of nanotube conductors. **Table 2 and Table 3** show a number of selected wires to demonstrate the steps taken in manipulating the nanotubes and wires to achieve improved electrical conductivity.

The manually fabricated wires (those made at Rice) were of non-uniform cross-section along the length. This is a product of the processing and would be eliminated with continuous growth. Therefore, the diameter was measured at different cross-sections along the wire length and minimum diameter, maximum diameter, average diameter, and the standard deviation for wires were identified and reported in **Table 4**. In this report the resistivity for the minimum diameters and average diameter conditions are reported as seen in **Table 2**. In engineering situations, the worse case scenario is often the value of interest and shall be the subject of future phases of this project. In Phase I, where research is being conducted to advance the electrical properties, the efforts focus on the properties that occur at the smallest diameters because they are more optimized, and on the average diameter because this speaks to the average properties of the wires. In a continuous processing mode, the minimum and maximum diameters approach the average diameter, and the standard deviation is reduced with continued processing. Therefore the average diameter yields the expected properties of the wire over time.

While the diameters vary because of the manual fabrication method, it should also be considered that the wire density and defect nature can also vary along the length of the wire. This means that the resistance likely changes with the length. The Rice Team understands this and shall focus on measuring the density of the wires along the length as the processing becomes more continuous.

Table 2. Resistivity of representative samples studied in Phase I.

Wire	Resistivity (minimum diameter)				Resistivity (average diameter)			
	Before doping		After doping		Before doping		After doping	
	Ω -kcmil/ft	(Ω cm)	Ω -kcmil/ft	(Ω cm)	Ω -kcmil/ft	(Ω cm)	Ω -kcmil/ft	(Ω cm)
EY092013					7.8	1.3×10^{-3}	0.474	7.89×10^{-5}
032513B2					7.8	1.3×10^{-3}	28	4.6×10^{-3}
GETH130408-2					45	7.5×10^{-3}	22	3.7×10^{-3}
GETH130408-1					5.4	8.9×10^{-4}	5.4	8.9×10^{-4}
YZ207s	4.8	7.97×10^{-4}	0.404	6.72×10^{-5}	5.62	9.34×10^{-4}	1.1	1.83×10^{-4}
YZ207b	1.56	2.59×10^{-4}			1.83	3.04×10^{-4}		
	1.67	2.78×10^{-4}	1.46	2.42×10^{-4}	4	6.6×10^{-4}	3.46	5.75×10^{-4}
THAP001	1.46	2.42×10^{-4}	0.338	5.62×10^{-5}	3.46	5.75×10^{-4}	0.8	1.33×10^{-4}
THAP002	4.66	7.74×10^{-4}	2.66	4.42×10^{-4}	5.81	9.66×10^{-4}	3.31	5.51×10^{-4}
THBDC001								
THBDC002					71	1.18×10^{-2}		
YZ213	1.4	2.33×10^{-4}			4.3	7.1×10^{-4}		
EW1A			8.4	1.4×10^{-3}				
EW1A					15.9	2.65×10^{-3}	5.86	9.74×10^{-4}
EW1B							11.9	1.98×10^{-3}
EW2F			15.5	2.58×10^{-3}				
TABP001	1.0	1.7×10^{-4}	0.423	7.04×10^{-5}	1.26	2.1×10^{-4}	0.52	8.7×10^{-5}

Table 3. Treatments done to representative samples studied in Phase I.

Wire	Ci	Acid treatment	Ca	Doping	Cd	Comments
EY092013	√	Yes		Yes		Small wire w/ small diameter. Purification+ Doping
032513B2	√					
GETH130408-2	√					
GETH130408-1	√					
YZ207s	√			At 200°C for 14 hours		Yao Zao, Batch 2, 7 cm long, smaller
YZ207b	√			Not done		Yao Zao, Batch 2, 7 cm long, bigger; the sample melted
THAP001	√	Yes				Out of TZ. Smaller one.
	√			At 200°C for 24 hours		Acid doping improved iodine doping
THAP002	√			For 2.5 hours		Out of TZ. Larger one.
THBDC001	√					
THBDC002	√					THB Batch, David Chan, 2 sample; Done electrical conditioning; to be checked with Boeing
YZ213	√			Not done		Yao Zao, Batch 2, 13cm long
EW1A	√			Yes		Also heat treatment is done for 30 minutes
EW1A	√			Yes, long		Also heat treatment is done for 30 minutes
EW1B	√			Yes		Also heat treatment is done for 30 minutes
EW2F	√					5 hour heat treatment
TABP001	√	Yes		Yes		More uniform diameter wire; full processing route used

Table 4. Wire Diameters.

Wire	Minimum diameter		Maximum diameter		Average diameter		Standard deviation	
	(mil)	(μm)	(mil)	(μm)	(mil)	(μm)	(mil)	(μm)
032513B2	15.16	384.96	38.96	989.58	24.54	623.33	5.98	151.82
GETH130408-1	0.96	24.29	1.14	28.99	1.03	26.06	0.058	1.48
GETH130408-2	31.26	794.09	33.19	842.95	32.12	815.89	0.82	20.88
EW1A	0.91	23.04	3.81	96.86	1.81	46.02	0.66	16.78
EW1B	1.56	39.55	4.43	112.46	3.08	78.12	0.76	19.42
EW2F	0.87	22.06	3.16	80.22	1.82	46.23	0.53	13.48
THAP001	1.13	28.74	7.38	187.41	2.67	67.87	0.92	23.47
THAP002	2.02	51.36	5.36	136.19	3.63	92.09	0.75	19.01
THBDC001	16.27	413.27	48.40	1229.33	34.70	881.43	9.15	232.38
THBDC002	3.00	76.26	17.01	431.96	10.14	257.55	2.94	74.79
YZ207	13.34	338.86	22.15	562.49	16.48	418.48	3.05	77.56
YZ213	0.61	15.50	3.65	92.66	1.33	33.66	0.43	10.89

For Phase 1, several sources of nanotubes were used and in some cases were sources from research conducted prior to this RPSEA project. Samples also were used in varying starting conditions and did not originate from the same initial properties. Since a range of starting conditions and sources were being used, a range of sample numbers appears in **Tables 2-4**. The details of each sample can be ascertained from **Table 2 and 3** but **Table 5** describing the sample numbers is included to give more details on a per sample basis. Basically, sample designations for **Tables 2-4** represent the person who was responsible for the sample processing at Rice or the initial person(s) that produced the wire. Other information has to do with the length of the wire, wire creation date, some aspects of how the sample was processed, and/or which sample it was (one of two for example). While these sample designations are not systematic at this time, a new numbering scheme has been established for samples studied following these samples in tables 2-4. **Table 6** shows a sample numbering scheme for samples that shall be used in this report (mostly that come from NanoRidge). While the current sample numbering scheme does not appear to have an order to them, Rice holds a sample database that has all the details of each of these samples.

Table 5. Descriptions of the sample numbers for samples identified in Tables 2-4.

Wire	Name Methodology
EY092013	EY – Sample creator’s initials ; 092913 – Wire creation date [Month/Day/Year] (13 should be 12)
032513B2	032513 – Wire Creation date; B2 – Region of NR burner surface [Month/Day/Year] (13 should be 12)

GETH130408-2	GETH – Sample creator’s initials; 130408 – Wire creation date; -2 – wire section [Year/Month/Day for date]
GETH130408-1	GETH – Sample creator’s initials; 130408 – Wire creation date; -1 – wire section [Year/Month/Day for date]
YZ207s	YZ - Sample creator’s initials; 2 – Batch Sample, 07 – Sample length; s – Wire #
YZ207b	YZ - Sample creator’s initials; 2 –Batch Sample, 07 – Sample length; b – Wire #
THAP001	TH – Sample source; A – Batch number; P – Purified; 001 – Wire #
THAP002	TH – Sample source; A – Batch number; P – Purified; 002 – Wire #
THBDC001	TH – Sample source; B – Batch number; DC – Sample creator’s initials; 001 – Wire #
THBDC002	TH – Sample source; B – Batch number; DC – Sample creator’s initials; 002 – Wire #
YZ213	YZ – Sample creator’s initials; 2 – Batch Sample, 13 – Sample length
EW1A	EW - Sample creator’s initials; 1 – Wire #; A - Section of wire
EW1B	EW - Sample creator’s initials; 1 – Wire #; B – Section of wire
EW2F	EW - Sample creator’s initials; 2 – Wire #; F – Section of wire
TABP001	TAB – Sample creator’s initials; P – Purified; 001 – Wire #

Table 6. Sample naming scheme for NanoRidge samples given to Rice on spools.

Sample name = NR (X₁) (#₁) (X₂) (#₂) (X₃) _ #_{Wire Number}

NR - Indicates that a spool with this number came from NanoRidge Materials.

If a sample is produced at Rice it shall be designated RU.

(X₁) – Letters A-Z-AA-ZZ indicate NanoRidge spool

(#₁) – Numbers 0-*n* indicate Purification process used

(X₂) - Letters A-Z-AA-ZZ indicate Acid Doping and or Washing process used

(#₂) - Numbers 0-*n* indicate Doping process used

(X₃) - Letters A-Z-AA-ZZ indicate Conditioning process used

2.2.3.1 NANORIDGE WIRE 032513B2

Source materials: NanoRidge wire (Sample no. 032513B2) was made from CNT (032513B2) grown at NanoRidge.

Processing and characterization:

The CNT was densified using acetone and made into a wire at NanoRidge. It was also treated with hydrochloric acid (HCl) and rinsed with de-ionized (DI) water at NanoRidge. The as received sample was characterized by SEM and Raman. The SEM micrographs of the as received sample are shown in **Figure 21 and 19**. EDX spectra are shown in **Figures 20 and 21**. The Raman spectra are shown in **Figure 22 and Figure 23**. Carbon nanotubes can be easily identified from SEM but particulate contaminants are also seen. **Figure 22** is a typical Raman spectrum for 032513B2 with 633 nm laser. The presence of fluorescence indicates that there are significant amount of impurities that make the interpretation of this Raman spectrum very difficult. The sample was also characterized using 514 nm laser excitation to avoid the influence of fluorescence. As shown in **Figure 23**, the intensity of D peak and relative intensity of G and D peaks indicate that there are defects and amorphous carbon. The absence of radial breathing mode peak indicates 032513B2 is multi-walled CNT.

The wire sample was untwisted and purified in hydrogen peroxide (H₂O₂) for three days and then HCl for one day in Rice lab. A wire (**Figure 24**) was made from the post-purified CNT and the resistivity was 7.8 Ω–kcmil/ft ($1.3 \times 10^{-3} \Omega \cdot \text{cm}$) with four-probe method. The average diameter of the wire is 623 μm. The wire was then doped with iodine for 20 minutes, and the resistivity increased to 28 Ω–kcmil/ft ($4.6 \times 10^{-3} \Omega \cdot \text{cm}$). The increase in resistivity was unexpected and the sample was characterized with SEM and Raman spectroscopy. As shown in **Figure 19**, there are impurities on the surface of the wire. In the Raman spectrum in **Figure 23**, between 500 - 1200 cm⁻¹, several peaks that do not belong to CNT appeared and the peaks between 100 - 500 cm⁻¹ are probably not from RBM of CNT because of the intensities. However, the exact origin of these peaks has not been identified.

To remove the impurities, the sample was sonicated in pure ethanol for 24 hours using an ultrasonication bath with the ethanol constantly replaced to insure maximum purification. Raman and EDX were used to characterize the sample. As shown in **Figure 23**, the unknown Raman peaks disappeared after ethanol wash but EDX spectrum (**Figure 20**) shows there is significant amount of iron residue even after ethanol wash. To remove iron and amorphous carbon, the sample was heat-treated at 350 °C in air for 30 minutes and characterized by EDX and Raman. From EDX spectrum (**Figure 21**), there is 47 weight percent of iron on the wire surface. The D peak in the Raman spectrum decreased and G/D ratio increase after heat treatment.

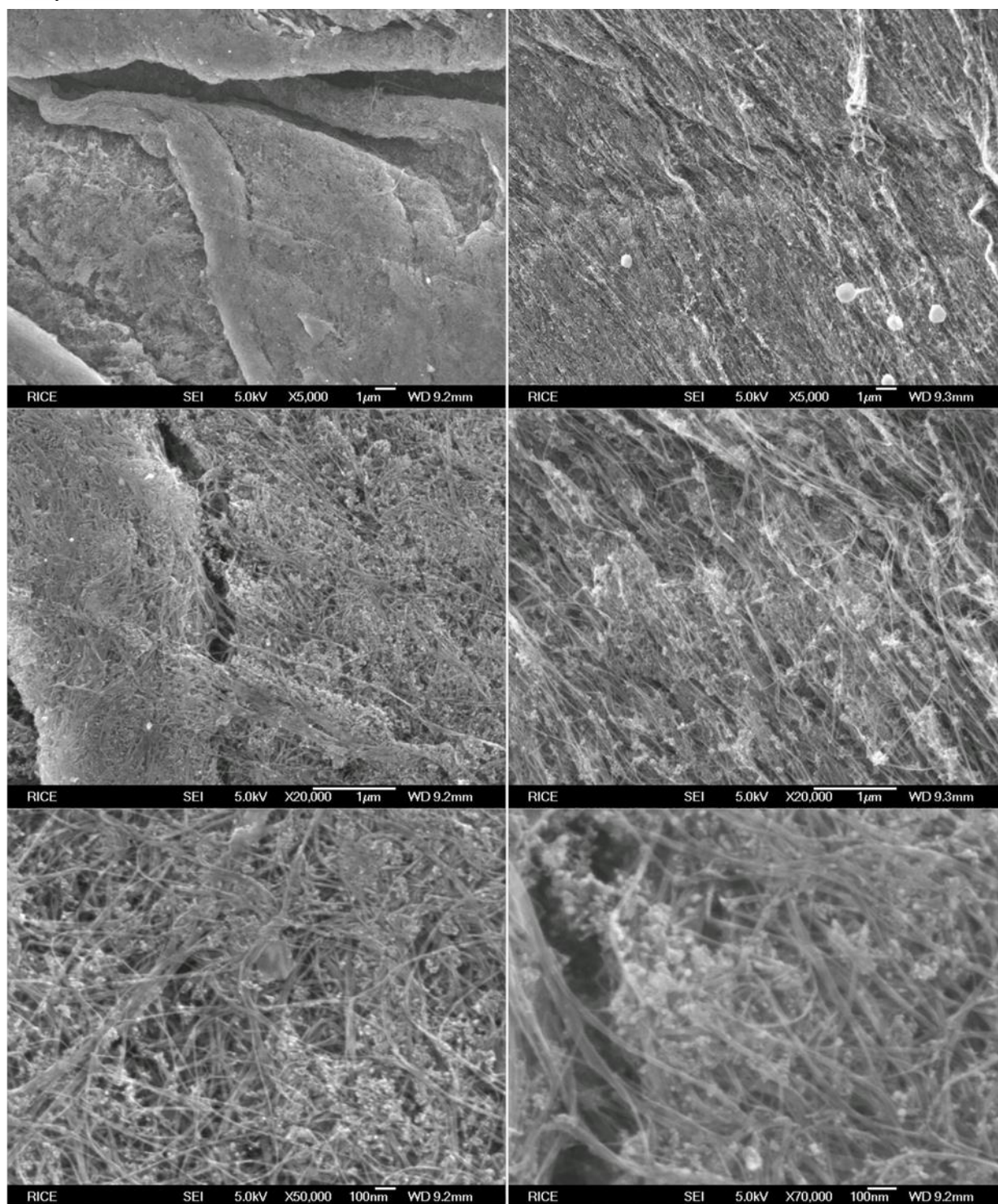


Figure 18. SEM micrographs of 032513B2 wire. Carbon nanotubes can be easily identified from SEM but particular contaminants are also seen.

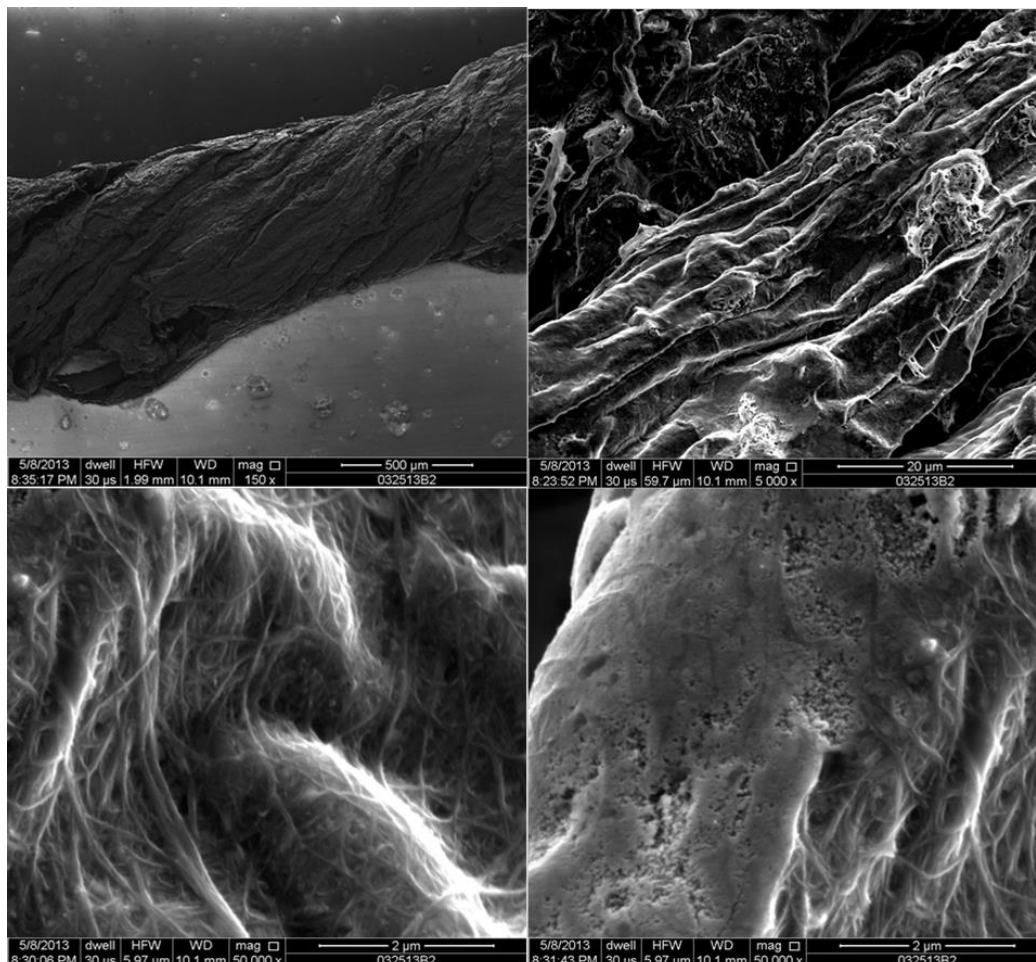


Figure 19. SEM micrographs of 032513B2 wire after purification and iodine doping. Carbon nanotubes can be easily identified from SEM but there is a crust of impurities covering part of the wire surface.

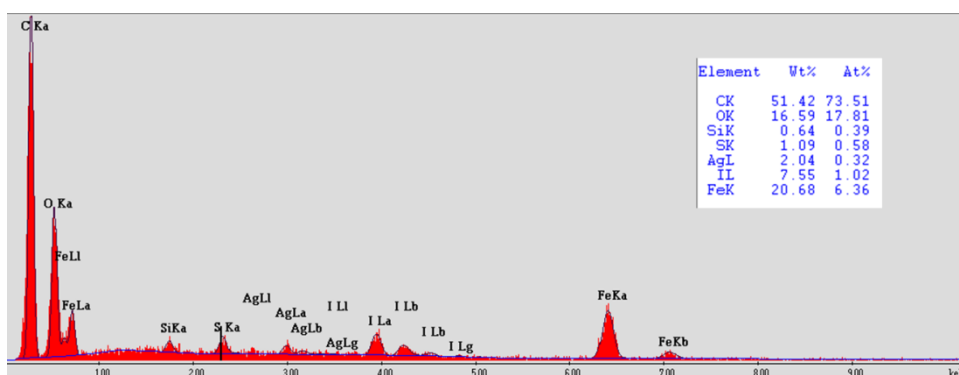


Figure 20. EDX spectrum of 032513B2 wire after ethanol wash. Besides carbon, there is also significant amount of iron and iodine dopant.

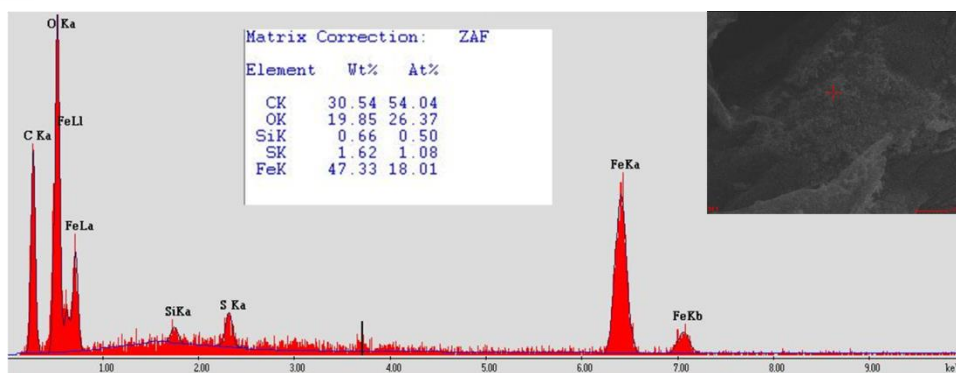


Figure 21. EDX spectrum of 032513B2 wire heat treatment in air. Besides carbon, there is also significant amount of iron oxide. Iodine peak is not visible.

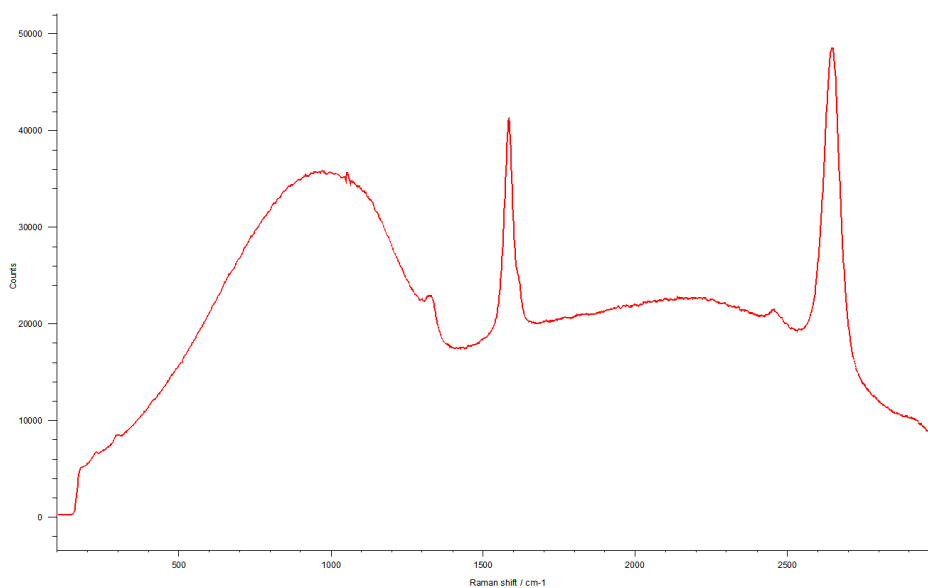


Figure 22. Raman spectrum of 032513 wire with 633 nm laser. The intense fluorescence from impurity makes interpretation of the spectrum difficult.

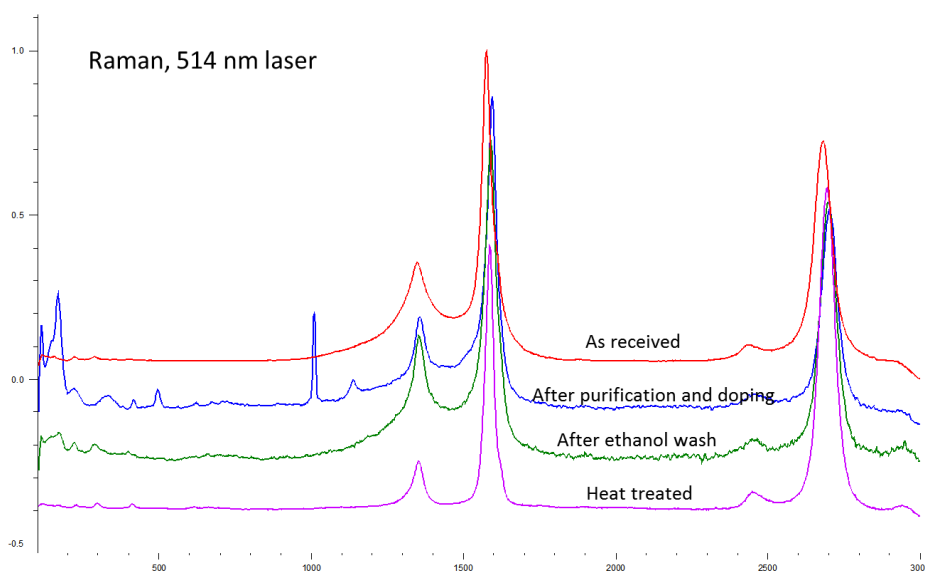


Figure 23. Raman spectra of 032513B2 with 514 nm laser.

The spectra are normalized. For the as received sample, the intensity of D peak and relative intensity of G and D peaks indicate that there are defects and amorphous carbon. The absence of radial breathing mode peak indicates 032513B2 is multi-walled CNT. The peaks from impurities appeared after purification and iodine doping. After ethanol wash, these impurity peak diminished. After heat treatment, D peak decreased and G/D ratio improved.

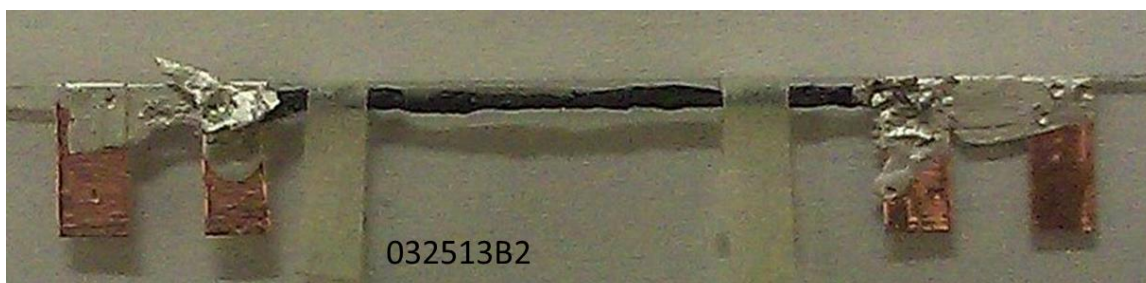


Figure 24. 032513B2 wire mounted on four-probe setup.

2.2.3.2 GETH130408 WIRES

Source materials: GETH130408-1 wire and GETH130408-2 wire are made from the same source material as THBDC001. The CNT was not purified.

Processing and characterization:

Figure 25 is the optical images of GETH130408-1 wire. The average diameter of the wire is 25 μm . The resistivity was 5.4 $\Omega\text{-kcmil/ft}$ ($8.9 \times 10^{-4} \Omega\cdot\text{cm}$) before iodine doping. The sample was doped with iodine at 70 °C for 20 minutes and resistivity is 5.4 $\Omega\text{-kcmil/ft}$ ($8.9 \times 10^{-4} \Omega\cdot\text{cm}$) after doping.

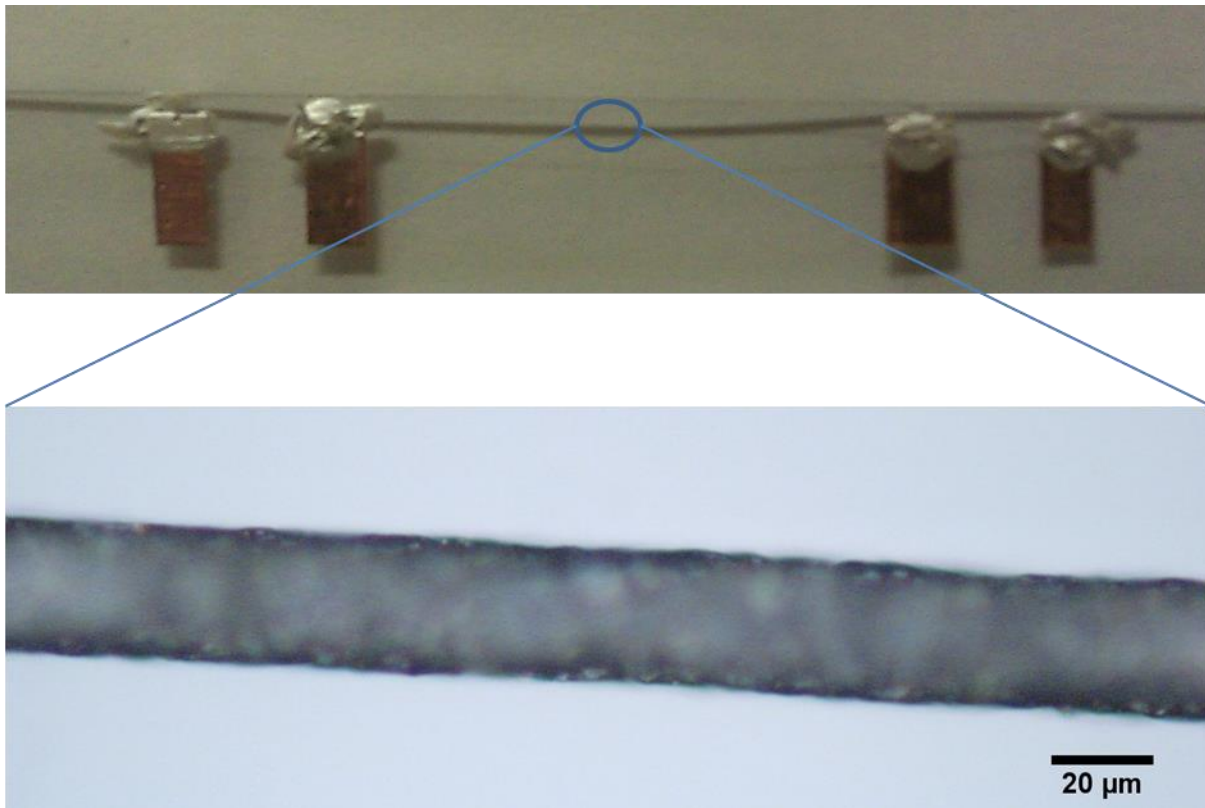


Figure 25. GETH130408-1 wire mounted on four-probe setup.

GETH130408-2 is a much thicker wire (**Figure 26**). The average diameter of the wire is 600 μm . The resistivity was 45 $\Omega\text{-kcmil/ft}$ ($7.5 \times 10^{-3} \Omega\cdot\text{cm}$) before iodine doping. The sample was doped with iodine at 70 °C for 20 minutes and resistivity was 22 $\Omega\text{-kcmil/ft}$ ($3.7 \times 10^{-3} \Omega\cdot\text{cm}$) after doping.

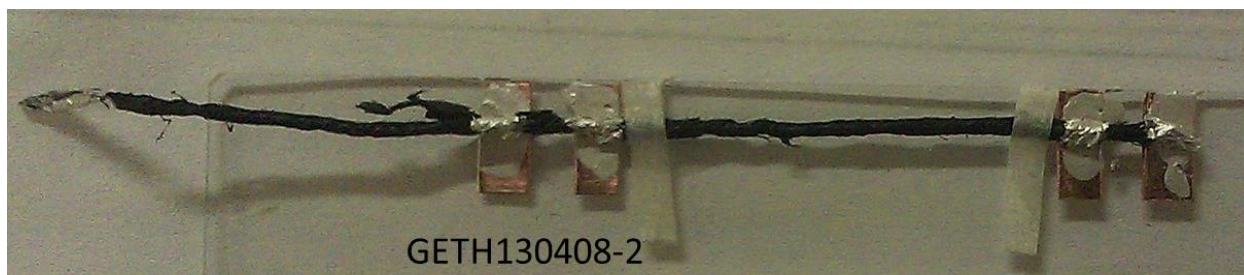


Figure 26. GETH130408-2 wire mounted on four-probe setup.

2.2.3.3 WIRE YZ207

Source material: THA batch.

The YZ207 wire (**Figure 27** and **Figure 28**) was characterized by Raman (**Figure 29**), SEM (**Figure 31**) and EDX (**Figure 30**). From the characterization data, the YZ207 wire has low impurities.

Figure 28 is the complete terminal to terminal images of the two wires after heat treatment. The final images were made up by overlapping of multiple SEM images.

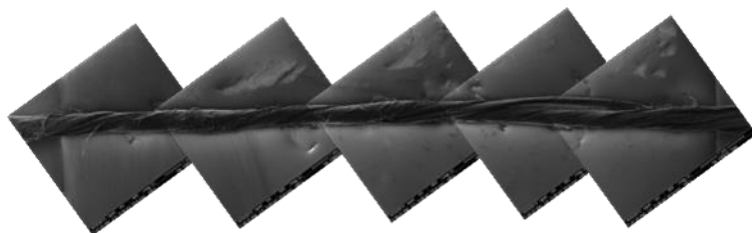


Figure 27. SEM micrographs of YZ207 wire between resistance measurement nodes.



Figure 28. YZ207 full length.

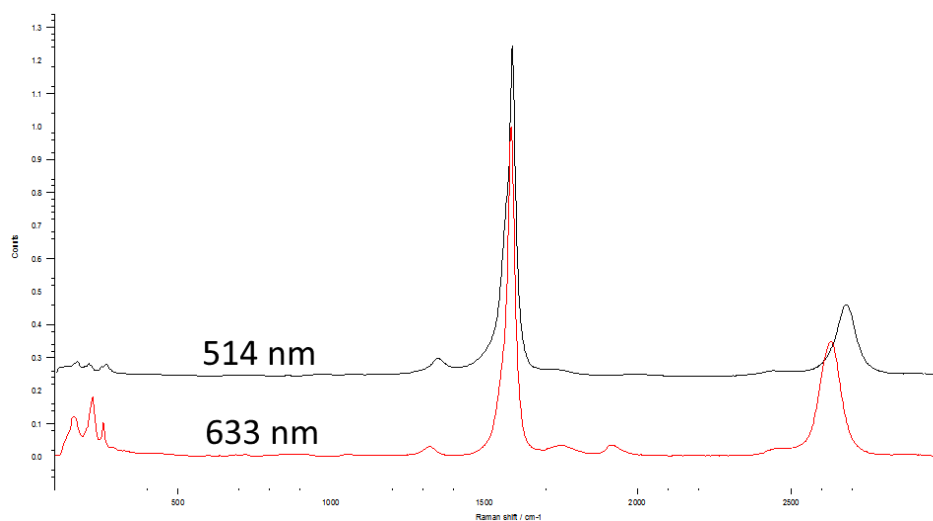


Figure 29. Raman spectra of YZ207 wire.

Raman spectra were obtained using both 514 nm and 633 nm laser excitation (**Figure 29**). Compared with 032513B2 wire, no fluorescence was observed from 633 nm Raman spectrum indicating low impurities. The RBM peaks indicated that these nanotubes were 1-3 walled CNT. The intensity of the G peak and high G/D ratio indicated that the YZ207 wire was made from high quality CNT. The EDX spectrum (**Figure 30**) showed that the sample was free of iron impurity. A minimal amount of chlorine was present due to the previous purification step.

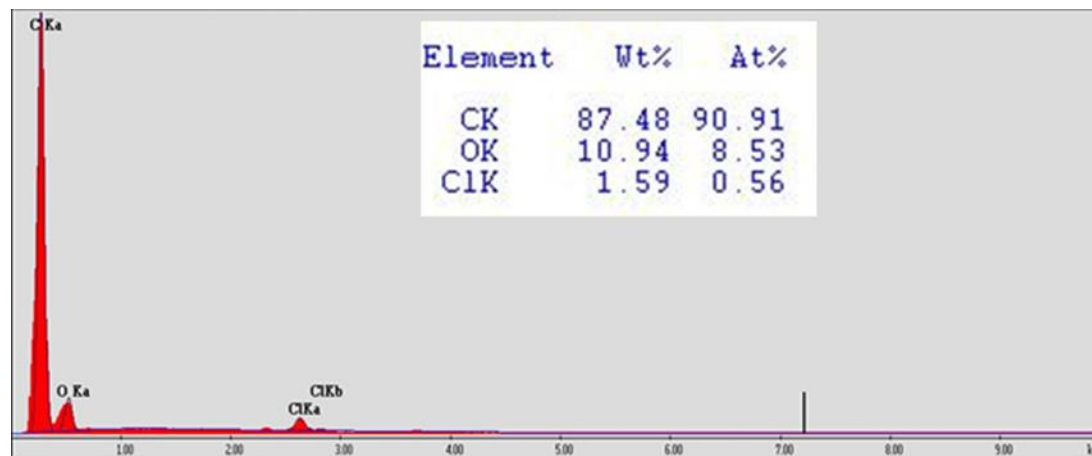


Figure 30. EDX spectrum of YZ207 wire. It shows that the sample is free of iron impurity. Minimal amount of chlorine is present due to previous purification step.

An analysis of SEM micrographs (**Figure 31**) showed that the sample was primarily free of impurities. The surface showed a slight oxidation coating with the nanotubes primarily aligned and densified. SEM allowed for diameter and length confirmation as well.

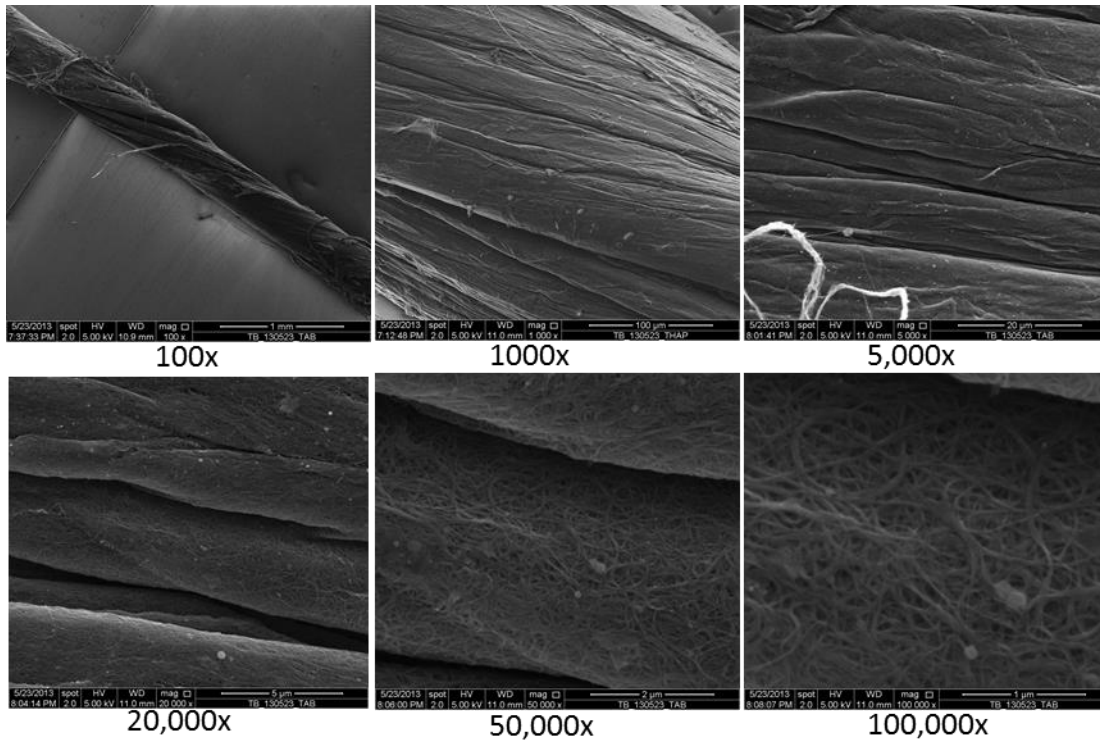


Figure 31. SEM micrographs of YZ207 wire.

- Current Resistivity (average diameter) = $1.83 \Omega\text{-kcmil/ft}$ ($3.04 \times 10^{-4} \Omega\cdot\text{cm}$)
- Current Resistivity (minimum diameter) = $1.56 \Omega\text{-kcmil/ft}$ ($2.59 \times 10^{-4} \Omega\cdot\text{cm}$)

The YZ207 wire was then doped for 20 hours in chlorosulfonic acid and the sample dissolved in the acid, creating a slurry. YZ207 slurry was poured into DI water to reconstitute it at room temperature. Upon this, four new wires were created:

- TABP001
- TABP002
- TABP003
- TABP004

TABP001 and TABP002 were chosen for testing and analysis due to their consistency in diameter and length.

TABP001

TABP001 was then Iodine doped at 200°C for 18 hours. After removing from the iodine and letting it sit for one hour the resistance was checked and resistivity was calculated.

- Current Resistivity (AVE diameter) = $0.523 \Omega\text{-kcmil/ft}$ ($8.70 \times 10^{-5} \Omega\cdot\text{cm}$)
- Current Resistivity (MIN diameter) = $0.423 \Omega\text{-kcmil/ft}$ ($7.04 \times 10^{-5} \Omega\cdot\text{cm}$)
- Average Diameter = $110 \mu\text{m}$
- Minimum Diameter = $99 \mu\text{m}$

EDX

EDX spectrum (**Figure 32**) revealed that several new elements had been introduced during the doping process.

- Na and Si from glass background
- S and Cl from acid doping
- from various Oxides
- Ca trace might have been another element

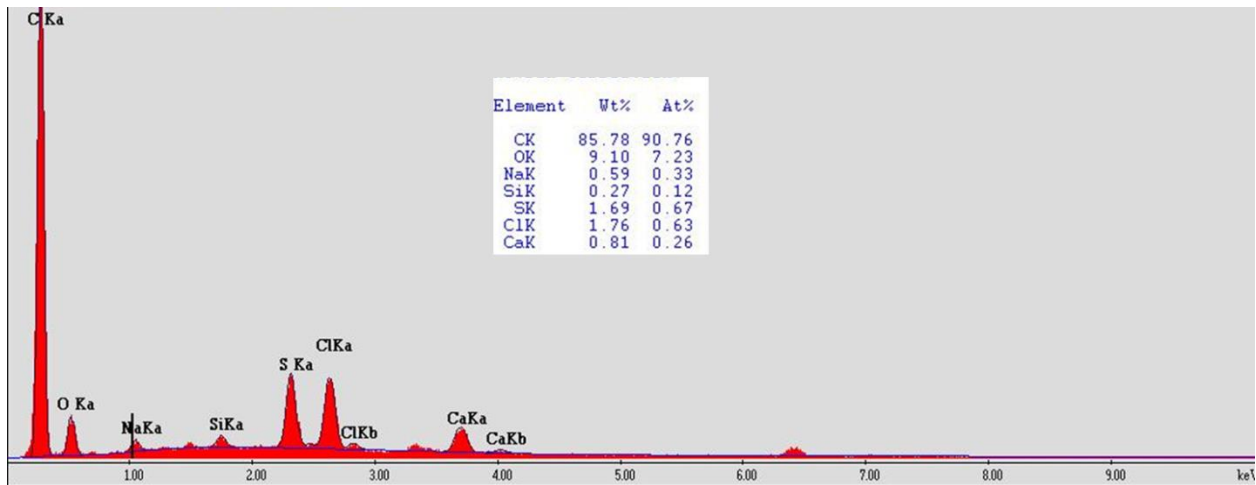


Figure 32. EDX spectrum of TABP001.

SEM

Minimal difference was observed with surface contamination from SEM images (**Figure 33**). Pure tubes with slight oxide were primarily present. Density seemed to remain intact, if not somewhat less than YZ207 wire as received.

Pictures after iodine doping are currently under development.

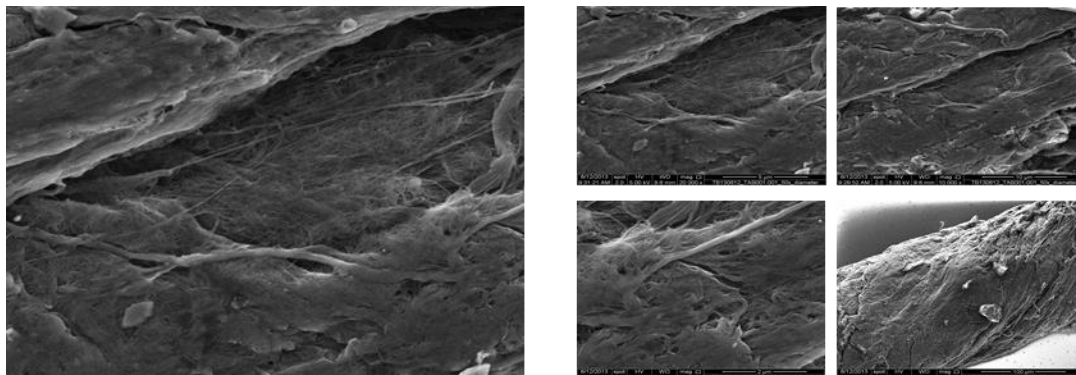


Figure 33. SEM micrographs of TABP001.

Resistance

- Before doping resistivity: 1.263 Ω-kcmil/ft (2.10×10^{-4} Ω•cm)(average diameter) 1.022 Ω-kcmil/ft (1.70×10^{-4} Ω•cm) (minimum diameter)
- After doping resistivity: 0.523 Ω-kcmil/ft (8.70×10^{-5} Ω•cm)(average diameter)
- 0.423 Ω-kcmil/ft (7.04×10^{-5} Ω•cm) (minimum diameter)

The TABP002 wire was created with a much smaller diameter than TABP001 ($56.3 \mu\text{m} < 110 \mu\text{m}$). This sample was not purified completely after acid doping, however, and hence produced results less significant from the iodine doping procedure. To better understand the process, additional research and steps are currently underway.

- Current Resistivity (AVE diameter) = 1.335 Ω-kcmil/ft (2.22×10^{-4} Ω•cm)
- Current Resistivity (MIN diameter) = 0.788 Ω-kcmil/ft (1.31×10^{-4} Ω•cm)
- Average Diameter = 56.3 μm
- Minimum Diameter = 43.27 μm

EDX

The EDX spectrum (**Figure 34**) revealed large amounts of elemental impurities. While research is underway to determine the exact source for the introduction of each impurity, the largest groups of impurities can be explained. Large amounts from both chloride (Cl) and sulfur (S) were not thoroughly rinsed from the sample after acid doping.

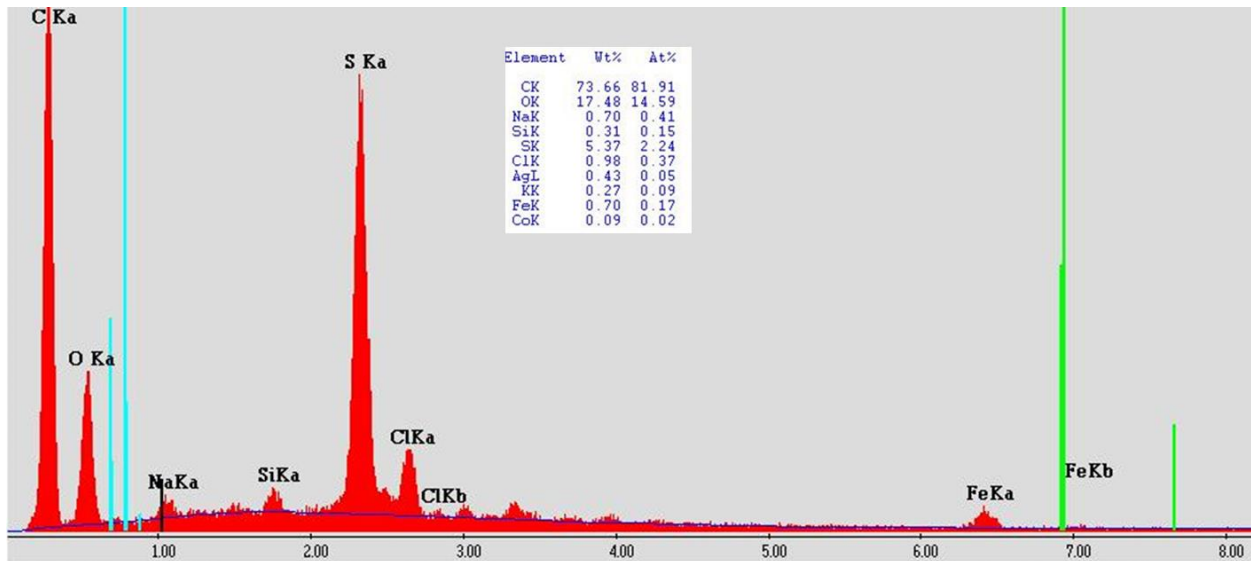


Figure 34. EDX spectrum of TABP002.

- Sodium (Na) and silicon (Si) from glass background
- S and Cl from acid doping¹
 - from various oxides
- Iron (Fe) traces from incomplete purification

¹

SEM

SEM images (**Figure 35**) revealed the wire to have poor alignment. While oxidation could be seen, the densification of the wire itself was fairly minimal, preventing the layer from collecting too thickly in any one area.

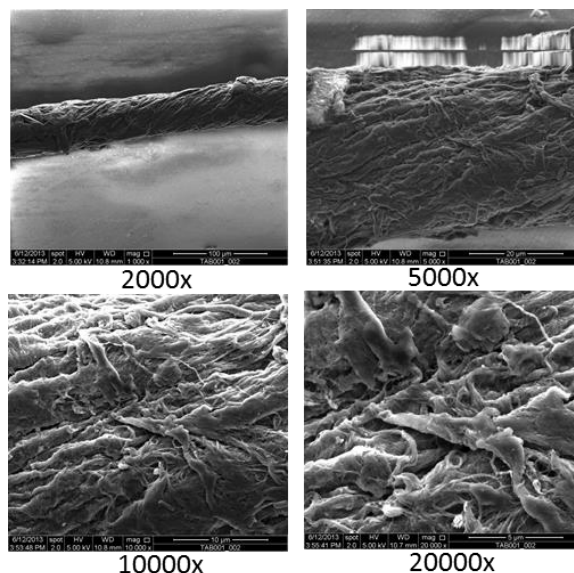


Figure 35. SEM of TABP002.

Resistivity

Before doping resistivity:

- 1.798 Ω -kcmil/ft ($2.99 \times 10^{-4} \Omega \cdot \text{cm}$) (average diameter)
- 1.064 Ω -kcmil/ft ($1.77 \times 10^{-4} \Omega \cdot \text{cm}$) (minimum diameter)

After doping resistivity:

- 1.329 Ω -kcmil/ft ($2.21 \times 10^{-4} \Omega \cdot \text{cm}$) (average diameter)
- 0.781 Ω -kcmil/ft ($1.30 \times 10^{-4} \Omega \cdot \text{cm}$) (minimum diameter)

After doping and HT to remove excess iodine:

- 1.335 Ω -kcmil/ft ($2.22 \times 10^{-4} \Omega \cdot \text{cm}$) (average diameter)
- 0.788 Ω -kcmil/ft ($1.31 \times 10^{-4} \Omega \cdot \text{cm}$) (minimum diameter)

2.2.3.4 THAP WIRES

THAP is purified THA CNTs. THAP is characterized using Raman and EDX.

From the analysis of Raman spectra (**Figure 36** and **Figure 37**), THAP has a very small D peak and very intense G peak. The 633 Raman spectrum is free of fluorescence which indicates that THAP is very clean.

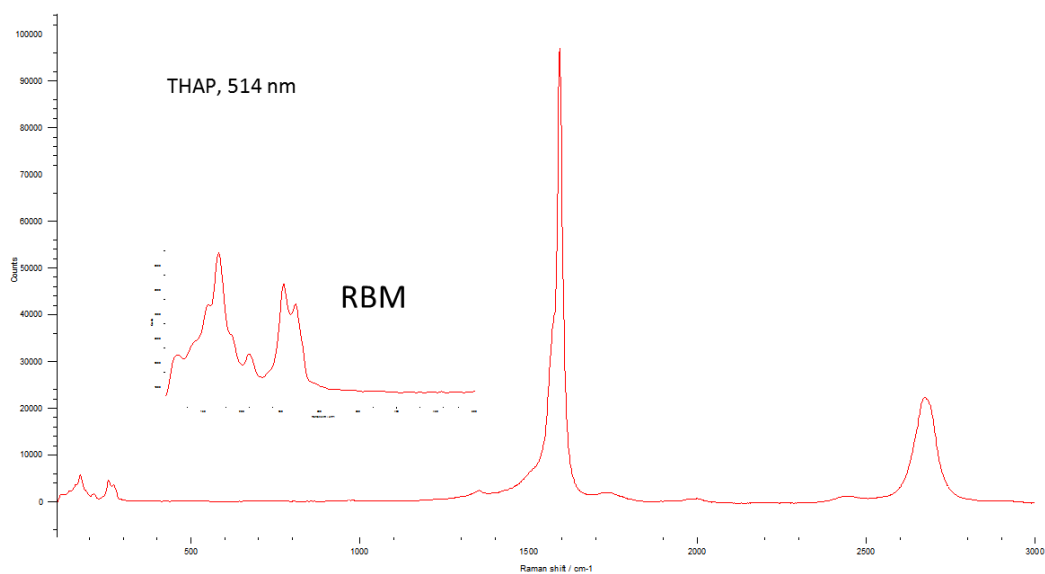


Figure 36. Raman spectrum of THAP wire with 514 nm laser.

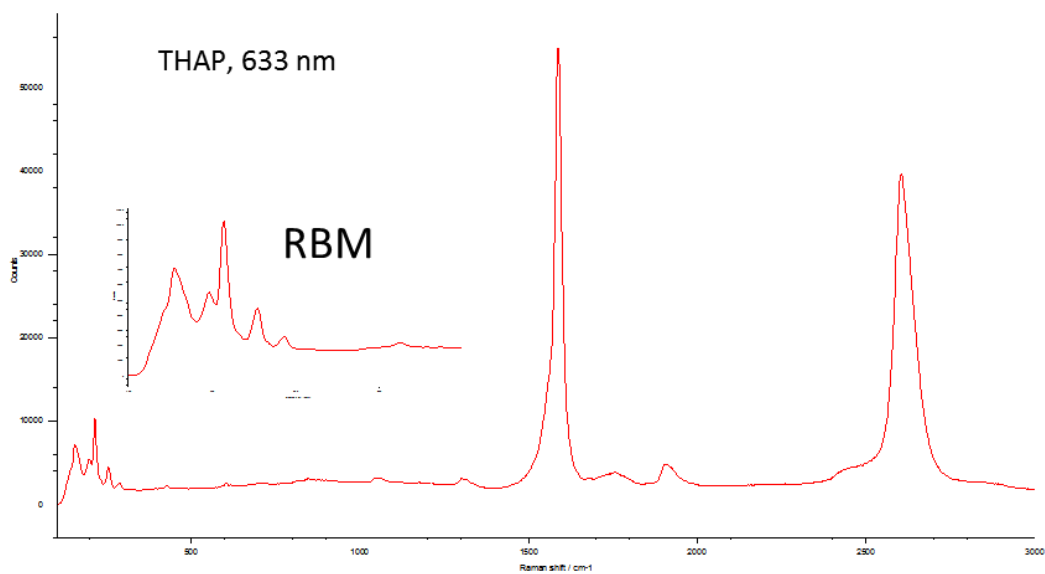


Figure 37. Raman spectrum of THAP wire

The EDX spectrum in **Figure 38** shows 16.9 percent of Fe, 9.3 percent of Cl, and S is misidentified as Mo.

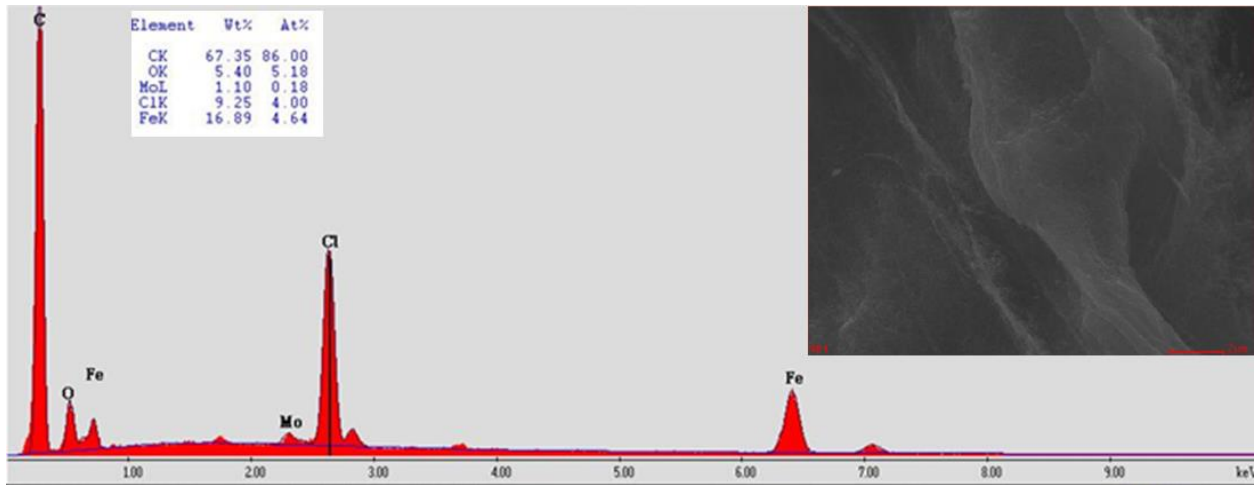


Figure 38. EDX spectrum of THAP.

Two wires were fabricated from THAP: THAP001 and THAP002. **Figure 39** and **Figure 40** are the SEM images of THAP001 wire before doping. After acid doping and iodine doping too, the SEM images were taken and shown in **Figure 41** and **Figure 42**, respectively.



Figure 39. SEM of THAP001 full length.

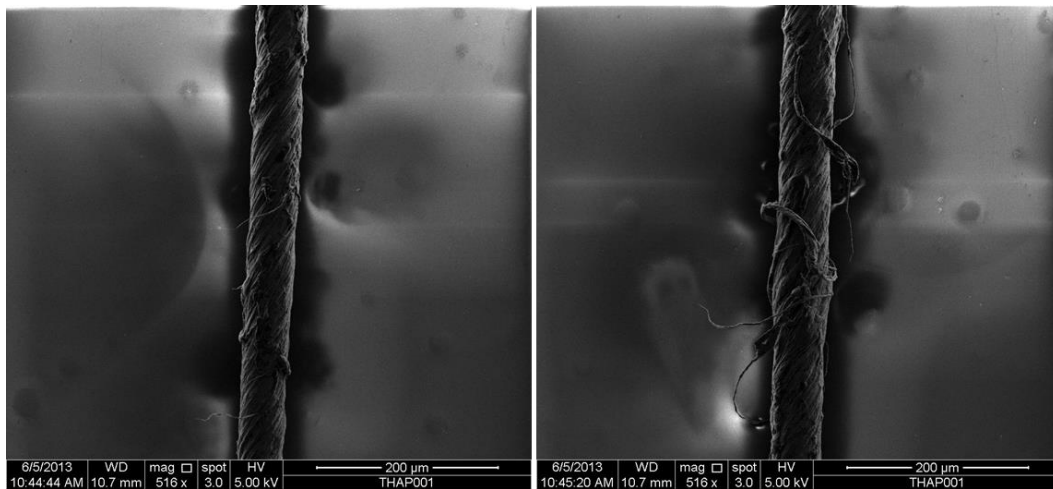


Figure 40. SEM micrographs of THAP001 before acid doping.

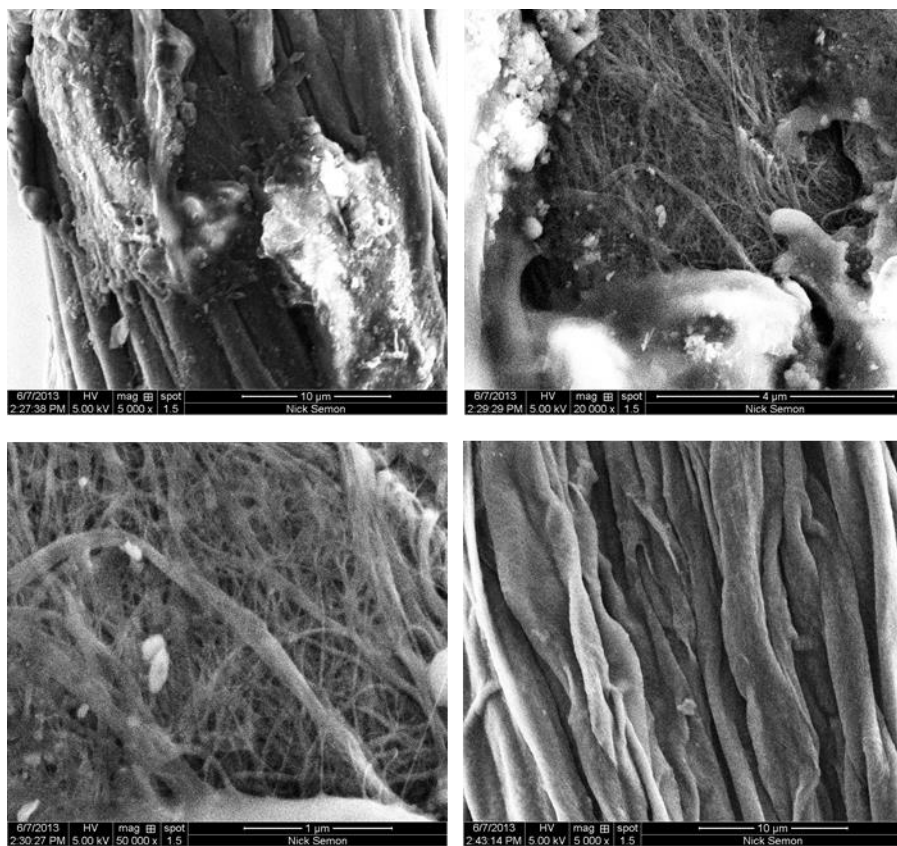


Figure 41. SEM micrographs of THAP001 after acid doping.

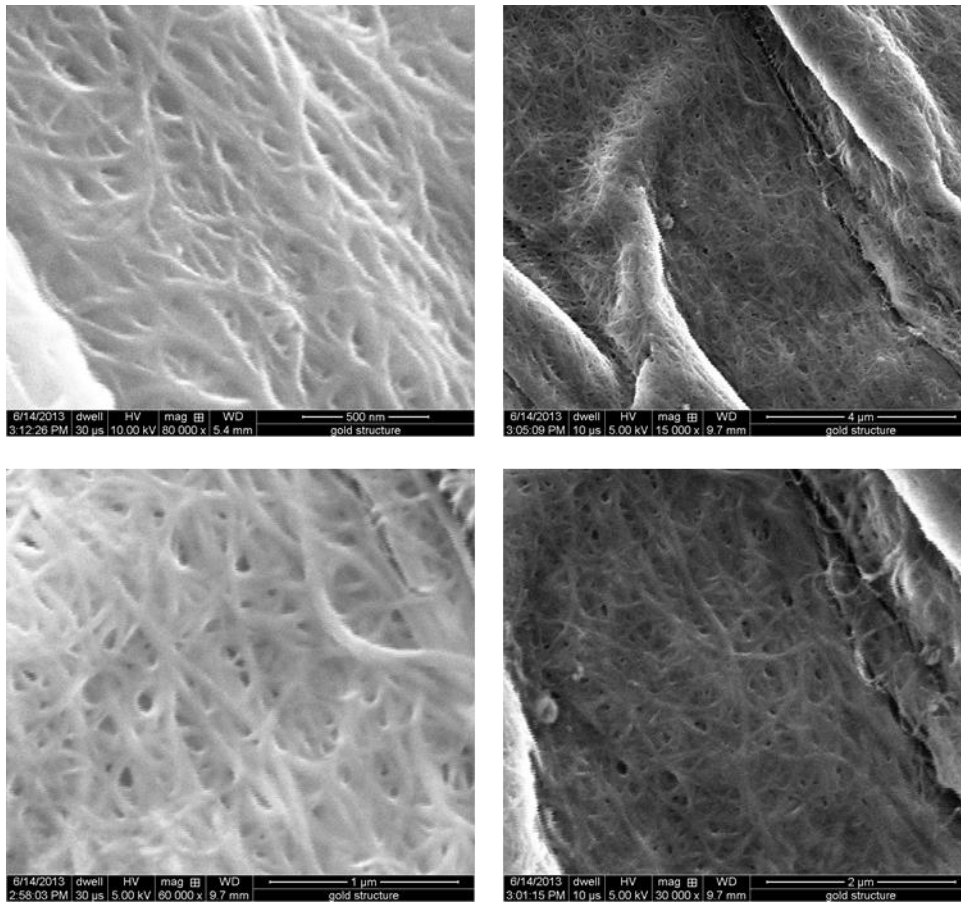


Figure 42. SEM micrographs of THAP001 after iodine doping.

The full wire image of THAP002 is shown in **Figure 43**. Some SEM images were also taken on this wire and shown in **Figure 44**.

THAP002 Full Wire Image



Figure 43. Full Wire Image of THAP002.

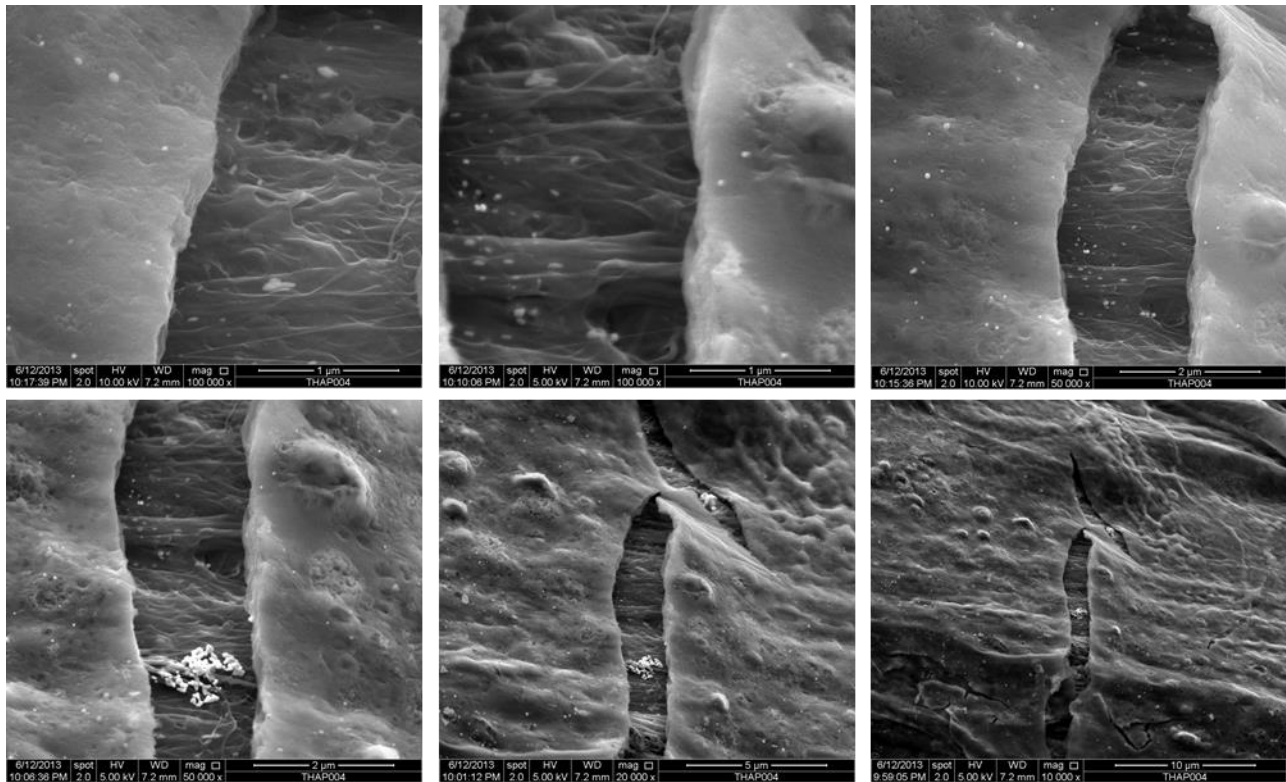


Figure 44. SEM micrographs of THAP002.

2.2.3.5 EW WIRES

Starting material was coiled wire and approximately 40 in (1 m) long. A small section was removed and identified as RAW source material. The remainder was purified in 30 percent H₂O₂ for 72 hours and 37 percent HCl for 24 hours as shown in **Figure 45**. During post-purification handling, the purified segment broke into two segments. The longer was approximately two-foot (60.96 cm) long and was designated EW1. The shorter was approximately 6 inches long (15.24 cm) and was designated EW2.



Figure 45. EW wire segment was introduced to H₂O₂. Prior to soaking in H₂O₂, the wire did not wet. However, after 72 hours of soaking, the wire wet with water and HCl.

The samples that were used are listed in **Table 7** below:

Table 7. Samples made from the EW Wire.

Wire	Processing	SEM	RAMAN	EDX
EW1A	Purification, 30 min. heat treatment (350°C).	√	√	√
EW2A	Purification	√		
EW2B	Purification	√		
EW2C	Purification	√		
EW2D	Purification	√		
EW2E	Purification	√	√	
EW2F	Purification, 5 hr. heat treatment (350°C).	√	√	√
RAW	None	√	√	√

The Purification Process used is as follows:

- 72 hours in 30 percent H₂O₂
- Washed with DI water
- 24 hours in 37 percent HCl
- Washed with DI water

After removal from DI water, a noticeable shrinkage occurred (the wire reduced in diameter).



Figure 46. Raw EW wire in H₂O₂. CO₂ bubbles were seen coming from the wire earlier in the process.

Raman spectroscopy was conducted on the samples and the spectra are shown in **Figure 47**.

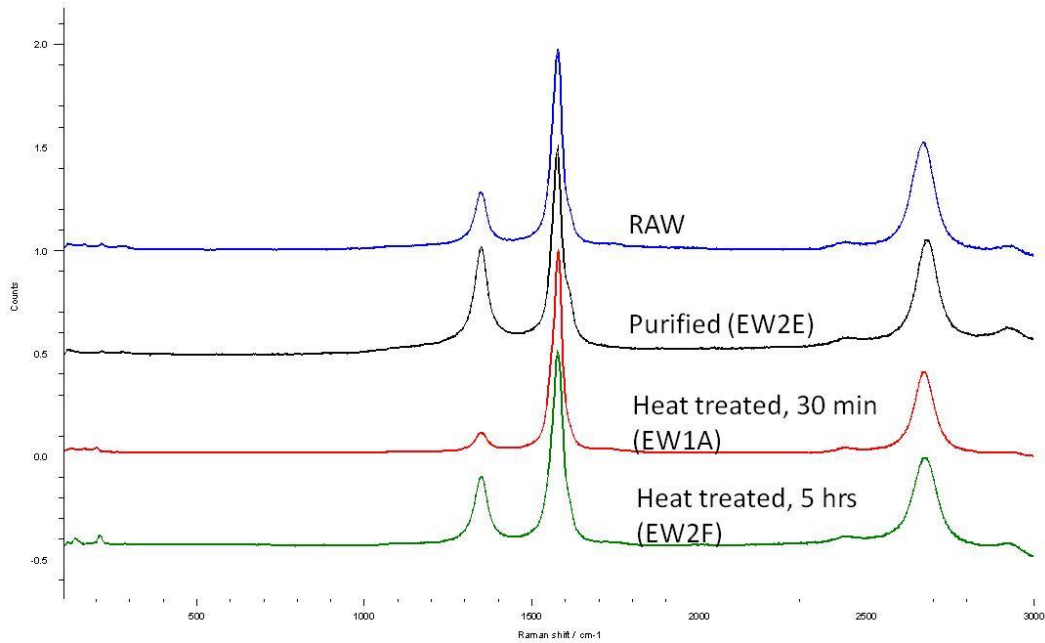


Figure 47. Raman spectra of the samples at 514 nm laser are (Blue) for sample RAW, (Black) for purified (EW2E), (Red) for EW1A sample heat-treated for 30 minutes and (Green) for EW2F sample heat-treated for 5 hours.

The following observations were made following purification and the heat treatments:

- The D peak increased after purification,
- 30 min heat treatment improved the G/D ratio, better than for the RAW sample; and after 5 hr of heat treatment, the D peak was higher than for the 30 min heat treatment.

The EDX was also done on the samples. The RAW sample showed a presence of almost 10 percent iron as seen in **Figure 48**.

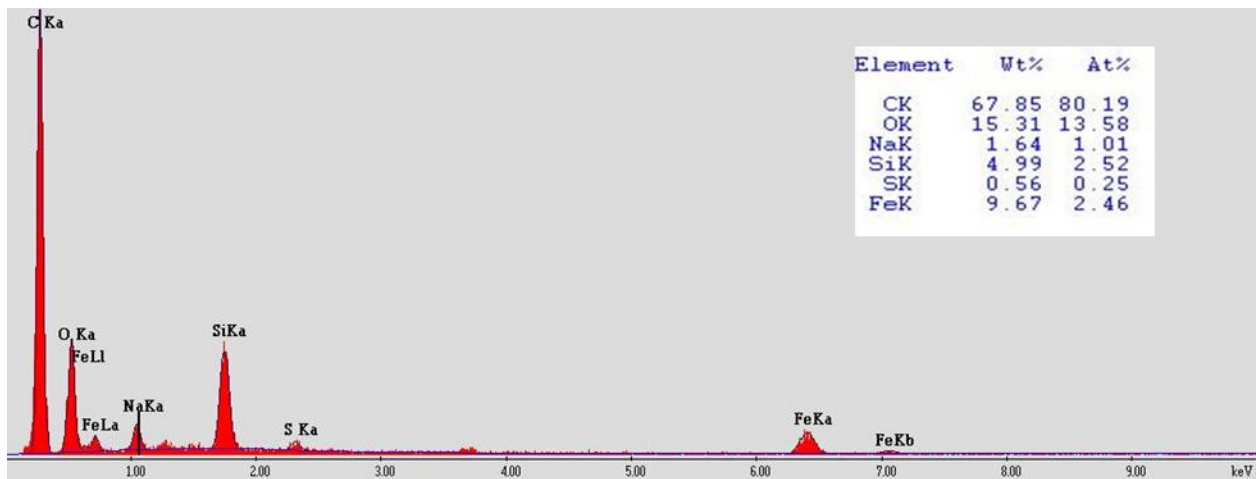


Figure 48. EDX of RAW sample with elemental composition shown.

For the purified sample with heat treatment for 5 hours (EW2F) more iron was seen in **Figure 49** compared to RAW. It is currently being studied to determine if the purification brought the iron to the surface and, if so, if this is the reason why more iron is seen after the purification.

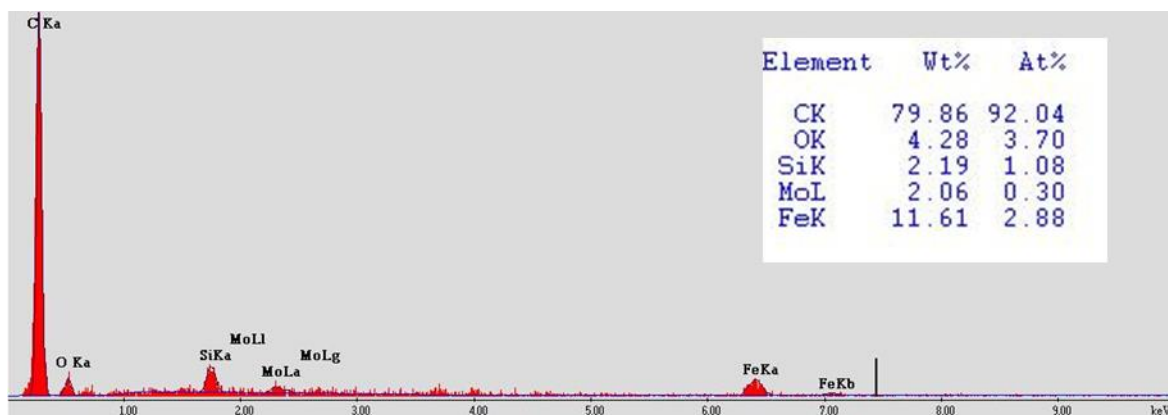


Figure 49. EDX of EW2F sample.

Point elemental composition of the sample showed that the crusty surface (seen in the micrograph) was iron oxide (rust) as shown in **Figure 50**.

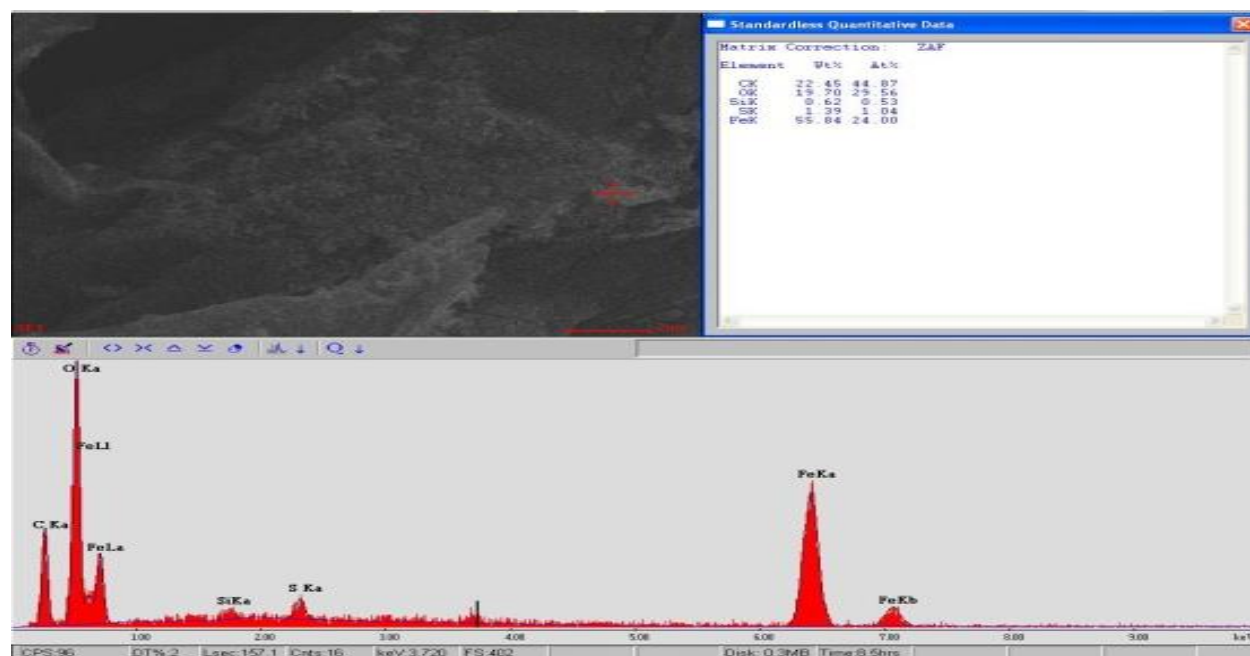


Figure 50. EDX point elemental composition and a corresponding micrograph.

The SEM images of the RAW sample showed good alignment, but a lot of contamination was observed as well, as seen in **Figure 51**.

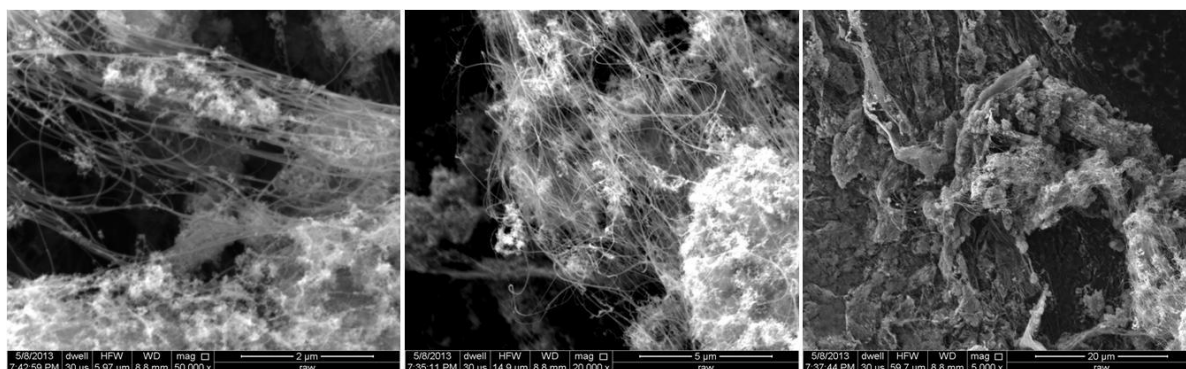


Figure 51. SEM images of the RAW sample before any treatments.

The SEM images of the purified samples (EW2C and EW2D) suggested that as the density of the wires increased, they only remained partially cleaned, as shown in **Figure 52**.

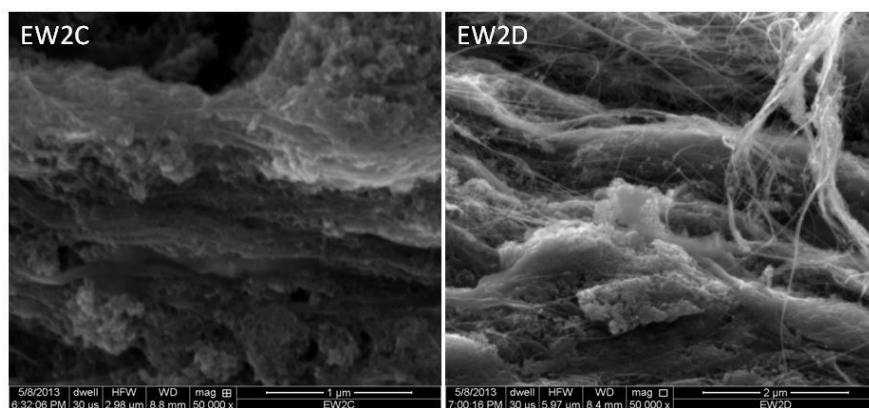


Figure 52. SEM images of purified samples EW2c and EW2d. Both Samples purified with 72 hr H₂O₂ 30%; 24 hr 37% HCl; SEM 50,000x Magnification.

The procedure followed for the heat treatments are shown below:

- Sample EW1A
 - Schedule
 - Select gas 2 (air)
 - Flow rate 0.0035 cfm (100 ml/min)
 - Ramp 40 °C/min to 350 °C
 - Isothermal for 30 min
 - Air cool on (fan for faster cooling)

- Sample EW2F
 - Schedule
 - Select gas 2 (air)
 - Flow rate 0.0035 cfm (100 ml/min)
 - Ramp 40 °C/min to 350 °C
 - Isothermal for 300 min
 - Air cool on (fan for faster cooling)

The SEM images of the sample EW1A showed increased density. However, contamination was still observed, as seen in **Figure 53**.

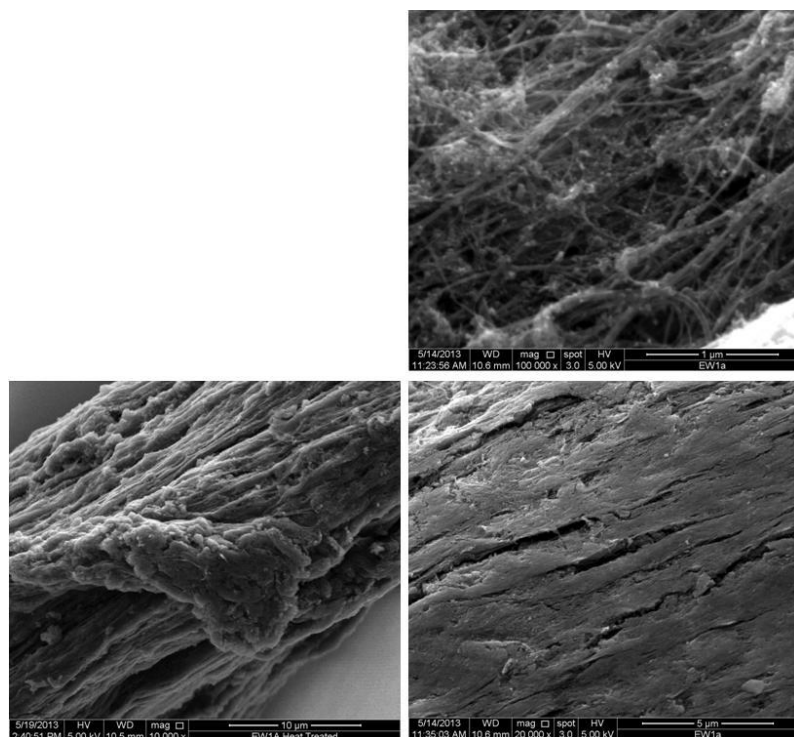


Figure 53. SEM images of EW1A sample. Purified and 30 minutes heat-treated is highly densified (bottom right and left). Still some particulate contamination (top right) was observed.

The SEM images of sample EW2F after 5 hours of heat treatment also showed a similar observation to that for EW1A. The images are shown in **Figure 54**.

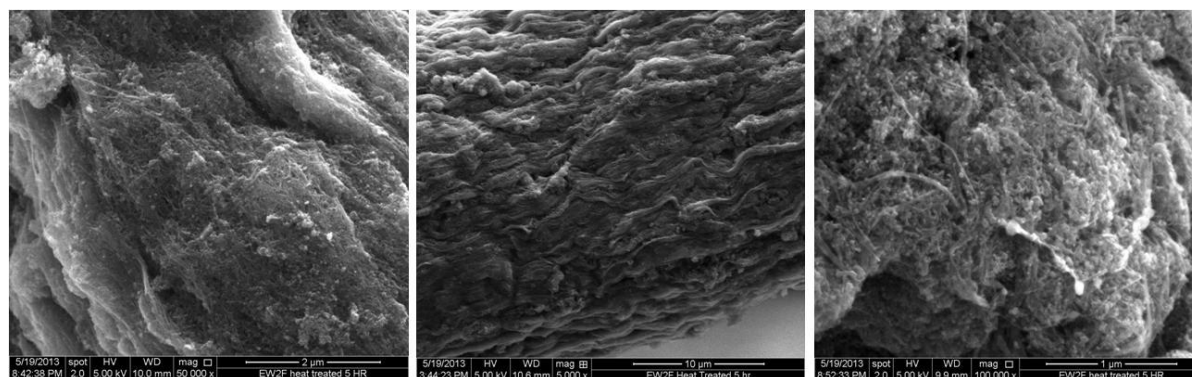
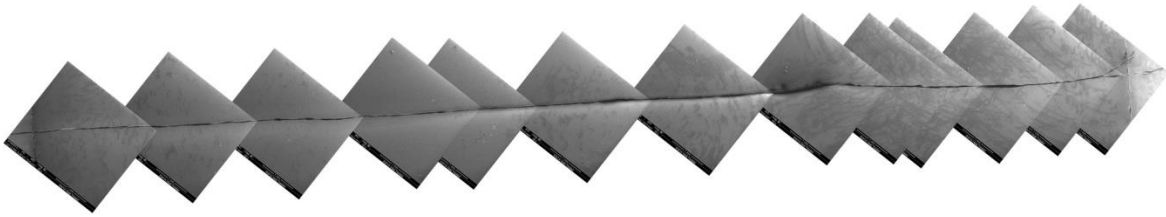


Figure 54. SEM images of sample EW2F-Purified and -heat-treated for 5 hours.

The images of wires EW1A and EW2F after purification and heat treatments are as shown in **Figure 55**.

EW1A heat treated for 30min



EW2F heat treated 5hr

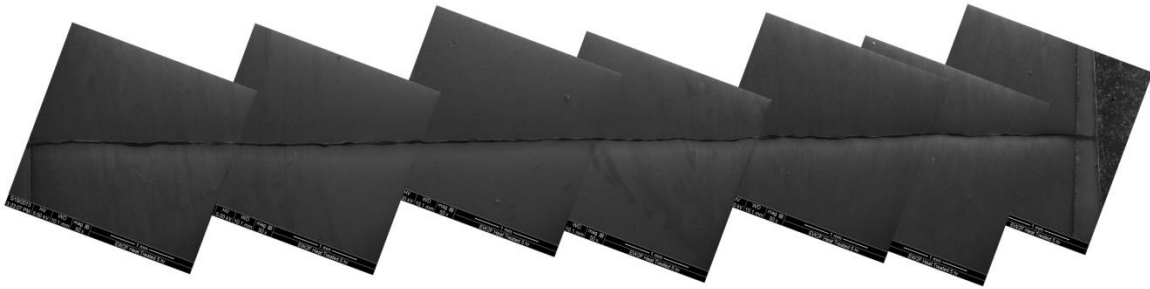


Figure 55. Wires of EW1A and EW2F as seen from SEM images.

Based on these studies the following findings were identified:

- The best resistivity seen so far was observed in the sample through purification and 30 min heat treatment.
- The longer heat treatment of 5 hr produced a wire close in resistivity.
- The 5 hr heat treatment also produced a less desirable Raman spectrum and appeared to decrease the tensile strength of the wire.
- The nanotubes still contain a significant amount of iron.
- Further acid treatment and/or doping shall be attempted to further improve this wire conductivity.

2.2.3.6 YZ213 WIRE

Raman spectroscopy was conducted on this sample using 514 and 633 nm lasers. The spectra are shown in **Figure 56** and **Figure 57**, respectively.

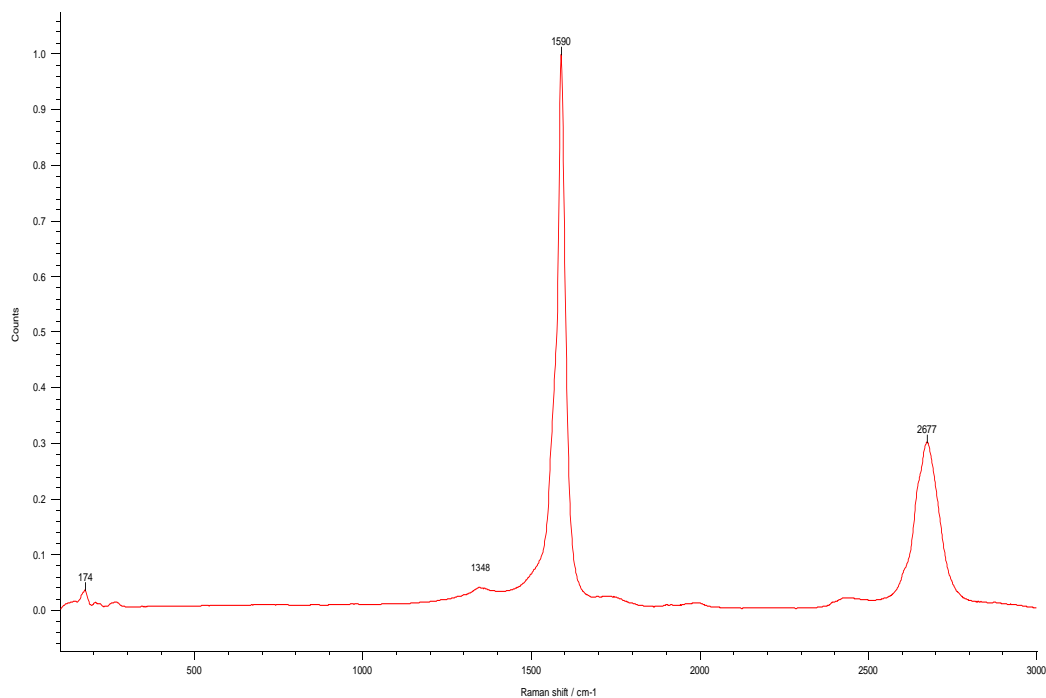


Figure 56. Raman spectra of sample YZ213 at 514 nm laser.

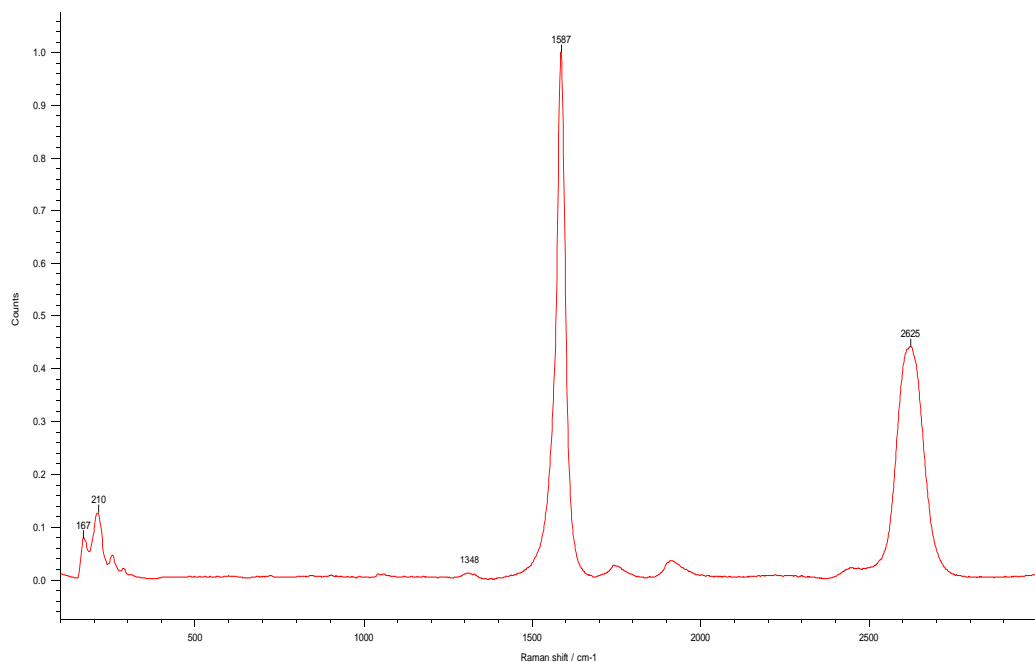


Figure 57. Raman spectra of sample YZ213 at 633 nm laser.

The Raman spectroscopy was conducted on this sample at 514 and 633 nm lasers for the RBM region. The spectra are shown in **Figure 58** and **Figure 59**, respectively.

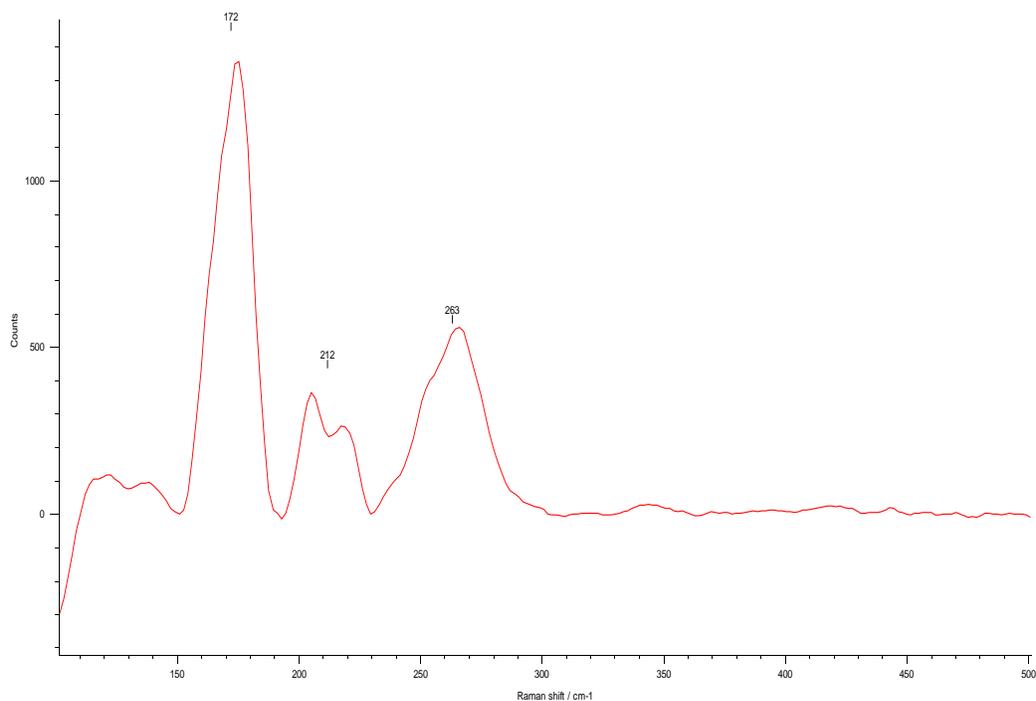


Figure 58. Raman in RBM at 514 nm laser.

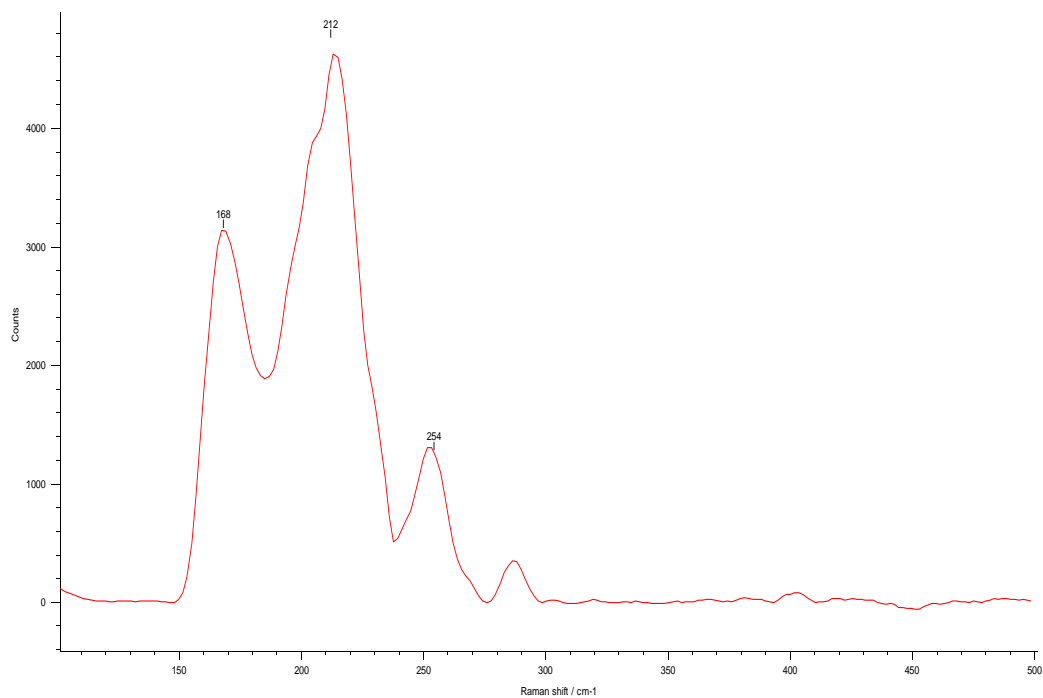


Figure 59. Raman in RBM at 633 nm laser.

Based on the Raman study (this sample was only studied at the end of this period so not all steps have been taken) the following findings were made:

A high G/D ratio was observed and a good quality RBM was observed, indicating the presence of DWNT. Low fluorescence with 633 nm laser showed the nanotubes to be of good quality and relatively clean.

An overview of the representative sample of wire was seen from SEM images, since the SEM image of whole wire could not be taken as it was too long to fit on the SEM stage, is shown in **Figure 60**.

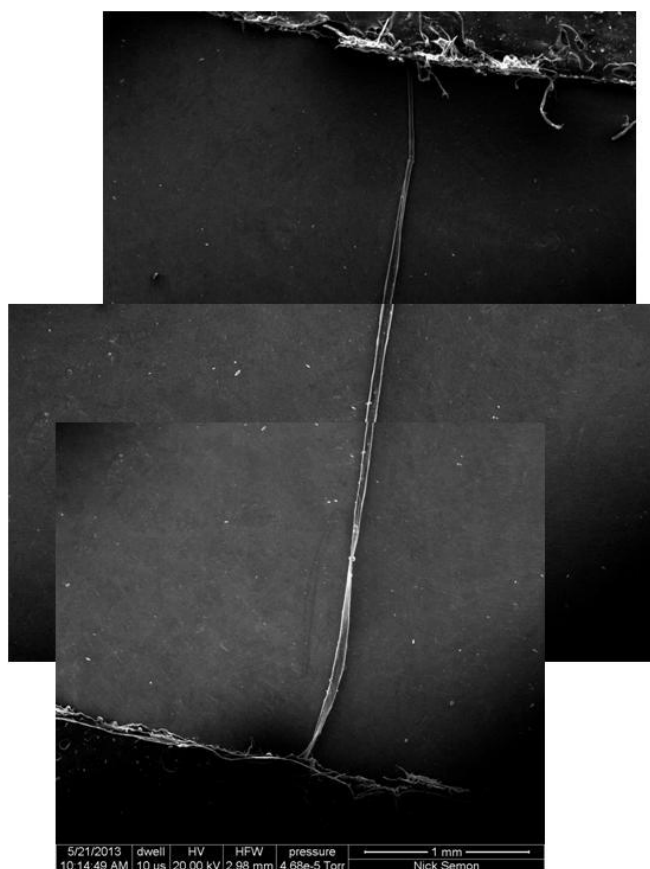


Figure 60. Overview of the representative of the sample wire through SEM images.

SEM images in **Figure 61** suggested that there existed a bend or compressed section which was earlier assumed to be a knot.

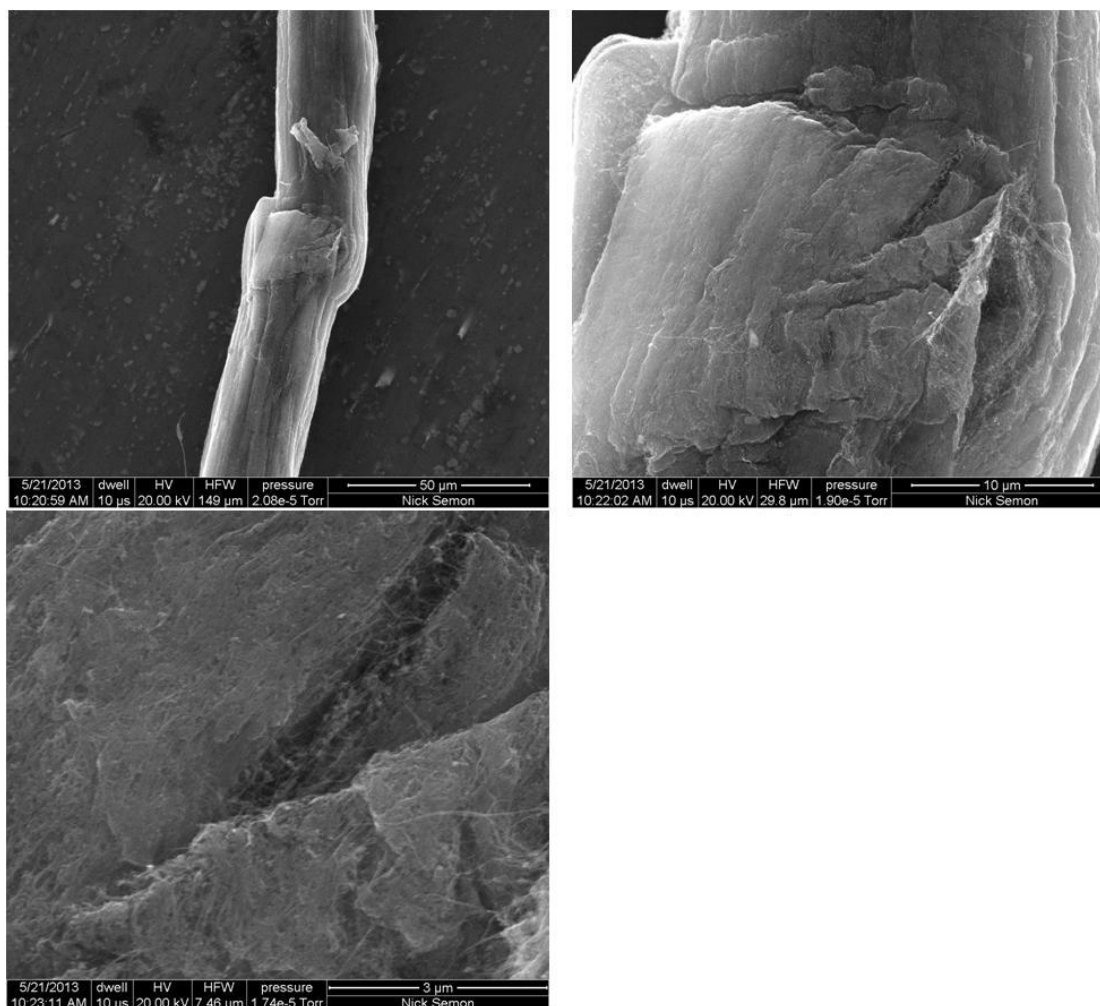


Figure 61. SEM images of the wire with magnifications 1,000x, 5,000x and 20,000x from top left.

The SEM investigations were conducted along the length of the tube. In **Figure 62**, the SEM images showed a typical section of the wire. These images also showed that sample YZ213 was clean and the nanotubes were well aligned. The average diameter for this section was 1.035 mils (26.28 μm). The resistivity for this diameter was 1.497 kcmil/ft ($2.49 \times 10^{-4} \Omega \cdot \text{cm}$).

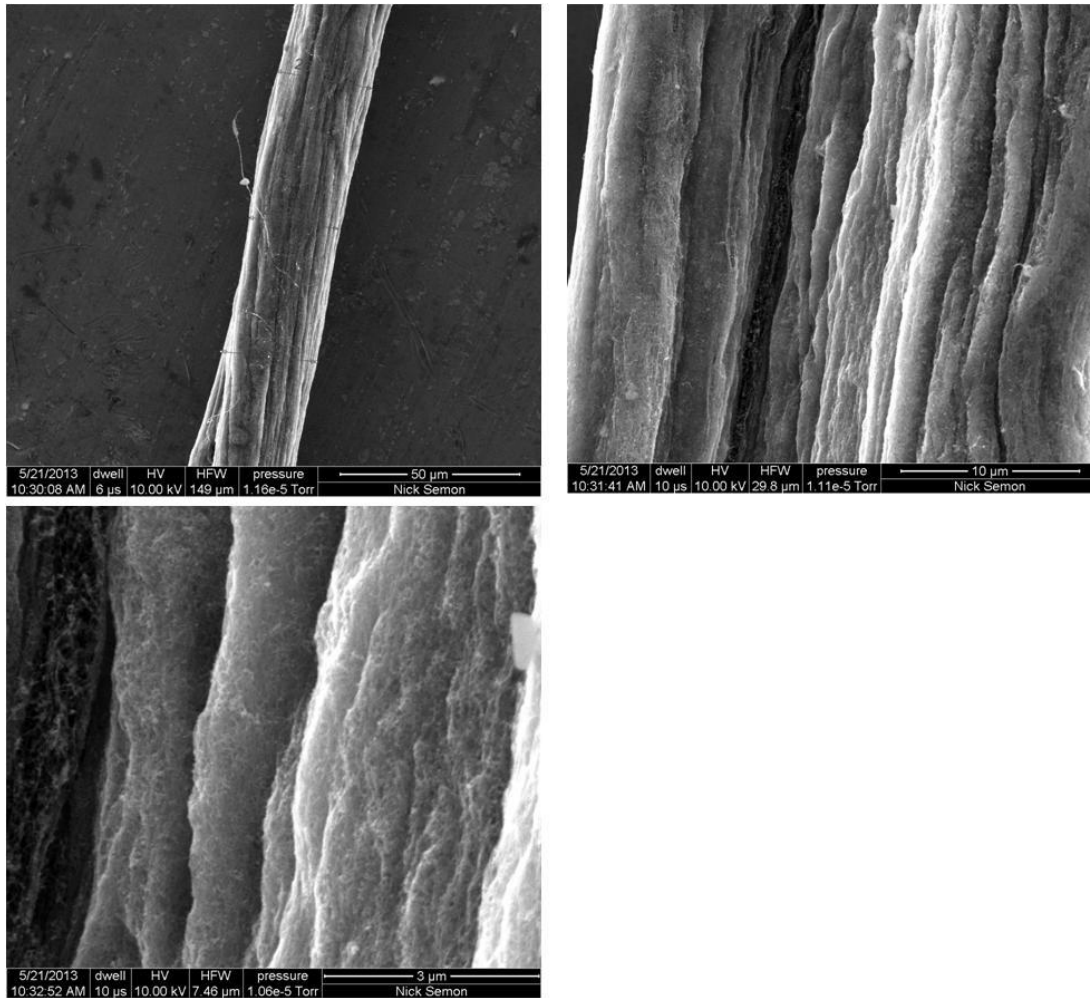


Figure 62. SEM images with magnifications 1,000x, 5,000x and 20,000x from top left.

In **Figure 63**, the SEM images show the sample when the wire widens out. It was less dense with tube alignment in favorable conditions. The average diameter for this section was 2.053 mils (52.13 μ m).

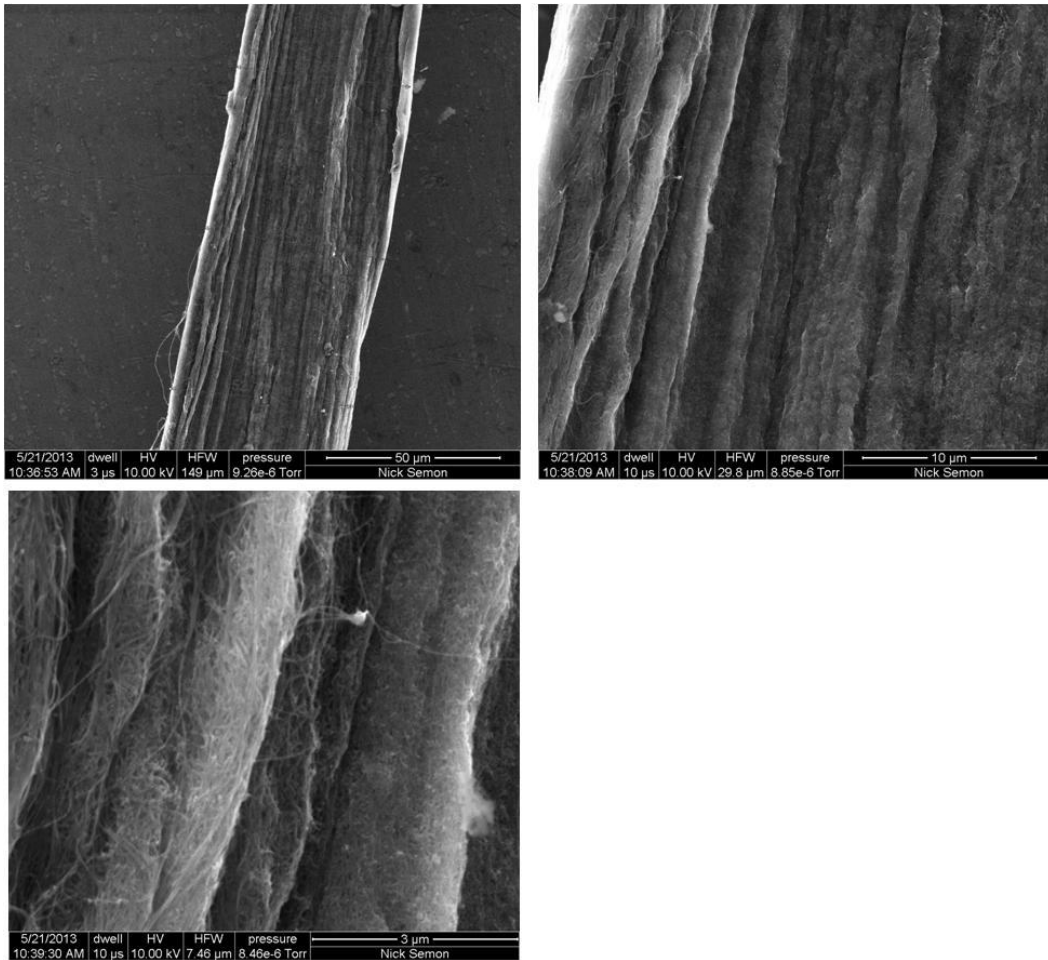


Figure 63. SEM images with magnifications 1,000x, 5,000x and 20,000x from top left.

The SEM image in **Figure 64** taken at magnification 1,000x showed an average diameter of the tube to be 47.9 μm , and the resistivity value for this diameter was found to be 4.975 $\Omega\text{-kcmil/ft.}$ ($8.27 \times 10^{-4} \Omega \cdot \text{cm}$). The red arrow indicated the thickest portion of the wire, which was 2.57 mils (65.28 μm).

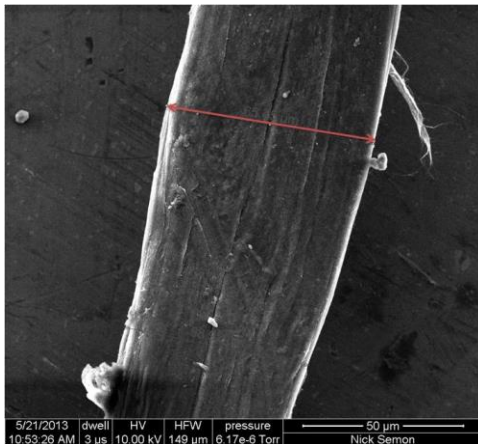


Figure 64. SEM image with magnification 1,000x.

The SEM image in **Figure 65** showed the presence of racked rust patch, further confirmed by EDX.

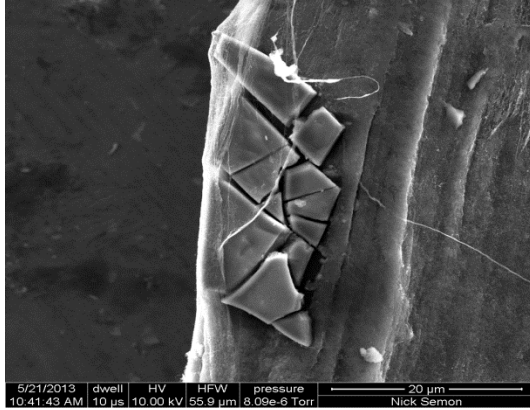


Figure 65. SEM image showing cracked rust patch.

In **Figure 66** the SEM images also showed presence of unidentified foreign particles. These particles could not be confirmed from EDX because it was difficult to charge them.

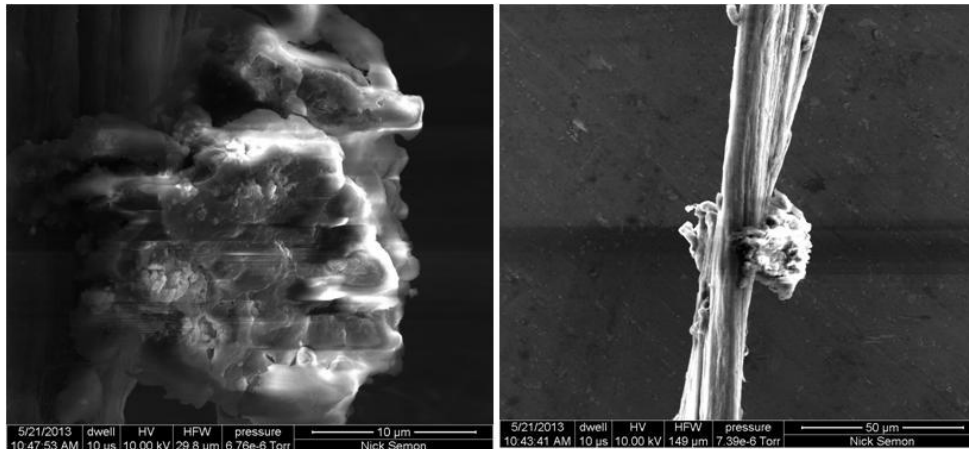


Figure 66. SEM image showing unidentified impurities.

The wire was subjected to EDX also to get some useful information. It was performed at several different locations to ensure the consistency of the wire. One notable result from this analysis was the absence of iodine. This wire was not doped and the resistivity can most likely be improved with iodine doping. The EDX analysis was shown by **Figure 67**, **Figure 68**, **Figure 69**, and **Figure 70**. In **Figure 67**, the print screen feature had an error, and for the **Figure 68** and **Figure 69** the element analysis was available but the graph of the distribution of elements was not. In **Figure 68** the presence of aluminum (Al) was attributed to stub. In **Figure 69** both full screen and spot analysis were carried out to confirm the presence of the rust discussed earlier in the SEM image shown on **Figure 65**.

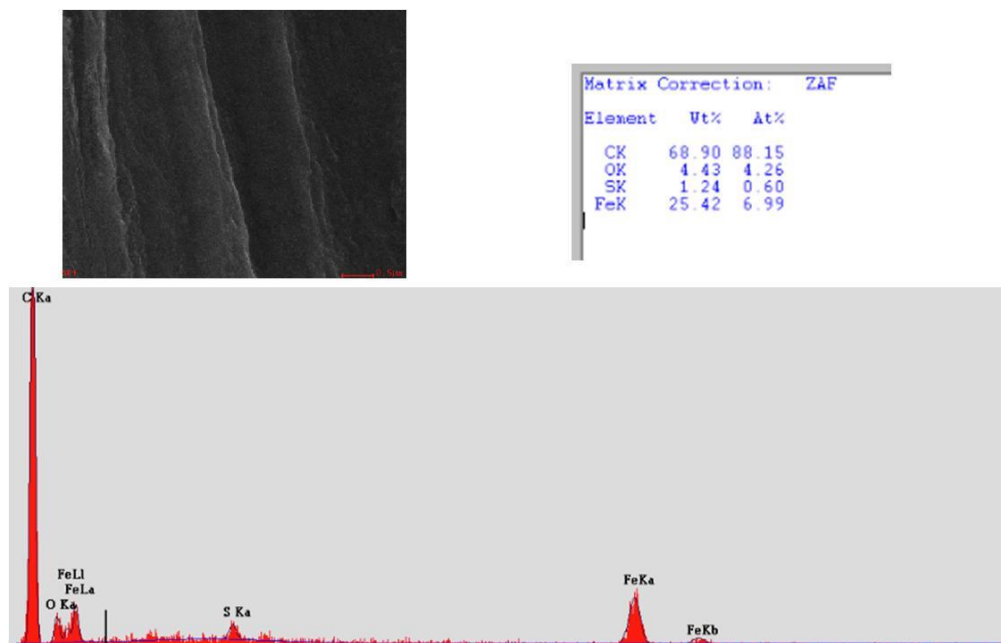


Figure 67. EDX analysis of the sample with elemental composition.

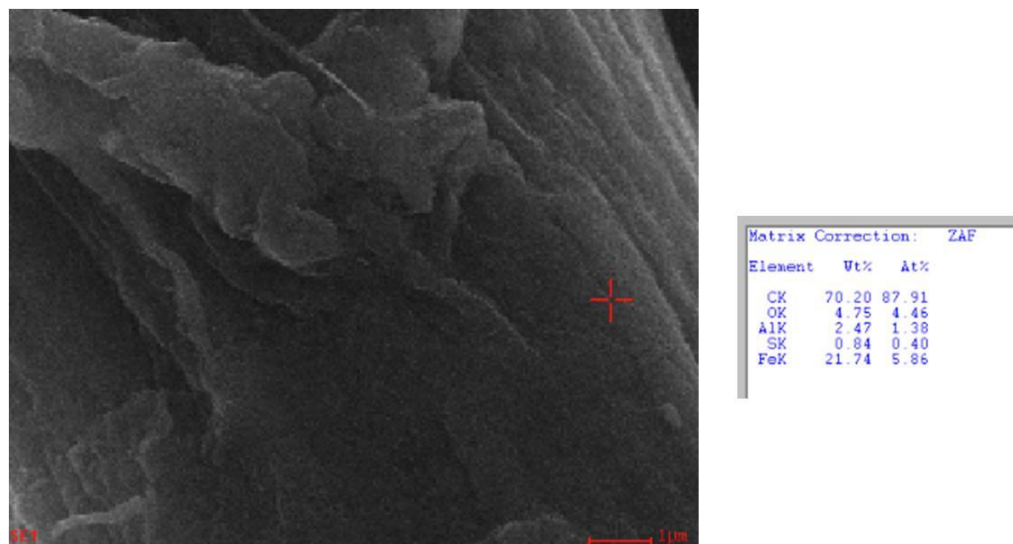
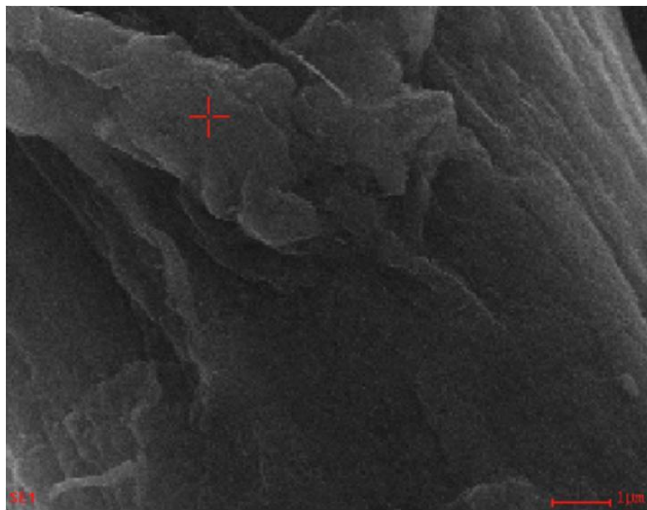


Figure 68. EDX analysis of the sample with elemental composition.

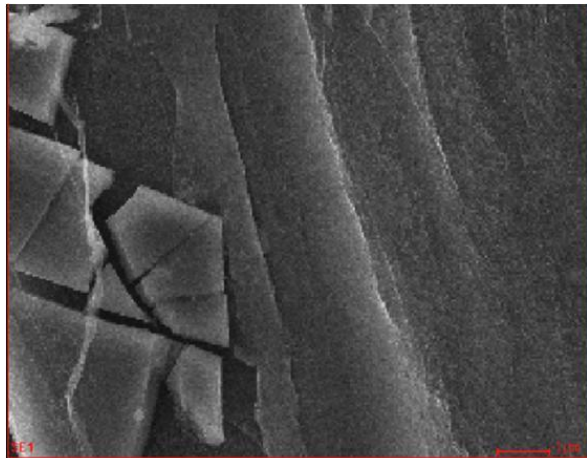


Matrix Correction: ZAF

Element	Wt%	At%
CK	67.89	88.52
OK	3.42	3.34
AlK	1.03	0.60
MoL	2.59	0.42
ClK	0.53	0.23
FeK	24.54	6.88



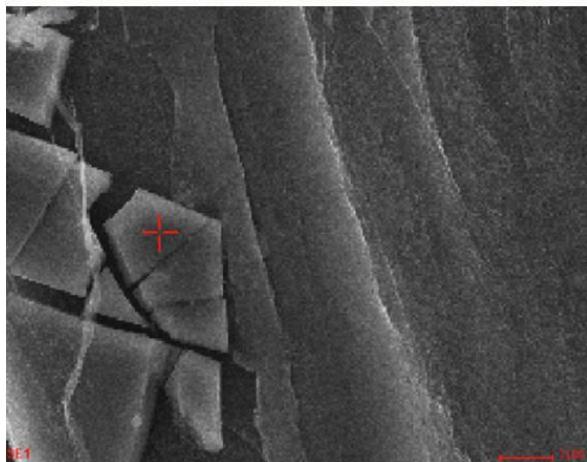
Figure 69. EDX analysis of the sample with elemental composition.



Matrix Correction: ZAF

Element	Wt%	At%
CK	63.69	83.94
OK	7.26	7.19
AlK	0.74	0.43
SK	1.34	0.66
ClK	0.80	0.36
FeK	26.16	7.41

Full screen element analysis



Matrix Correction: ZAF

Element	Wt%	At%
CK	14.79	29.73
OK	28.50	43.00
AlK	0.66	0.59
PK	7.05	5.50
FeK	48.99	21.18

Spot analysis on defect: confirms rust

Figure 70. EDX full screen and spot analysis of the sample.

Final observations for the YZ213 wire:

This wire shows to be clean and with good alignment of the nanotubes. It also shows far fewer nanotube entanglements. These conditions lead to good values of resistivity as seen for measurements for the wire using both the average and smallest diameters. This wire shall likely be iodine doped without any further purification steps.

2.2.4 CNT PURIFICATION

Purification was optimized to shorten purification time. In the original purification process, the sample is treated with 30 percent H_2O_2 for three days, but CNT is hydrophilic and the purification did not start until the H_2O_2 solution was able to infiltrate into CNT. It was found that 50 percent ethanol makes the CNT sample wettable to 30 percent H_2O_2 , so this additional ethanol wash step was added before H_2O_2 treatment. The CNT sample was rinsed with 50 percent ethanol for 10 - 20 seconds, then rinsed with DI water and dried on a hot plate at $120^\circ C$ for 10 minutes.

The CNT is then put in 30 percent H_2O_2 solution and mechanically stirred in a glass beaker. The 30 percent H_2O_2 solution immediately penetrates into CNT network. During purification, bubbles formed due to oxidation of carbon. After a few hours, bubbling from oxidation stopped, and then the CNT sample were rinsed with DI water for 3 minutes and recovered by filtration. The CNT formed a peelable membrane.

Acid treatment time was also shortened to 5 - 10 minutes when CNT was mechanically stirred in a 37 percent HCl solution. The solution turned yellowish due to Fe^{3+} ion formation. The samples were rinsed with DI water and collected by filtration. The yield was more than 90 wt percent.

2.2.5 CNT GROWTH

Objective: Growth of continuously spinnable CNT yarn of very high conductivity

Variables and effects:

Carbon source: Xylenes and ethanol were used as carbon sources. Ferrocene was used as a catalyst. In this study, we found that a 5-10 percent ethanol/xylene mixture and 3-6 percent ferrocene produced clean, spinnable material.

Temperature: Growth temperature varied from $1000 - 1200^\circ C$. It was found that higher temperature and 10:1 iron/sulfa ratio favor DWNT growth.

Carrier gas flow rate: The carrier gas flow rate varied from 0.5 - 8 SLM. A high gas flow rate of between 0.0883 - 0.1236 SCFM (2.5-3.5 SLM) reduced amorphous carbon contamination and favored spinnable material.

From SEM (**Figure 71** and **Figure 72**) and Raman (**Figure 73**) characterization, one can see that a spinnable CNT has been achieved by optimization. The yield of CNT was still low and not sufficient to produce a wire. Additional optimization is needed to improve the yield.

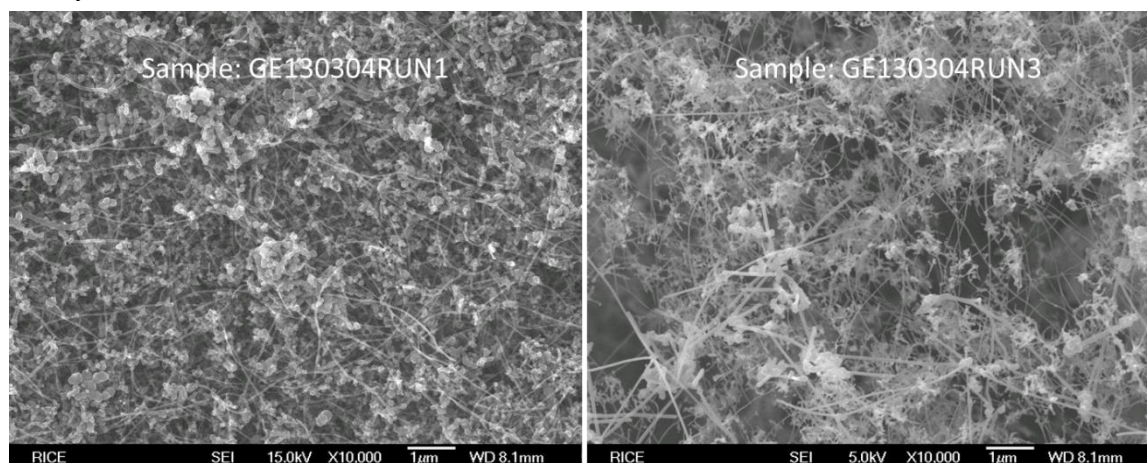


Figure 71. SEM micrograph of as grown CNT before optimization. Lots of particulate material from these runs.

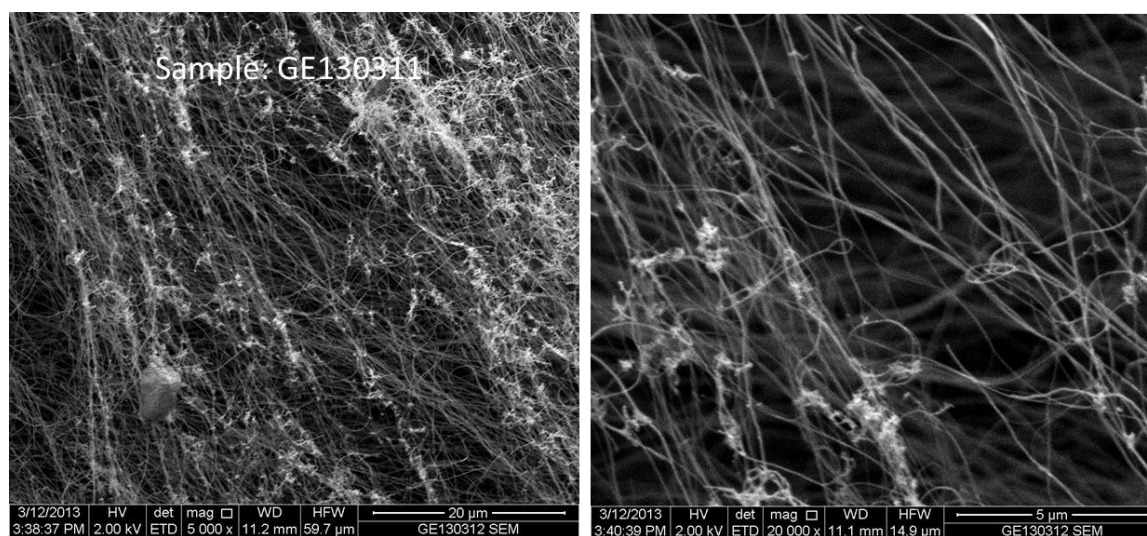


Figure 72. SEM micrograph of as grown CNT after optimization of carbon source, flow rate, and temperature. Particulate contamination is minimized.

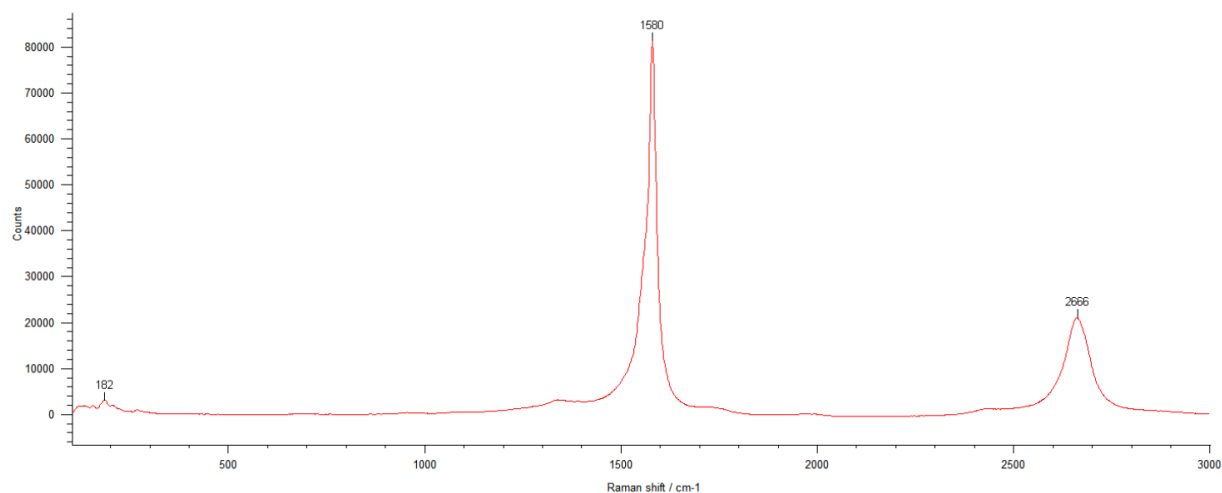


Figure 73. Raman spectrum of as grown CNT. The intense G peak and small D peak indicate the CNT are of good quality.

2.2.6 MANIPULATION AND CONTACT

[This section was taken from RPSEA Monthly Report 042513] Investigation of the bulk carbon nanotube (CNT) wire-polymer interface was refocused on SWNT buckypaper-polymer interface. The polymer of interest in this study is polystyrene (PS). Previous work examined solution casted PS, dissolved in toluene. However, the solvent evaporation rate was too fast. Therefore, a solvent blend (**Table 8**) was substituted. A solvent blend was used to apply the polymer to the nanotubes.

Table 8. Solvent blend composition.

Component	Weight percent (%)
MEK	14.7
MIBK	19.7
Xylene	24.3
Toluene	18.2
n-Butyl alcohol	17.3
1-Methoxy-2-propyl acetate	5.7

For the study, PS was dissolved in the solvent blend in two concentrations, 5 and 15 g/cL. The buckypaper was then dipped into the dissolved solution once, twice, and three times to compare coating coverage. **Figure 74** shows SEM micrographs of the surface and the edge of the buckypaper, uncoated. The CNT network was clearly visible, even at low magnifications.

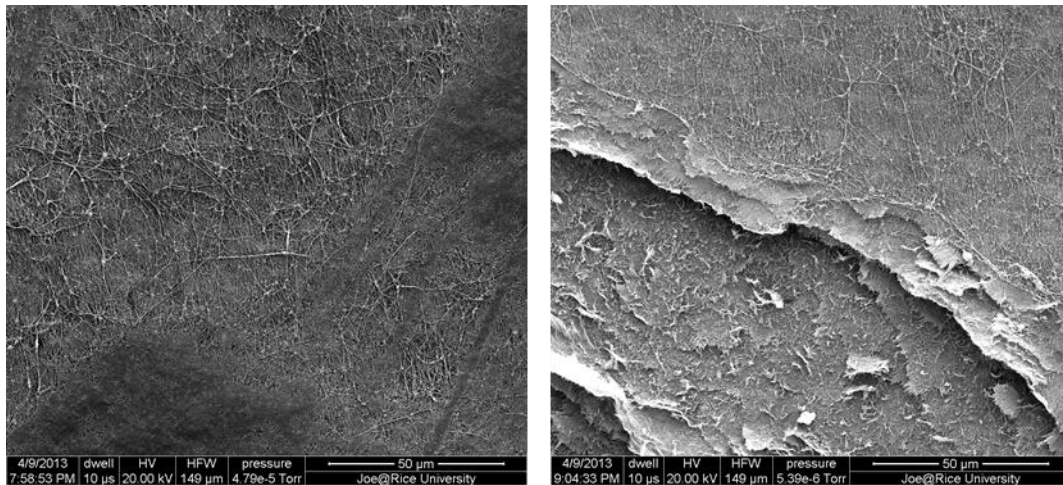


Figure 74. SEM micrograph of uncoated buckypaper surface (left) and edge (right).

First, the dissolved PS/solvent blend at 5 g/mL concentration was examined. When coated, the new solvent blend solution did not suffer from the porosity effects, as expected. However, it is evident that one coat did not provide sufficient coverage. **Figure 75** is an SEM micrograph of buckypaper coated one time with a 5 g/mL dissolved solution - the lighter areas are exposed buckypaper, as evidenced by the higher magnification image on the right.

When the buckypaper was coated twice (and three times), the paper was fully coated, and no nanotubes were exposed (**Figure 76**). This is indicated by the smooth, feature-free surface. While there have been many studies on individual CNT-polymer interface, we are most interested in the bulk CNT-polymer interface. SEM micrographs of the edges of the coated polymer were taken to infer the interface. The interface was prepared for imaging by sectioning after coating, to expose the CNTs of the buckypaper.

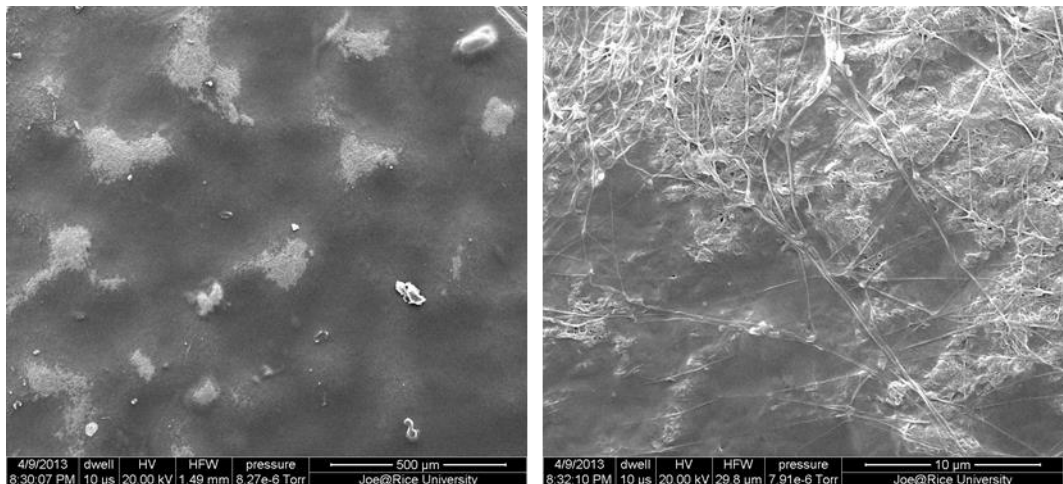


Figure 75. SEM micrograph of buckypaper coated one time with 5 g/cL dissolved PS solution in low mag (left) and higher mag (right).

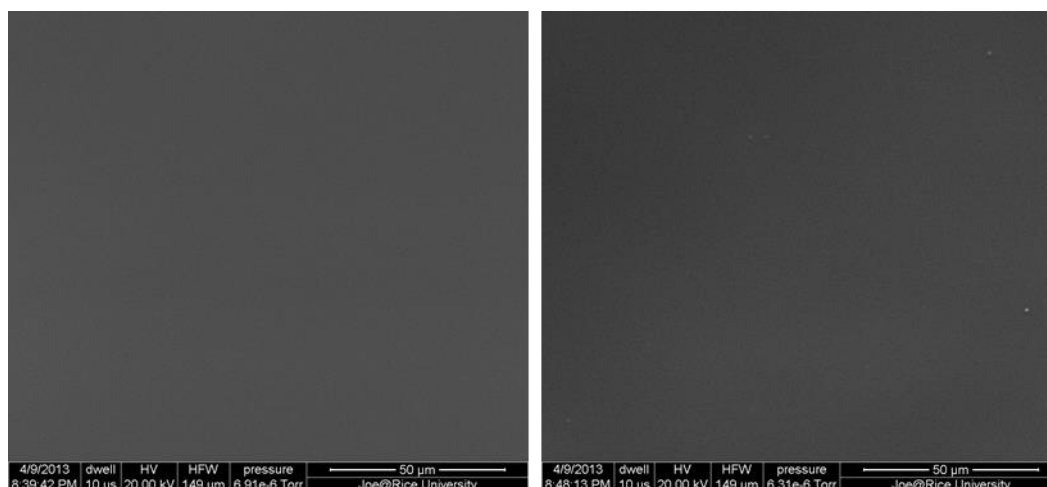


Figure 76. SEM micrograph of buckypaper coated twice (left) and three times (right) with 5 g/CL dissolved PS solution. Note the absence of any evidence of CNTs.

As seen in the two images in **Figure 77**, the interface between the bulk CNT of the buckypaper and the polymer is distinct. Indeed, in the image on the right, the reader can make out the polymer (foreground) – CNT (mid-plane) – polymer (background) layering. Clearly, as indicated by the stretching of the nanotubes, there is some interaction between the nanotubes and the polymer.

Next, we shall examine the dissolved PS/solvent blend at 15 g/mL concentration. Again, the surface coverage did not experience the porosity effects with the new solvent blend (**Table 8**), and indeed one coat of the dissolved polymer sufficiently covered the surface of the buckypaper. **Figure 78** is a micrograph of one, two, and three coats. The reader shall notice lack of surface porosity in all three.

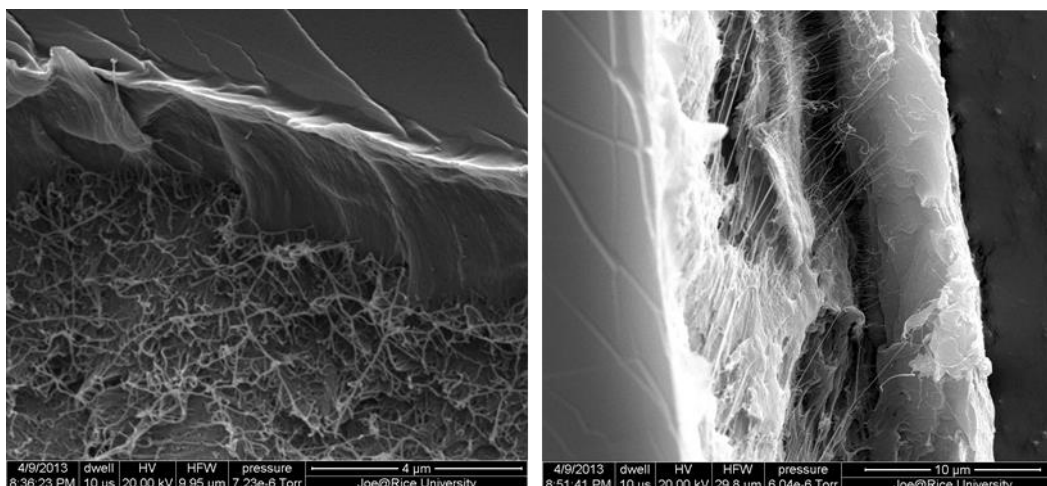


Figure 77. SEM micrograph of buckypaper/PS interface. Dissolved PS was a 5 g/CL concentration coated once (left) and three times (right).

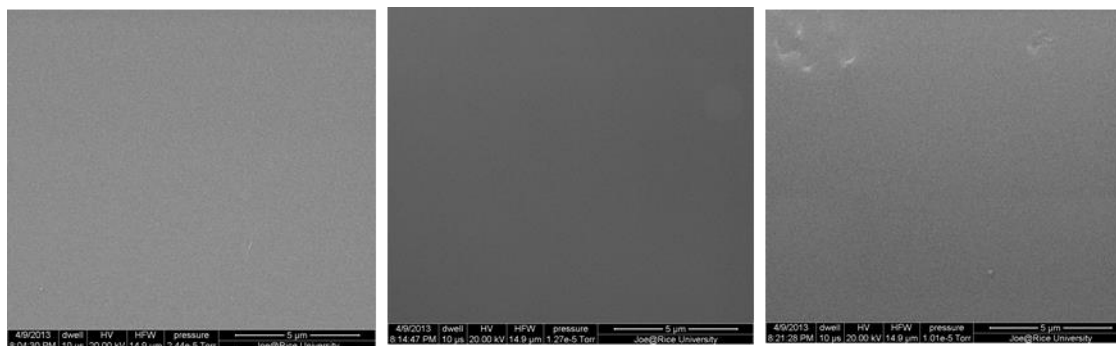


Figure 78. SEM micrographs of buckypaper coated with 15 g/cL dissolved PS, coated once (left), twice (middle) and three times (right).

When the edge is examined, there is evidence that the thickness of the polymer coating affects the examining cut. **Figure 79** is a micrograph of a prepared cut, where the reader can see an interaction between the nanotubes of the buckypaper and the polystyrene, but the layering is nonetheless distinct.

Additionally, we also studied the interface of thermally processed polystyrene and buckypaper. In this study, buckypaper was driven into molten polystyrene (260 °C), and excess molten polystyrene was folded over the paper. The sample was then placed back into the oven to allow the polystyrene to flow and relax into a non-stressed state. The result was buckypaper emerged in crystal polystyrene. The sample was cut using a diamond saw and the cross-section was prepared for imaging. **Figure 80** demonstrates the buckypaper having little to no interaction with the polystyrene. Indeed, when looking at the interface there is a very discrete gap between the two.

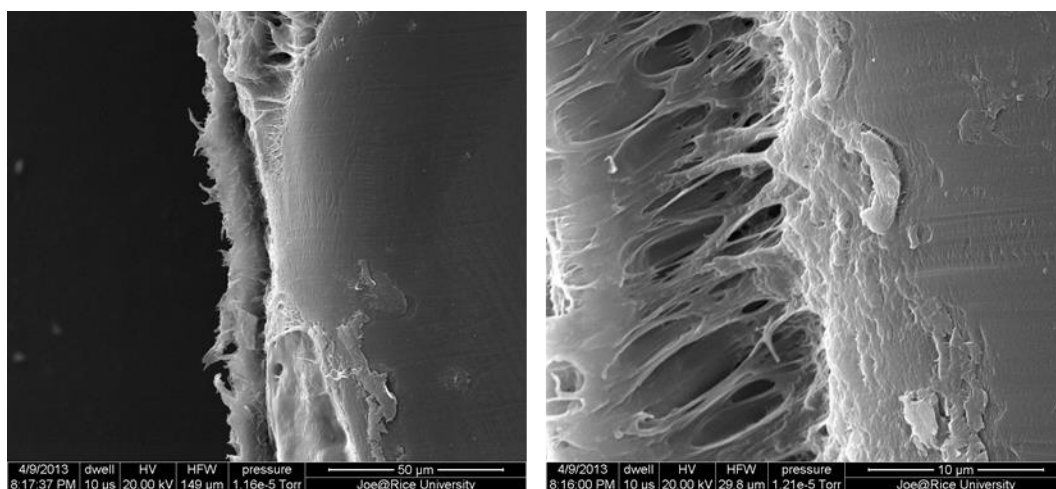


Figure 79. SEM micrograph of a prepared edge of buckypaper coated twice with 15 g/cL dissolved PS.

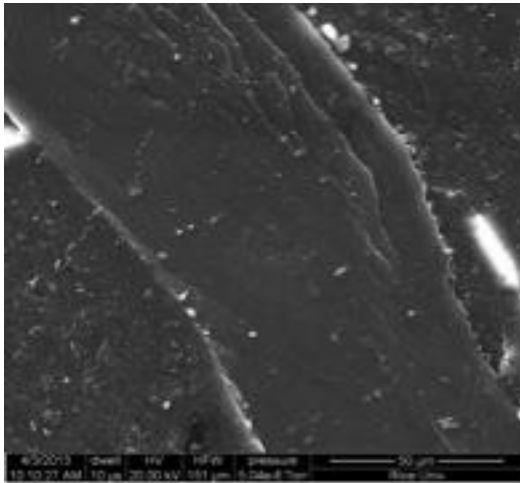


Figure 80. SEM micrograph of buckypaper sandwiched between thermally processed polystyrene.

Summary:

1. The new solvent blend resulted in a smooth polystyrene polymer coating.
2. One coating of a 5 g/cL dissolved solution did not sufficiently coat the buckypaper.
3. Subsequent coating using the 5 g/cL dissolved solution provided full coverage.
4. One coating of a 15 g/cL dissolved solution fully covered the buckypaper.
5. The interface of a buckypaper and dissolved polymer processed via solution casting is distinct, though with some interaction.
6. The interface of thermally processed polystyrene and buckypaper is distinct, with no obvious interaction.

2.2.7 IMPACT TO PRODUCERS

Thus far in Year 1, the research team has achieved resistivity of $10^{-5} \Omega \cdot \text{cm}$ with several carbon nanotube wires. Years 2 and 3 shall allow the team to further develop continuous processes and perform limited production to generate a prototype umbilical. A working prototype would allow risk-averse entities to more fully participate in the product development. The DWNT bare and jacketed conductor has many applications. In this project, we have restricted our focus to the oil and gas offshore market. We not only expect to reach the $10^{-6} \Omega \cdot \text{cm}$ target by Year 3, but anticipate the wire, cable to be lightweight with mechanical properties better than steel. Some oil and gas producers are keenly interested in the strength aspects of the DWNT conductor. The team has approached or been approached by several companies. These include Petrobras, EMGS, and Southwire. All have product needs and these vary between companies. We fully expect the impact of this product to be far reaching not only in the oil and gas market but also in the entire power transmission arena. The question we field primarily is “How much shall it cost?” Figure 81 shows our current cost projections of the product of this effort (LiteWire) as compared to Cu underground and Al overhead transmission lines. **Table 9** compares our conductor to Cu and Al, as well as to the literature. Our product is competitive with Cu underground cable but not reasonable as an Al overhead line replacement.

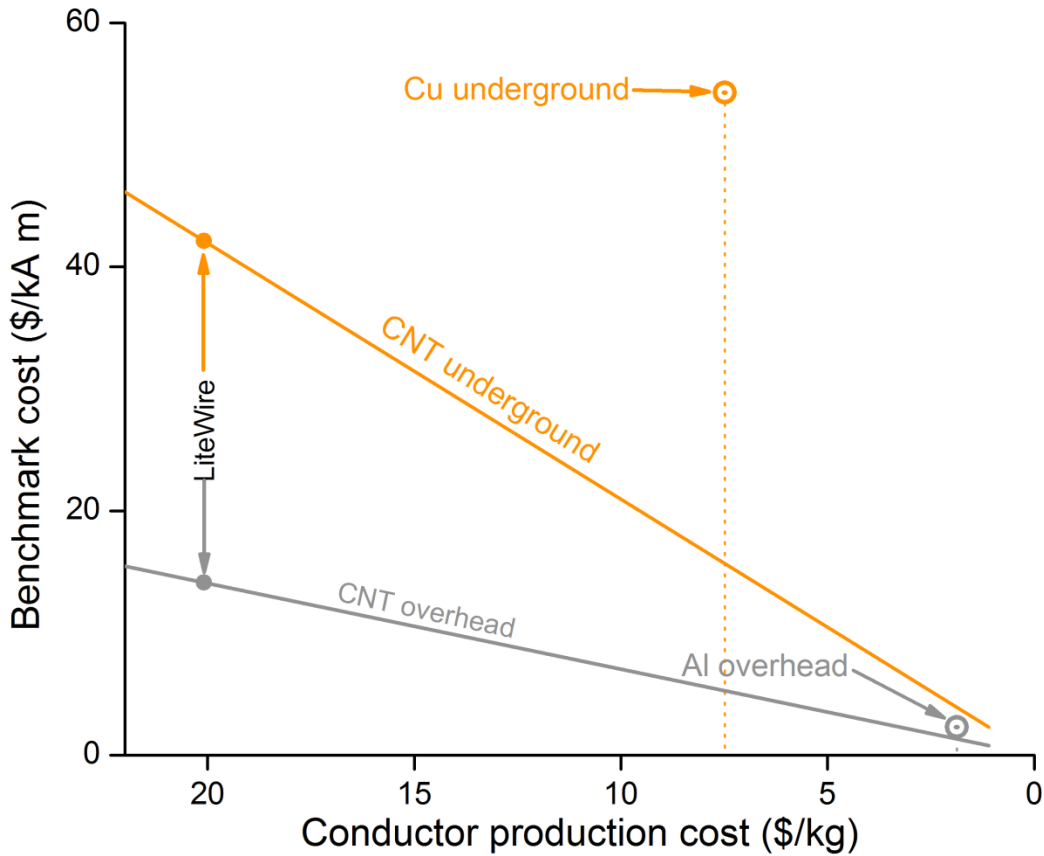


Figure 81. Benchmark cost projection of the conductor as a function of production cost.

Table 9. Literature survey and calculated benchmark cost for CNT-based conductors.

Conductor Type	ρ	Specific conductivity	75 °C Benchmark	90 °C Benchmark
-	$\Omega \cdot \text{cm}$	$\text{S} \cdot \text{m}^2 / \text{kg}$	$\$/\text{kA} \cdot \text{m}$	$\$/\text{kA} \cdot \text{m}$
Al	2.82×10^{-6}	6.65×10^3		54.30
Cu	1.68×10^{-6}	1.30×10^4	2.31	
SWNT[18]	3.33×10^{-4}	1.00×10^3	252	763
MWNT[19]	7.40×10^{-5}	4.50×10^3	56	169
SWNT[20]	1.00×10^{-3}	3.33×10^2	757	2290
SWNT[21]	2.50×10^{-4}	1.33×10^3	189	572
SWNT[22]	1.00×10^{-2}	3.33×10^1	7570	22900
MWNT[13]	1.20×10^{-4}	2.77×10^3	91.20	276
SWNT[23]	1.82×10^{-4}	1.83×10^3	138	416
SWNT[24]	3.33×10^{-4}	1.00×10^3	252	763
SWNT[25]	1.50×10^{-1}	2.22	114000	381000
SWNT[26]	7.10×10^{-1}	4.69×10^{-1}	537000	1800000
SWNT[27]	2.00×10^{-4}	1.67×10^3	151	458
SWNT[28]	3.30×10^{-4}	1.01×10^3	250	755

MWNT[29]	3.30×10^{-3}	1.01×10^2	2500	7550
MWNT[30]	2.40×10^{-3}	1.39×10^2	182	5490
MWNT[31]	1.10×10^{-3}	3.03×10^2	833	2520
DWNT[32]	2.00×10^{-4}	1.67×10^3	151	458
Not specified[33]	7.69×10^{-5}	4.33×10^3	58.20	176
DWNT[5]	5.00×10^{-5}	7.14×10^3	35.30	107
DWNT[5]	1.50×10^{-5}	2.02×10^4	12.50	37.80

2.2.8 TECHNOLOGY TRANSFER EFFORTS

The technology transfer effort for year 1 has been substantial. The RPSEA specific forums are as follows:

- RPSEA 2012 UDW Technology Conference – September 19, 2012
- Subsea Systems TAC Meeting – January 22, 2013
- Offshore Technology Conference presentation – May 08, 2013
- Subsea Systems TAC Meeting – May 28, 2013

In addition, the NanoRidge -Rice team members have had several discussions with Petrobras and Southwire. Several additional presentations were made where this project was highlighted. They are:

- Enrique V. Barrera, “Nanotube Conductor”, Invited Talk, Tec de Monterrey, Monterrey, Mexico.
- Mexico
- Brazil (two talks)
- EMGS
- Barrera, “Nanotube Conductor”, Depto de Química – ICEx, Universidade Federal de Minas Gerais, (UFMG) Campus Pampulha - C.P. 702, 31270-901 Belo Horizonte, MG-Brazil, December 17, 2012.
- E. V. Barrera, “Nanotube Conductor”, Petrobras, Rio de Janeiro, Brazil, December 18, 2012.
- E. V. Barrera, “Nanotube Conductor”, Telecom meeting with EMGS, March 23, 2013.
- Eric Lange, Adrian Yao, Liehui Ge, and E. V. Barrera, “A Carbon Nanotube Based Electrical Conductor,” poster for Rice Undergraduate Research Symposium (RURS), April 12, 2013.
- Luke Boyer and E. V. Barrera, “Modifying Asphalt Bitumen with Carbon Nanotubes,” TechConnect Conference, Washington, DC, May 14, 2013.
- E. V. Barrera and Chris Dyke, “Southwire Meeting: Research at Rice University for the Polymer Nanotube Umbilical Project”, Carrollton, GA, June 12, 2013. Others in attendance for this meeting were Chris Lundberg (NanoRidge) and Liehui Ge (Rice).

2.2.9 CONCLUSIONS

For Phase I, the NanoRidge team has been successful at meeting the first year gate objectives. Several wire samples (four) have been produced with $10^{-5} \Omega \cdot \text{cm}$ electrical resistivity. In Year 1 the wire diameters have been increased and the wire lengths have been increased beyond that of the first laboratory scale wires reported in Nature Scientific Reports [5]. The following items are outcomes from Phase I:

- A lab scale production furnace is situated at NanoRidge and outfitted for continuous wire formation in a vertical configuration.
- A number of improvements have been made to the conduction measurement method (four-point probe) to ensure accuracy in the measurements and to provide for measurement for a larger range of wire treatments (i.e., higher temperature).
- Diameters and lengths have been increased by an order of magnitude for the wires with $10^{-5} \Omega \cdot \text{cm}$ resistivity.
- Small diameter wires still tend to show better conductivity properties because they are likely processed with more optimal properties but these properties are being translated to larger diameter wires.
- Acid washing of the nanotubes seemed to reduce resistivity but primarily led to improved doping which leads to a lower wire resistivity.
- Methods to reduce purification time have been identified.

Numerous members of the Rice portion of the team have been trained to characterize the wire samples. More training shall be conducted in Phase II so that the team is fully prepared to handle samples from NanoRidge.

2.2.10 RECOMMENDATIONS

Since the deliverable has been achieved, the NanoRidge team recommends this project transitions to Phase II. Year 2 provides the resources necessary to produce the wire continuously and streamline the approach. Continuous production includes CNT formation, wire spooling, purification, doping and drawing. In addition, it provides resources to our subcontractor DUCO for wire jacketing. Technology transfer efforts and extensive testing shall provide the team with additional avenues to impact producers. **Appendix A** describes Year 2 research efforts as they relate to Phase I lessons learned.

3. FIGURES AND TABLES

Below are the lists of figures and tables.

List of Figures

Figure 1. Tree structure view of the Phase I tasks and subtasks.....	9
Figure 2. Engineering schematic of CM Furnace 1000K-0412-36-3Z-HTFS-240V-1PH.	11
Figure 3. Schematic of furnace in the horizontal.	12
Figure 4. A DWNT and an MWNT [9].....	13

Figure 5.	SWNT of distinct chiralities with band structure for each. Metallic SWNT have no band gap.....	14
Figure 6.	Two-point measurement setup.....	19
Figure 7.	Four probe configuration.	19
Figure 8.	Gold-plated four-point setup.	20
Figure 9.	Wire secured by silver paint.	20
Figure 10.	Basic Cu resistance measurement setup.	21
Figure 11.	In-situ resistance measurement setup. A. Wire setup constructed to obtain resistance reading from attached sample. B. Empty chamber ready for wire sample, vacuum, and iodine crystals. C. Sketch of iodine doping measurement system.	22
Figure 12.	Cu wires with surface contamination (green) from iodine doping.....	22
Figure 13.	A typical Raman spectrum of carbon nanotube.	23
Figure 14.	Fluorescence from impurity.....	24
Figure 15.	SEM sample of THAP002 at 50,000x magnification. Interior reveals dense tubes in alignment with an outer oxidation shell covering the bare wire.	25
Figure 16.	Example of EDX spectrum.	26
Figure 17.	TGA of THB sample shown above. Different drops correspond to the release of water, amorphous carbon, and other impurities.	27
Figure 18.	SEM micrographs of 032513B2 wire. Carbon nanotubes can be easily identified from SEM but particular contaminants are also seen.	34
Figure 19.	SEM micrographs of 032513B2 wire after purification and iodine doping. Carbon nanotubes can be easily identified from SEM but there is a crust of impurities covering part of the wire surface.....	35
Figure 20.	EDX spectrum of 032513B2 wire after ethanol wash. Besides carbon, there is also significant amount of iron and iodine dopant.	35
Figure 21.	EDX spectrum of 032513B2 wire heat treatment in air. Besides carbon, there is also significant amount of iron oxide. Iodine peak is not visible.	36
Figure 22.	Raman spectrum of 032513 wire with 633 nm laser. The intense fluorescence from impurity makes interpretation of the spectrum difficult.	36
Figure 23.	Raman spectra of 032513B2 with 514 nm laser.....	37
Figure 24.	032513B2 wire mounted on four-probe setup.....	37
Figure 25.	GETH130408-1 wire mounted on four-probe setup.....	38
Figure 26.	GETH130408-2 wire mounted on four-probe setup.....	39
Figure 27.	SEM micrographs of YZ207 wire between resistance measurement nodes.	39
Figure 28.	YZ207 full length.	39
Figure 29.	Raman spectra of YZ207 wire.	40
Figure 30.	EDX spectrum of YZ207 wire. It shows that the sample is free of iron impurity. Minimal amount of chlorine is present due to previous purification step.....	40
Figure 31.	SEM micrographs of YZ207 wire.	41
Figure 32.	EDX spectrum of TABP001.	42
Figure 33.	SEM micrographs of TABP001.....	42
Figure 34.	EDX spectrum of TABP002.	43

Figure 35. SEM of TABP002.....	44
Figure 36. Raman spectrum of THAP wire with 514 nm laser.	45
Figure 37. Raman spectrum of THAP wire	45
Figure 38. EDX spectrum of THAP.....	46
Figure 39. SEM of THAP001 full length.	46
Figure 40. SEM micrographs of THAP001 before acid doping.....	46
Figure 41. SEM micrographs of THAP001 after acid doping.	47
Figure 42. SEM micrographs of THAP001 after iodine doping.	48
Figure 43. Full Wire Image of THAP002.	48
Figure 44. SEM micrographs of THAP002.	49
Figure 45. EW wire segment was introduced to H ₂ O ₂ . Prior to soaking in H ₂ O ₂ , the wire did not wet. However, after 72 hours of soaking, the wire wet with water and HCl.	50
Figure 46. Raw EW wire in H ₂ O ₂ . CO ₂ bubbles were seen coming from the wire earlier in the process.	50
Figure 47. Raman spectra of the samples at 514 nm laser are (Blue) for sample RAW, (Black) for purified (EW2E), (Red) for EW1A sample heat-treated for 30 minutes and (Green) for EW2F sample heat-treated for 5 hours.	51
Figure 48. EDX of RAW sample with elemental composition shown.	51
Figure 49. EDX of EW2F sample.	52
Figure 50. EDX point elemental composition and a corresponding micrograph.....	52
Figure 51. SEM images of the RAW sample before any treatments.	53
Figure 52. SEM images of purified samples EW2c and EW2d. Both Samples purified with 72 hr H ₂ O ₂ 30%; 24 hr 37% HCl; SEM 50,000x Magnification.	53
Figure 53. SEM images of EW1A sample. Purified and 30 min heat-treated is highly densified (bottom right and left). Still some particulate contamination (top right) was observed.....	54
Figure 54. SEM images of sample EW2F-Purified and -heat-treated for 5 hours.	54
Figure 55. Wires of EW1A and EW2F as seen from SEM images.....	55
Figure 56. Raman spectra of sample YZ213 at 514 nm laser.....	56
Figure 57. Raman spectra of sample YZ213 at 633 nm laser.....	56
Figure 58. Raman in RBM at 514 nm laser.....	57
Figure 59. Raman in RBM at 633 nm laser.....	57
Figure 60. Overview of the representative of the sample wire through SEM images.	58
Figure 61. SEM images of the wire with magnifications 1,000x, 5,000x and 20,000x from top left.	59
Figure 62. SEM images with magnifications 1,000x, 5,000x and 20,000x from top left.	60
Figure 63. SEM images with magnifications 1,000x, 5,000x and 20,000x from top left.	61
Figure 64. SEM image with magnification 1,000x.....	62
Figure 65. SEM image showing cracked rust patch.	62
Figure 66. SEM image showing unidentified impurities.	62
Figure 67. EDX analysis of the sample with elemental composition.....	63
Figure 68. EDX analysis of the sample with elemental composition.....	63
Figure 69. EDX analysis of the sample with elemental composition.....	64

Figure 70.	EDX full screen and spot analysis of the sample.....	64
Figure 71.	SEM micrograph of as grown CNT before optimization. Lots of particulate material from these runs.....	66
Figure 72.	SEM micrograph of as grown CNT after optimization of carbon source, flow rate, and temperature. Particulate contamination is minimized.	66
Figure 73.	Raman spectrum of as grown CNT. The intense G peak and small D peak indicate the CNT are of good quality.	67
Figure 74.	SEM micrograph of uncoated buckypaper surface (left) and edge (right).	68
Figure 75.	SEM micrograph of buckypaper coated one time with 5 g/cL dissolved PS solution in low mag (left) and higher mag (right).	68
Figure 76.	SEM micrograph of buckypaper coated twice (left) and three times (right) with 5 g/cL dissolved PS solution. Note the absence of any evidence of CNTs.....	69
Figure 77.	SEM micrograph of buckypaper/PS interface. Dissolved PS was a 5 g/cL concentration coated once (left) and three times (right).....	69
Figure 78.	SEM micrographs of buckypaper coated with 15 g/cL dissolved PS, coated once (left), twice (middle) and three times (right).	70
Figure 79.	SEM micrograph of a prepared edge of buckypaper coated twice with 15 g/cL dissolved PS.....	70
Figure 80.	SEM micrograph of buckypaper sandwiched between thermally processed polystyrene.	71
Figure 81.	Benchmark cost projection of the conductor as a function of production cost.	72

List of Tables

Table 1.	List of project participants and their characterization method training.	17
Table 2.	Resistivity of representative samples studied in Phase I.	29
Table 3.	Treatments done to representative samples studied in Phase I.	30
Table 4.	Wire Diameters.	31
Table 5.	Descriptions of the sample numbers for samples identified in Tables 2-4.	31
Table 6.	Sample naming scheme for NanoRidge samples given to Rice on spools.	32
Table 7.	Samples made from the EW Wire.	50
Table 8.	Solvent blend composition.....	67
Table 9.	Literature survey and calculated benchmark cost for CNT-based conductors.....	72

4. REFERENCES

The references in this document are listed in this section.

1. RPSEA Project Number 1302, "Ultrahigh Conductivity Umbilicals," Final Report, **2010**.

2. E. V. Barrera, D. K. Chakravarthi, "Electric Field-Vacuum Spray Process to Produce Highly Conductive Carbon nanotube-Polymer Composite Thin Films, Fibers, and Wires," US Patent Application No. 13/640,028 (**2010**).
3. E. V. Barrera, P. M. Ajayan, Yao Zhao, and J. Wei, "DWNT Fibers of a Better Specific Conductivity than Copper and Aluminum," PCT No. PCT/US2012/026982 (**2012**).
4. E. V. Barrera, P. M. Ajayan, and Padraig Moloney, CNT with Antimony Pentafluoride Intercalate," PCT No. PCT/US2012/026949 (**2012**).
5. Zhao, Y.; Wei, J.; Vajtai, R.; Ajayan, P. M.; Barrera, E. V. "Iodine doped carbon nanotube cables exceeding specific electrical conductivity of metals." *Scientific Reports* **2011**, 1,1-5.
6. Behabtu, N.; Young, C. C.; Tsentelovich, D. E.; Kleinerman, O.; Wang, X.; Ma, A. W.; Bengio, E. A.; ter Waarbeek, R. F.; de Jong, J. J.; Hoogerwerf, R. E.; Fairchild, S. B.; Ferguson, J. B.; Maruyama, B.; Kono, J.; Talmon, Y.; Cohen, Y.; Otto, M. J.; Pasquali, M. "Strong, light, multifunctional fibers of carbon nanotubes with ultrahigh conductivity." *Science* **2013**, 339, 182-186.
7. Li, Y.-L.; Kinloch, I. A.; Windle, A. H. "Direct Spinning of Carbon Nanotube Fibers from Chemical Vapor Deposition Synthesis." *Science* **2004**, 304, 276-278.
8. Wei, J.; Jiang, B.; Wu, D.; Wei, B., Large-Scale Synthesis of Long Double-Walled Carbon Nanotubes. *The Journal of Physical Chemistry B* **2004**, 108 (26), 8844-8847.
9. http://www.exaenc.com/product/en_pro6_1.asp. Accessed 06/16/2013
10. Dresselhaus, M. S.; Dresselhaus, G.; Eklund, P. C., *Science of fullerenes and carbon nanotubes*. Academic Press: San Diego, 1996; p xviii, 965 p.
11. Searfass, M. T. "Carbon nanotube-based electrical connectors. US Patent no. US20100144205A1(2011).
12. Wang, Y.; Kim, M. J.; Shan, H.; Kittrell, C.; Fan, H.; Ericson, L. M.; Hwang, W. F.; Arepalli, S.; Hauge, R. H.; Smalley, R. E., Continued growth of single-walled carbon nanotubes. *Nano Lett* **2005**, 5 (6), 997-1002.
13. Li, Y.-L.; Kinloch, I. A.; Windle, A. H., Direct Spinning of Carbon Nanotube Fibers from Chemical Vapor Deposition Synthesis. *Science* **2004**, 304 (5668), 276-278.
14. White, C. T.; Todorov, T. N., Carbon nanotubes as long ballistic conductors. *Nature* **1998**, 393 (6682), 240-242.
15. Buldum, A.; Lu, J. P., Contact resistance between carbon nanotubes. *Physical Review B* **2001**, 63 (16), 161403.
16. Hsu, W. K.; Chu, S. Y.; Muñoz-Picone, E.; Boldú, J. L.; Firth, S.; Franchi, P.; Roberts, B. P.; Schilder, A.; Terrones, H.; Grobert, N.; Zhu, Y. Q.; Terrones, M.; McHenry, M. E.; Kroto, H. W.; Walton, D. R. M., Metallic behaviour of boron-containing carbon nanotubes. *Chem. Phys. Lett.* **2000**, 323 (5-6), 572-579.

17. Chun, K.-Y.; Lee, C. J., Potassium Doping in the Double-Walled Carbon Nanotubes at Room Temperature. *The Journal of Physical Chemistry C* **2008**, *112* (12), 4492-4497.
18. Lee, R. S.; Kim, H. J.; Fischer, J. E.; Thess, A.; Smalley, R. E., Conductivity enhancement in single-walled carbon nanotube bundles doped with K and Br. *Nature* **1997**, *388* (6639), 255-257.
19. Wei, B.; Spolenak, R.; Kohler-Redlich, P.; Ruhle, M.; Arzt, E., Electrical transport in pure and boron-doped carbon nanotubes. *Applied Physics Letters* **1999**, *74* (21), 3149-3151.
20. Sreekumar, T. V.; Liu, T.; Kumar, S.; Ericson, L. M.; Hauge, R. H.; Smalley, R. E., Single-Wall Carbon Nanotube Films. *Chemistry of Materials* **2002**, *15* (1), 175-178.
21. Zhou, W.; Vavro, J.; Guthy, C.; Winey, K. I.; Fischer, J. E.; Ericson, L. M.; Ramesh, S.; Saini, R.; Davis, V. A.; Kittrell, C.; Pasquali, M.; Hauge, R. H.; Smalley, R. E., Single wall carbon nanotube fibers extruded from super-acid suspensions: Preferred orientation, electrical, and thermal transport. *Journal of Applied Physics* **2004**, *95* (2), 649-655.
22. Badaire, S. p.; Pichot, V.; Zakri, C. c.; Poulin, P.; Launois, P.; Vavro, J.; Guthy, C.; Chen, M.; Fischer, J. E., Correlation of properties with preferred orientation in coagulated and stretch-aligned single-wall carbon nanotubes. *Journal of Applied Physics* **2004**, *96* (12), 7509.
23. Geng, H.-Z.; Kim, K. K.; So, K. P.; Lee, Y. S.; Chang, Y.; Lee, Y. H., Effect of Acid Treatment on Carbon Nanotube-Based Flexible Transparent Conducting Films. *Journal of the American Chemical Society* **2007**, *129* (25), 7758-7759.
24. Skákalová, V.; Kaiser, A. B.; Dettlaff-Weglikowska, U.; Hrnčariková, K.; Roth, S., Effect of Chemical Treatment on Electrical Conductivity, Infrared Absorption, and Raman Spectra of Single-Walled Carbon Nanotubes. *The Journal of Physical Chemistry B* **2005**, *109* (15), 7174-7181.
25. Steinmetz, J.; Glerup, M.; Paillet, M.; Bernier, P.; Holzinger, M., Production of pure nanotube fibers using a modified wet-spinning method. *Carbon* **2005**, *43* (11), 2397-2400.
26. Kozlov, M. E.; Capps, R. C.; Sampson, W. M.; Ebron, V. H.; Ferraris, J. P.; Baughman, R. H., Spinning Solid and Hollow Polymer-Free Carbon Nanotube Fibers. *Advanced Materials* **2005**, *17* (5), 614-617.
27. Ericson, L. M.; Fan, H.; Peng, H.; Davis, V. A.; Zhou, W.; Sulpizio, J.; Wang, Y.; Booker, R.; Vavro, J.; Guthy, C.; Parra-Vasquez, A. N. G.; Kim, M. J.; Ramesh, S.; Saini, R. K.; Kittrell, C.; Lavin, G.; Schmidt, H.; Adams, W. W.; Billups, W. E.; Pasquali, M.; Hwang, W.-F.; Hauge, R. H.; Fischer, J. E.; Smalley, R. E., Macroscopic, Neat, Single-Walled Carbon Nanotube Fibers. *Science* **2004**, *305* (5689), 1447-1450.

28. Jang, E. Y.; Kang, T. J.; Im, H.; Baek, S. J.; Kim, S.; Jeong, D. H.; Park, Y. W.; Kim, Y. H., Macroscopic Single-Walled-Carbon-Nanotube Fiber Self-Assembled by Dip-Coating Method. *Advanced Materials* **2009**, *21* (43), 4357-4361.
29. Zhang, M.; Atkinson, K. R.; Baughman, R. H., Multifunctional Carbon Nanotube Yarns by Downsizing an Ancient Technology. *Science* **2004**, *306* (5700), 1358-1361.
30. Zhang, X.; Li, Q.; Tu, Y.; Li, Y.; Coulter, J. Y.; Zheng, L.; Zhao, Y.; Jia, Q.; Peterson, D. E.; Zhu, Y., Strong Carbon-Nanotube Fibers Spun from Long Carbon-Nanotube Arrays. *Small* **2007**, *3* (2), 244-248.
31. Liu, K.; Sun, Y.; Lin, X.; Zhou, R.; Wang, J.; Fan, S.; Jiang, K., Scratch-Resistant, Highly Conductive, and High-Strength Carbon Nanotube-Based Composite Yarns. *ACS Nano* **2010**, *4* (10), 5827-5834.
32. Zhong, X.-H.; Li, Y.-L.; Liu, Y.-K.; Qiao, X.-H.; Feng, Y.; Liang, J.; Jin, J.; Zhu, L.; Hou, F.; Li, J.-Y., Continuous Multilayered Carbon Nanotube Yarns. *Advanced Materials* **2010**, *22* (6), 692-696.
33. Alvarenga, J.; Jarosz, P. R.; Schauerman, C. M.; Moses, B. T.; Landi, B. J.; Cress, C. D.; Raffaele, R. P., High conductivity carbon nanotube wires from radial densification and ionic doping. *Applied Physics Letters* **2010**, *97* (18), 182106-3.

5. LIST OF ACRONYMS AND ABBREVIATIONS

Below is a table listing the acronyms and abbreviations included in this document.

Al	Aluminum
AQW	Armchair Quantum Wire
C	Characterization
CFM	Cubic Feet per Minute
CNT	Carbon Nanotubes
Cu	Copper
CVD	Chemical Vapor Deposition
D	Diameter
DFG	Dry Flow Growth
DUCO	DUCO, Inc.
DWNT	Double Walled Carbon Nanotubes
E&P	Exploration and Production
EDX	Energy-Dispersive X-Ray Spectroscopy
EH&S	Environmental Health & Safety
I	Current
IP	Intellectual Property
MWNTS	Multi-Walled Carbon Nanotubes
NanoRidge	NanoRidge Materials, Inc.
NIST	National Institute of Standard and Technology
OTC	Offshore Technology Conference
PAC	Project Advisory Committee
PMP	Project Management Plan

PNU®	Polymer Nanotube Umbilical
Psig	Pounds per square inch gauge
Raman	Raman Spectroscopy
RFP	Request for Proposal
Rice	Rice University
RP1302	RPSEA Project 1302
RP4302	RPSEA Project 4302
RPM	Revolution per minute
RPSEA	Research Partnership to Secure Energy for America
SCFM	Standard Cubic Feet per Minute
SEM	Scanning Electron Microscope
SLM	Standard Liter per Minute
SWNT	Single Walled Carbon Nanotubes
TAC	Technical Advisory Committee
Technip	Technip, USA
TEM	Transmission Electron Microscope
TGA	Thermal Gravimetric Analysis
UDW	Ultra-Deepwater

6. APPENDICES

The appendices are:

- **Appendix A – Phase II Next Steps**

APPENDIX A

Phase II Next Steps

NanoRidge Materials, Inc. – 10121-4302-01

Ultra-High Conductivity Umbilicals: Polymer Nanotube Umbilicals (PNUs)

1. PHASE I SUMMATION

The technical team includes NanoRidge Materials (Prime), Rice University, and Cambridge University. In Phase I, the focus of the technical team was primarily, achievement of the Phase I deliverable, evidence of a conductor with resistivity between 1×10^{-5} and $9 \times 10^{-5} \Omega \cdot \text{cm}$, and secondarily, continuous production of a DWNT wire. Previous to the Project Kick-Off meeting, a Statement of Work was negotiated between the Department of Energy and NanoRidge. This necessitated the primary focus of Phase I. The relevant portion of the Statement of Work is reproduced below:

“

D. DELIVERABLES OF THE DEFINED EFFORT

This is a complete listing of all contractual deliverables for this contract:

1. **Project Management Plan draft** - due in MS Word format within thirty (30) calendar days of the Project Kick-Off Meeting.
2. **Project Management Plan** - due within fifteen (15) calendar days after receipt of RPSEA's comments.
3. **Technology Status Report** - due within thirty (30) calendar days of the Project Kick-Off Meeting.
4. **Technology Transfer Plan** - due within thirty (30) calendar days of the Project Kick-Off Meeting.

Technical Deliverables:

Phase I:

1. The product deliverable shall be **evidence of a conductor** with resistivity between 1×10^{-5} and $9 \times 10^{-5} \Omega \cdot \text{cm}$. It shall be due prior to the Phase I End of Performance Period.
2. **Phase 1 Final Technical Report Draft** in MS Word format, to include all Task 5.0 project activity, shall be submitted 45 calendar days prior to the Phase I End of Performance Period.
3. **Phase I Final Technical Report** shall be submitted to RPSEA 14 calendar days after receiving comments on draft report and prior to the End of the Phase I End of Performance Period.
4. **Phase I Final Presentation materials** shall be submitted to RPSEA within 14 calendar days of the Phase I Final Presentation, but prior to the Phase I End of Performance

Period according to RPSEA requirements.

“

In addition to satisfaction of the deliverable, several key observations were made and processes developed. The ones critical to the success of Phase II are bulleted below:

- The Rice team was assembled including new hires. Many of the team members were trained on advanced analytical techniques. The group in total is trained on all of the analytical techniques necessary to complete the 3 year project.
- Purification techniques were assessed and their efficacy determined. We have the knowledge to purify carbon nanotube wires and place the purification in line with the production furnace.
- Doping was investigated, and two techniques were identified. Doping gives an order of magnitude increase in conductivity. This is a broad generalization, however, if the as-produced wire is $10^{-5} \Omega \cdot \text{cm}$, one may expect to achieve $10^{-6} \Omega \cdot \text{cm}$ by combining purification and doping techniques. Both shall be added in line with the furnace if required to achieve the Phase II and III goals.
- Polymer jacketing was explored. This was a minor investigation, but shall benefit Phase II.
- The production furnace was put in place at NanoRidge. Peripherals were added. The total system was procured not leased. We remained at or under budget for the entire system.
- Two spinning or continuous production strategies were ruled out. They were 1) stringing a take-up system by hand while the furnace is in a horizontal configuration (none of the attempts led to continuous operation nor showed promise), and 2) placing a spindle in the hot end of the furnace. The “spindle” approach allowed the team to make wire and optimize growth. The material was of high quality, but the wires were not.
- A spinning strategy was decided after the previous two were investigated and a Technical Review was completed. The decided spinning configuration has led to promising wire formation. The system shall be completed by the end of Phase I or early Phase II.

In brief, carbon nanotube wire was formed and low resistivity was achieved in Phase I. Several prerequisite research topics were investigated with many of them completed. We achieved our primary aim, and the other key focus, continuous wire formation, has yielded wire of good quality. Continuous wire formation is the exclusive focus of NanoRidge from now until the process is robust and reproducible.

2. PHASE II NEXT STEPS

The current, agreed Phase II Gantt (**Figure A-1**) includes efforts on continuous wire production. This is the current focus of NanoRidge and is to be completed by the end of September. The remainder of the tasks includes a) integrating key process into continuous production, b) extensive wire characterization and testing, and c) engineering processes to further the

prototype development. DUCO shall be added to the Phase I team in Year 2 to aid in the accomplishment of these tasks.

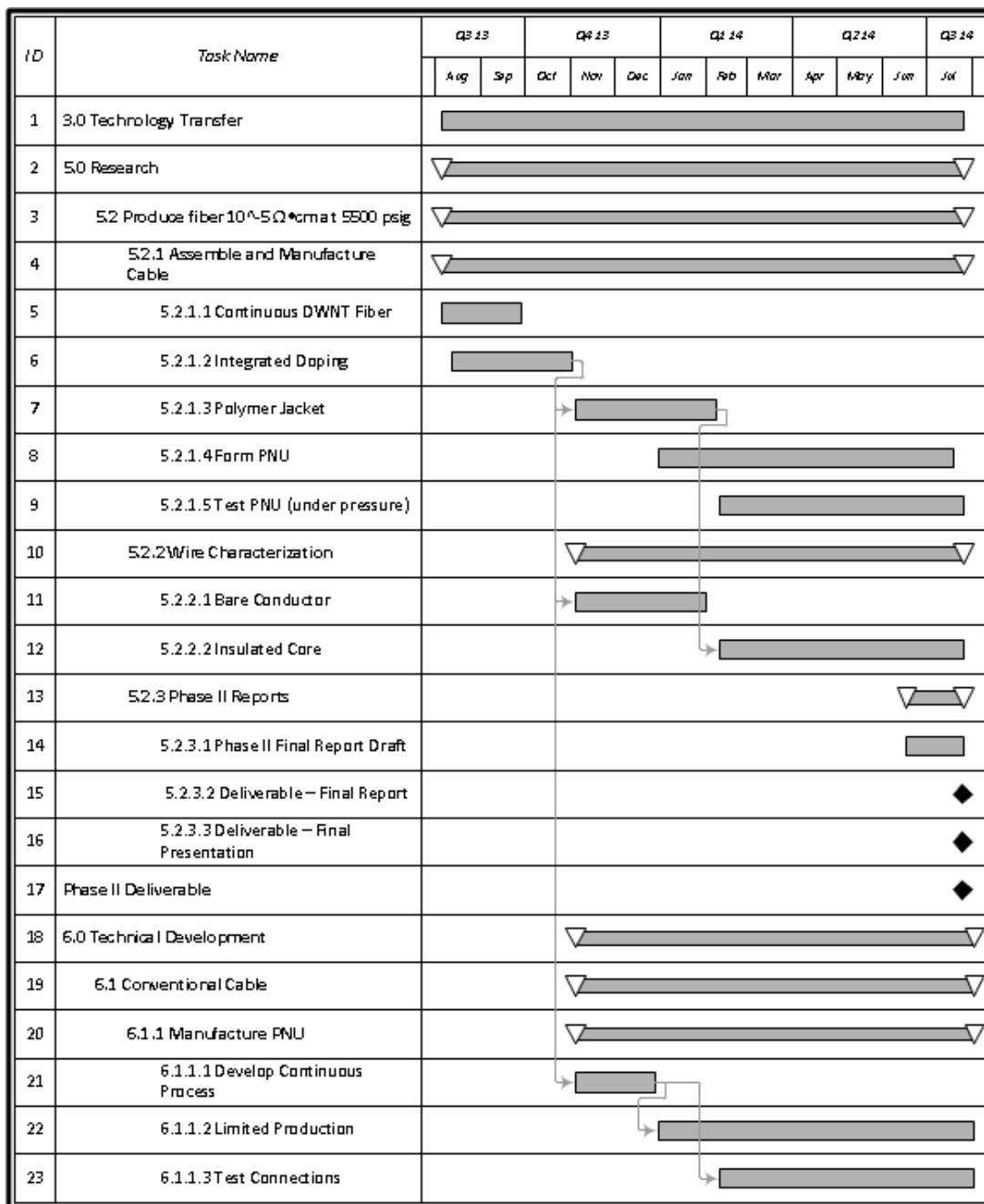


Figure A-1. Phase II Gantt chart.

As stated, the main thrust of Q1, Year 2 is completion of continuous wire forming processes. Currently, wire is being collected on a take-up spool and delivered to Rice for characterization and resistivity measurements. Although, the system is yielding spooled material, improvements are needed to make the process more consistent. **Figure A-2** shows the current

furnace configuration. Once the vertical configuration was decided, several systems were installed. These include:

- Exit flange with large exit port and gas management capabilities
- Pressure control to manage the hydrogen and growth zone flow profile
- Acetone spray nozzles to densify the fiber as it forms
- Chiller to for thermal management
- Take-up spool positioned with spool edge tangential to the furnace center
- Preheaters to adjust thermal profile
- Several flow meters to monitor flow velocity at various locations

The most challenging issue at the moment is the adherence of the nanotubes to the cold quartz wall. Spinning begins and proceeds smoothly for a time. Ultimately spinning ceases due to fiber thinning caused by adherence of nanotubes to the production tube. A second generation flange and an inert gas ring are being designed. The inert gas ring shall cause a vortex and thus holding the fiber true to center. Nevertheless, the system provides meters of fiber. Phase II shall provide the resources necessary to complete the continuous system.



Figure A-2. Production furnace in vertical configuration.